Long-Term Effects of Cathodic Protection on Prestressed Concrete Bridge Components

FOREWORD

This interim report documents the initial 30 months of progress that has been achieved in an overall 5-year study to determine the feasibility of applying cathodic protection as a corrosion control strategy for steel tendons in pretensioned concrete structural members. The report will be of interest to design firms and designers, bridge engineers, inspectors, and construction contractors who are involved with pretensioned concrete bridges, and to owners of such structures.

Charles J. Nemmers, P.E.
Director, Office of Engineering
Research and Development

NOTICE

This document is disseminated under the sponsorship of the Department of Transportation in the interest of information exchange. The United States Government assumes no liability for its contents or use thereof. This report does not constitute a standard, specification, or regulation.

The contents of this report reflect the views of the authors, who are responsible for the facts and accuracy of the data presented herein. The contents do not necessarily reflect the official policy of the Department of Transportation.

The United States Government does not endorse products or manufacturers. Trade or manufacturers' names appear herein only because they are considered essential to the object of this document.

1. Report No. FHWA-RD-96-029	2. Government Accession No.	3. Recipient's Catalog No.
4. Title and Subtitle LONG-TERM EFFECTS OF CATHODIC PROTECTION ON PRESTRESSED CONCRETE BRIDGE COMPONENTS		5. Report Date November 1996
		6. Performing Organization Code
7. Author(s) W. HARTT, E. JOUBERT, and S. KLISZOWSKI		8. Performing Organization Report No.
9. Performing Organization Name and Address CENTER FOR MARINE MATERIALS DEPARTMENT OF OCEAN ENGINEERING FLORIDA ATLANTIC UNIVERSITY BOCA RATON, FLORIDA 33431		10. Work Unit No. (TRAIS) 3D4b
		11. Contract or Grant No. DTFH61-92-C-00058
12. Sponsoring Agency Name and Address Office of Engineering and Highway Operations R & D Federal Highway Administration 6300 Georgetown Pike McLean, VA 22101-2296		13. Type of Report and Period Covered INTERIM REPORT OCT., 1992 to MAR., 1995
		14. Sponsoring Agency Code

15. Supplementary Notes

Contracting Officer's Technical Representative (COTR): Y. P. Virmani, HNR-10

16. Abstract

While cathodic protection effectively reduces or stops ongoing corrosion of reinforcing steel in concrete, applicability of this technology to prestressing steel has been limited because of concerns of possible bond loss and hydrogen embrittlement. Within this context the present research was intended as a comprehensive, multifaceted undertaking to elevate the understanding of prestressed concrete cathodic protection to the same level as for reinforced concrete. The experimental part of the program involved three approaches: 1) constant extension rate tests (CERT) upon straight tendon wire, 2) monitoring of cathodically polarized prestressed beams for both bond loss and hydrogen embrittlement, and 3) concrete block pull-out tests involving both tendon and wire. Findings to-date include the following: 1) High chromium bearing microalloyed prestressing steel is more susceptible to embrittlement than ordinary steel, and the previously proposed -0.90 v (SCE) lower potential limit is not conservative in this case. 2) Prestressed concrete structures can be qualified for cathodic protection based upon the amount of uniform and localized corrosion wire cross section loss. 3) Loss of bond within the anticipated remaining service life of most prestressed concrete structures should not be a concern provided current density is within the normal range and is not locally concentrated. These and related findings are evaluated within the context of standards for prestressing steel and criteria for cathodic protection.

17. Key Words		18. Distribution Statement	
Cathodic protection, corrosion prestressed concrete, pretensioned concrete, cathodic protection criteria, bond loss, hydrogen embrittlement, bridges		No restrictions. This document is available to the public through the National Technical Information Service, Springfield, VA 22161	
19. Security Classif. (of this report) Unclassified	20. Security Classif. (of this page) Unclassified	21. No. of Pages 120	22. Price

Form DOT F 1700.7   (8-72)   Reproduction of completed page authorized

SI* (MODERN METRIC) CONVERSION FACTORS

APPROXIMATE CONVERSIONS TO SI UNITS

Symbol	When You Know	Multiply By	To Find	Symbol
LENGTH				
in	inches	25.4	millimeters	mm
ft	feet	0.305	meters	m
yd	yards	0.914	meters	m
mi	miles	1.61	kilometers	km
AREA				
in²	square inches	645.2	square millimeters	mm²
ft²	square feet	0.093	square meters	m²
yd²	square yards	0.836	square meters	m²
ac	acres	0.405	hectares	ha
mi²	square miles	2.59	square kilometers	km²
VOLUME				
fl oz	fluid ounces	29.57	milliliters	mL
gal	gallons	3.785	liters	L
ft³	cubic feet	0.028	cubic meters	m³
yd³	cubic yards	0.765	cubic meters	m³

NOTE: Volumes greater than 1000 l shall be shown in m³.

Symbol	When You Know	Multiply By	To Find	Symbol
MASS				
oz	ounces	28.35	grams	g
lb	pounds	0.454	kilograms	kg
T	short tons (2000 lb)	0.907	megagrams (or "metric ton")	Mg (or "t")
TEMPERATURE (exact)				
°F	Fahrenheit temperature	5(F-32)/9 or (F-32)/1.8	Celcius temperature	°C
ILLUMINATION				
fc	foot-candles	10.76	lux	lx
fl	foot-Lamberts	3.426	candela/m²	cd/m²
FORCE and PRESSURE or STRESS				
lbf	poundforce	4.45	newtons	N
lbf/in²	poundforce per square inch	6.89	kilopascals	kPa

APPROXIMATE CONVERSIONS FROM SI UNITS

Symbol	When You Know	Multiply By	To Find	Symbol
LENGTH				
mm	millimeters	0.039	inches	in
m	meters	3.28	feet	ft
m	meters	1.09	yards	yd
km	kilometers	0.621	miles	mi
AREA				
mm²	square millimeters	0.0016	square inches	in²
m²	square meters	10.764	square feet	ft²
m²	square meters	1.195	square yards	yd²
ha	hectares	2.47	acres	ac
km²	square kilometers	0.386	square miles	mi²
VOLUME				
mL	milliliters	0.034	fluid ounces	fl oz
L	liters	0.264	gallons	gal
m³	cubic meters	35.71	cubic feet	ft³
m³	cubic meters	1.307	cubic yards	yd³
MASS				
g	grams	0.035	ounces	oz
kg	kilograms	2.202	pounds	lb
Mg (or "t")	megagrams (or "metric ton")	1.103	short tons (2000 lb)	T
TEMPERATURE (exact)				
°C	Celcius temperature	1.8C + 32	Fahrenheit temperature	°F
ILLUMINATION				
lx	lux	0.0929	foot-candles	fc
cd/m²	candela/m²	0.2919	foot-Lamberts	fl
FORCE and PRESSURE or STRESS				
N	newtons	0.225	poundforce	lbf
kPa	kilopascals	0.145	poundforce per square inch	lbf/in²

* SI is the symbol for the International System of Units. Appropriate rounding should be made to comply with Section 4 of ASTM E380.

(Revised September 1993)

ii

TABLE OF CONTENTS

TABLE OF CONTENTS (continued)

LIST OF FIGURES

LIST OF TABLES

ix

CHAPTER I: INTRODUCTION

BACKGROUND

Utilization of prestressed concrete in bridge construction has evolved during the past 45 years to the point where in the late 1980's 50 percent of all new construction and a total of in excess of 55,000 bridges in the United States were of this material class. (1) Correspondingly, during the past three-plus decades, corrosion of steel in reinforced concrete bridges and related transportation structures has evolved to become the single most costly problem of its type in the United States. While corrosion induced deterioration of prestressed concrete is not presently widespread, it is anticipated that damage from this cause will become increasingly important in the next few years as structures of this type age. Thus, although the alkaline nature of the cement paste in concrete (pH~12.5-13.8) facilitates formation and maintenance of a protective, passive film and low corrosion rate, chloride intrusion into the concrete from exposure to either deicing salts or a marine environment (or both) can compromise this situation and, in the presence of moisture and oxygen, cause corrosion rate to become unacceptably high. (2) This, in turn, leads to accumulation in the cement pore space near the embedded steel-concrete interface of solid corrosion products which give rise to tensile hoop stresses and, eventually, to concrete cracking and spalling.

Factors which influence corrosion of embedded steel in concrete include 1) type of exposure, 2) inherent cement alkalinity, 3) concrete permeability and 4) concrete resistivity. Parameters in the first of these categories include temperature, concentration of deleterious species (chlorides, for example), as well as water and oxygen, and the frequency and intensity of alternate wetting and drying. Concrete permeability (item 3) is important as it influences the transport of influential species (chloride, water and oxygen) to the steel-concrete interface, whereas item 4 (resistivity) is critical to functioning of the electrochemical cell(s), particularly when anodes and cathodes exist on a macroscopic scale as is often the case in bridge components. Past research investigations have concluded that as little as 0.025-0.033 percent Cl^- (concrete weight basis) can cause localized loss of passivity for steel in concrete, thereby facilitating corrosion at a rate controlled by water and oxygen availability at cathodic sites. (3,4) Related experiments involving simulated cement pore water electrolytes have indicated that the ratio of chlorides to hydroxides, $[Cl^-]/[OH^-]$, is the parameter with which compromise of passivity best correlates. (5)

Prestressed concrete can be either pre- or post-tensioned, where tendon in the former case is bonded directly to the concrete and in the latter is contained within plastic ducts (see reference 6 for background information regarding prestressed concrete principles and practice). While most corrosion studies have focused historically upon reinforced as opposed to prestressed concrete, it is generally considered that the mechanism of corrosion attack and the role of influential variables are the same in the pre-tensioned case. Corrosion damage to post-tensioning, on the other hand, is more related to presence of water and other detrimental species within ducts which house the tendon, as may arise either in association with inadequate

1

quality control during construction or the protective nature of the duct being compromised during service.

Cathodic protection (cp) is presently recognized as the only existing technology that is both sufficiently mature and proved in practice for reducing or stopping ongoing corrosion of embedded steel in concrete. This approach to corrosion control is being promoted and employed increasingly for bridge structure life extension in conjunction with conventional repair of areas where corrosion induced concrete damage has already occurred. In the sense that the corrosion mechanism is considered to be the same for both reinforcing steel and pre-tensioned tendon in concrete, as discussed above, so also cathodic protection should be equally effective in arresting corrosion for either material. At the same time, questions have been identified that are critical to the effective utilization of cathodic protection in the pre-tensioned concrete case and which render this technology distinctive compared to cp of reinforcing steel in concrete. These are a consequence of the fact that, first, pre-tensioned members are often more critically designed than ones with reinforcing steel such that loss of a relatively small number of tendons can compromise structural integrity and, second, the high strength steel from which tendon is fabricated can be susceptible to hydrogen embrittlement. Consider, for example, seven wire spiral tendon (the typical type of prestressing element) which is stressed to 70 percent of its ultimate strength, as is normally thought to be the case. Here, even a modest local cross section loss on a single wire could cause an overload fracture of the wire which, in turn, leads to load transference to the remaining six wires such that an even smaller corrosion penetration upon one or more of these will cause failure of the tendon. Once this occurs, the prestress is compromised over a certain length of the concrete member; and additional stress is transmitted to adjacent tendons making them increasingly susceptible to overload fracture. Further, if hydrogen uptake within the steel occurs, either in association with corrosion or with cathodic protection, then the material becomes embrittled, its strength is lowered and the tolerance for any cross section loss from corrosion is further reduced. With these concerns in mind, certain questions must be resolved before cathodic protection can be confidently employed in association with prestressing steel members and structures. These questions are:

1. Are further refinements necessary regarding the operating parameters for cathodic protection of prestressing steel in concrete?

2. Is there a relationship between tendon steel properties (composition and microstructure) and the tendency for occurrence of cathodic protection induced (hydrogen) embrittlement?

3. To what extent and how significant is any reduction of tendon-concrete bond in association with cathodic protection of steel in concrete?

4. How can a particular prestressed concrete member be best qualified for cathodic protection?

5. What are the most effective operating parameters and field techniques for cathodically protecting prestressing steel in concrete?

2

The last of these (question 5) is being addressed in a companion research project, while it is the objective of the present research to consider the first four. (7) This report presents results of experiments and analyses performed to-date with completion of approximately 50 percent of this project.

STATE-OF-KNOWLEDGE DEFINITION

General

Based upon the questions which are relevant to advancement of prestressing cathodic protection technology (see above) and development of a practical methodology for its application, the state-of-knowledge pertaining to 1) tendon material, 2) cp criteria for steel in concrete, 3) hydrogen embrittlement of prestressing steel, 4) qualification of a prestressed concrete structure or component for cathodic protection and 5) tendon-concrete bond reduction or loss in association with cp has been defined as presented below.

Tendon Material

Tendon for prestressed concrete construction consists of a center wire with six helically placed outer wires with overall diameter ranging from 6.35 to 15.24 mm. (8) Two grades (250 and 270) are specified, where the number designates minimum ultimate strength in ksi units (1725 and 1860 MPa, respectively). The wire is cold drawn high carbon steel with a wrought pearlitic microstructure. Fabrication is followed by a thermal treatment to affect either a low relaxation or stress relieved condition. The standard specification addresses mechanical properties (strength, ductility and relaxation or creep) and dimensions of the final product only with selection of steel composition being left to the fabricator. (8) It has been determined, however, that the requisite strength in a drawn pearlitic microstructure can best be achieved using either a plain carbon steel of near eutectoid composition (0.77 w/o carbon) or with microalloying, where a small amount of either chromium, vanadium or chromium plus vanadium is included. The microalloying elements facilitate the strengthening that is realized upon cold drawing and better assure that the requisite mechanical strength will be attained.

Cathodic Protection Criteria for Steel in Concrete

As noted above, cathodic protection is presently the only recognized and routinely practiced methodology for reducing or arresting ongoing corrosion of steel in concrete. (9,10) The characteristics, relevant design parameters, limitations, installation procedures, materials and hardware components, and performance history of numerous types of cp systems for concrete structures containing reinforcing steel have been extensively researched and documented. At the same time, this technology continues to evolve. Particularly critical to satisfactory performance and longevity of cp systems for reinforcing and prestressing steel in concrete is specification of an appropriate protection criterion. Alternatives that have been employed historically are:

1. Polarization to a prescribed cathodic potential (potential criterion).

2. Cathodic polarization by 300 mV relative to the corrosion or unpolarized potential (potential shift criterion).

3. Cathodic polarization by sufficient magnitude that a 100 mV potential decay occurs at anodic sites with time subsequent to current interruption (potential decay criterion).

4. Application of a prescribed net cathodic current (current criterion).

The first of these (potential criteria) has been widely employed for natural water and, to a lesser extent, soil exposure applications, where polarization to -0.78 v (SCE) has been shown to arrest corrosion of steel.[1]   Such an approach has a first principles basis in that the potential in question corresponds to the reversible value for the anodic reaction. Unfortunately, the nature of the reversible potential and an inability to define its value, either from theoretical considerations or experimentation, for alloys in environments of interest often relegate any criterion based upon this approach to one which is practice based. A further limitation is that, while corrosion is certainly arrested upon polarization to the reversible potential for the anodic reaction, such polarization may be unnecessarily excessive for exposures where the metal may passivate, as is the case for steel in concrete. This follows since for a passive metal adequate protection is also afforded by maintaining potential within the passive regime, which requires less polarization than to achieve the reversible potential. Even in situations where the embedded steel or portions thereof are initially active, production of hydroxides at, and electromigration of chlorides from, the metal-electrolyte interface may reestablish passivity over a period of time. This is illustrated schematically by the pseudo-Pourbaix diagram in figure 1 for the iron-water system but with the influence of chlorides of concentration 10^{-3}, 10^{-2}, 10^{-1} and 10^0 molarity (identified by '-3', '-2', '-1' and '0', respectively, in the figure) upon the potential-pH regimes of "protection" and "pitting" also being shown. Thus, the "protection" (actually passive) regime extends over a more broad range of potential and pH as the chloride ion concentration decreases. The situation projected here is consistent with the onset of corrosion for steel in concrete conforming to occurrence of a specific value for chloride-to-hydroxide ratio, as discussed above. Conversely, actively corroding steel in concrete should repassivate if $[Cl^-]/[OH^-]$ drops below a certain value (not necessarily the same as required to compromise passivity to begin with). Because the cathodic current to arrest corrosion upon an active metal is likely to be greater than that to maintain protection of a passive one, the corrosion state transition from active to passive that can result from production of hydroxides and electrochemical migration of chlorides could result in current being unnecessarily high. Consequently, the magnitude of polarization and the current necessary to affect this polarization are likely to change with time; and the implications of this with regard to cp of prestressing steel may be important. In this regard, several authors have given consideration and performed experiments and analyses relevant to a cp criterion based upon the chloride profile in a particular concrete, as affected by 1) diffusion and 2) electromigration. (13,14) While such an approach has the advantage of being first principles based, it does not alleviate the difficulty of the criterion associated with it being a function of time. Development of a quantitative criterion based upon such a method is projected to be a long-term effort.

---

[1] This potential (-0.78 v (SCE)) is equivalent to -0.85 v (CSE) and -0.80 v (Ag/AgCl).

4
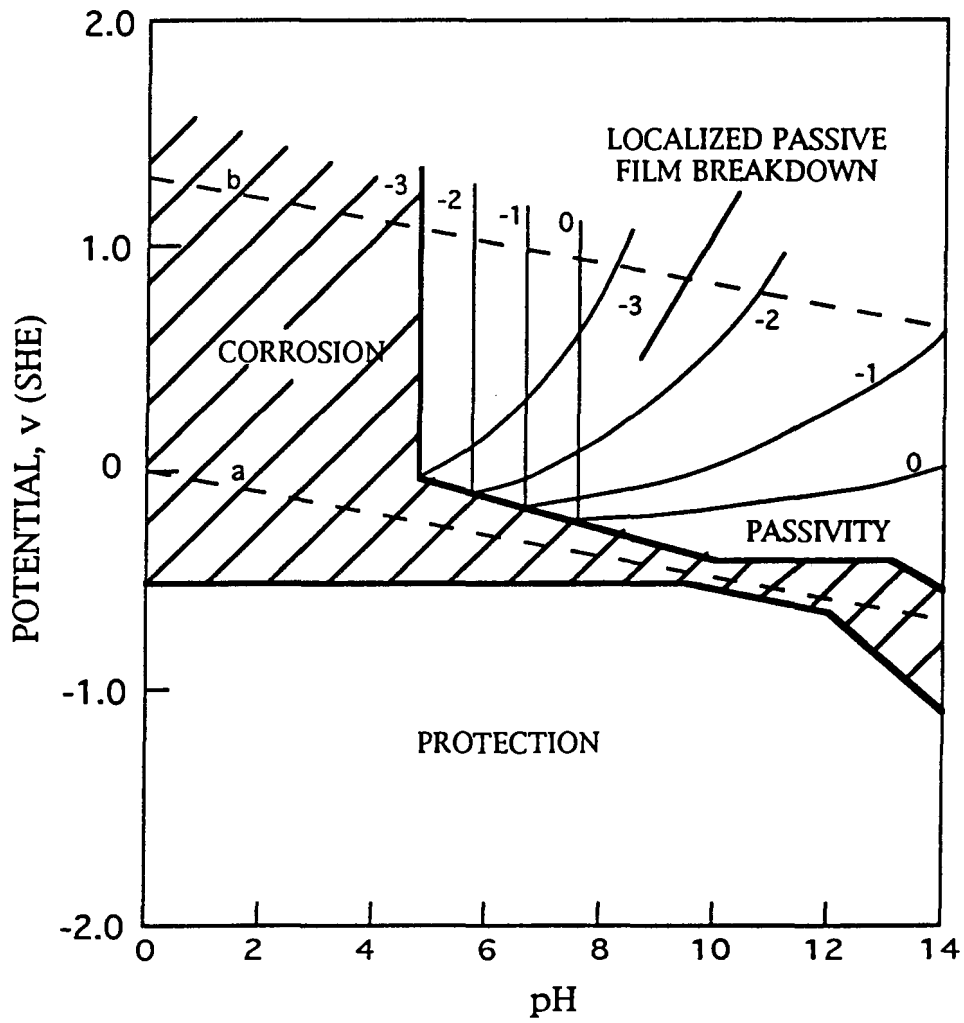
Figure 1: Modified Pourbaix diagram illustrating the influence of chloride concentration on the potential-pH range of passive film stability. (12)

The second criterion above (300 mV polarization) has been widely employed historically in conjunction with energizing cathodic protection systems for buried pipelines, where a large amount of service experience has indicated that protection of such structures is affected when cathodic polarization is of this magnitude. A limitation of this criterion is that a voltage (IR) drop of undefined magnitude constitutes a portion of the 300 mV. Consequently, this criterion can lead to underprotection in situations where IR drop is large and overprotection when it is small. The latter situation is apparent when this criterion is compared with the potential based one for the case of steel in sea water. Thus, a typical corrosion potential for steel in sea water is -0.60 v (SCE); and so the potential criterion indicates that protection is achieved with less than 200 mV of cathodic polarization, whereas the 300-mV polarization criterion, in turn, requires that the steel be polarized to -0.90 v (120 mV more polarization than required for protection). Energizing a cp system for steel in atmospherically exposed concrete according to the 300-mV polarization criterion is considered inappropriate because of the large uncertainty which exists regarding magnitude of the IR component. Also, even if the procedure is useful for initial activation of a cp system, it is not intended, nor is it applicable, as a monitoring tool.

The 100-mV depolarization approach measures potential decay over a prescribed period (normally 4-h) subsequent to current interruption and elimination of the IR drop. Definition of the level of protection according to this procedure, like the 300-mV polarization one, is imperical. It affords the advantage, however, of being independent of IR drop. While this criterion is now widely employed in association with cp of steel in concrete, appropriateness of the 100 mV per se has been projected by some as unconservative. (15-17)

The net current criterion approach to cp (item 4 above) is, in effect, synonymous with the preceding three in the sense that only potential or current, but not both, is an independent variable; and so specification of one for a particular situation, defines the other. Numerous cp systems employed in conjunction with protection of steel in concrete are operated on a constant current (current control) basis with the magnitude of the protective current being defined by the E-log I test procedure, which is also imperical. (18) However, operation of an impressed current rectifier in a constant current mode of control for cp of atmospherically exposed concrete is likely to result in overprotection during periods when the concrete is dry and of high resistivity. This, in turn, can lead to embrittlement of prestressing steel, as discussed subsequently. To reduce the possibility of this occurring, rectifier control in the constant current mode but with a voltage limit has been proposed. (19) Thus, as the concrete dries, the voltage required to provide the specified current increases until the prescribed limit is reached. Upon further drying the rectifier output voltage remains constant, and current is reduced according to magnitude of the resistance increase.

A related but more sophisticated approach is that of Bazzoni and Lazzari who proposed a cp criterion for prestressing steel in concrete based upon the equation: (20)

$$E = \phi_a + \phi_c + E_m + E_\alpha \tag{1}$$

where

> E = rectified voltage output (constant),
> ϕ_a = anode potential,
> ϕ_c = cathode potential,
> E_m = metallic path Ohmic drop and
> E_c = concrete path Ohmic drop.

These authors reasoned that with a mixed metal oxide anode a stable value for ϕ_a is realized. They considered also that 1) E_m is constant and measurable, 2) -0.85 v (SCE) is the minimum acceptable value for ϕ_c if hydrogen evolution is to be avoided and 3) the minimum likely value for E_c is 50 mV. Accordingly, a microprocessor based control unit/data acquisition system was designed and constructed which interrogated the cp system to measure the sum of ϕ_a (current-off) and E_m, calculated E (assuming ϕ_c + E_m = -0.90 v) and adjusted the rectifier output accordingly. Typical values for the latter parameter (E) were about 1.5 v. The procedure could be repeated iteratively and the degree of protection checked according to the 100-mV depolarization criterion. Subject to appropriateness of the selected minimum value for the concrete path Ohmic drop, overprotection should be avoided; however, periods of underprotection may arise when the concrete is dry and of high resistivity (high E_c). This shortcoming is not necessarily of major consequence, however, since corrosion of the prestressing should be minimal during such times. Also, in the long-term chlorides may be electromigrated away from the steel, active areas passivated and cp current demand reduced. Wagner and Funahashi performed small scale laboratory experiments which confirmed potential utility of such a voltage control based criterion. (21)

More recently, Bennett et al. have proposed a procedure termed Corrosion Null Probe (CNP) whereby a section of existing corroding steel is isolated and instrumented with the cathodic protection criterion defined according to the current required to balance the macrocell current between this section and other steel in the structure. (22) Both laboratory and field test data were presented which supported this approach. Interestingly, it was determined that while the current demand increased by about two orders of magnitude as chloride ion concentration increased from 0.6 to 11.9 kg/m^3 , the corresponding magnitude of depolarization for protection was invariably in the range 100 to 150 mV. The CNP approach has the advantage that reference electrodes of long-term stability and reliability are not required. However, for this criterion to be effective, the most active area of steel must be identified for the probe. Also, because current demand should decrease with time, periodic monitoring is required if overprotection is to be avoided. Of course, isolating a section of prestressing steel is not normally an option. However, it is possible that the isolated probe could be reinforcing steel that is also present; but it would have to be confirmed that this can be sectioned without compromising any adjacent tendons.

Most experiments directed toward evaluation of cathodic protection for reinforcing and prestressing steel in concrete have involved atmospheric exposures. Also important, however, are marine bridge substructure components, prestressed pilings in particular. In this regard, Pangrazzi et al. performed natural sea water exposure experiments upon simulated prestressed piling specimens that were cathodically polarized locally in the splash zone and found that 4-h depolarization in excess of 100 mV was realized only if

7

potential was -0.85 v (SCE) or more negative, and depolarization was less than 100 mV for potentials of -0.77 v and more positive. (23) Follow-on experiments by Chaix et al. determined that the magnitude of depolarization was dependent upon atmospheric relative humidity and moisture content in the specimen. (17) These authors pointed out that, while a criterion based upon the magnitude of depolarization appears to be appropriate from the standpoint of protection per se, such an approach does not yield information regarding possible overprotection. A cp criterion based upon both the magnitude of depolarization and potential was recommended.

With the advent of modern microelectronics based data acquisition instrumentation and communications technology, the capability exists for remotely activating, adjusting, monitoring and testing the cp system on a particular structure. The capacity to do this is particularly attractive in the case of prestressed structures, where closer control of the protection system is warranted compared to situations involving reinforced concrete. However, effective utilization of remote monitoring and control units requires that reference electrodes be both stable and reliable in the long term; and data is presently insufficient to confidently conclude that this can be achieved with the options which presently exist.

Hydrogen Embrittlement of Prestressing Steel

It is generally recognized that as strength of a metal or alloy is increased so also is its susceptibility to brittle fracture and to environmentally assisted cracking. Of particular concern with regard to cathodic protection of prestressing steel in concrete is the possibility of hydrogen embrittlement, since, first, the strength of prestressing steel is certainly in the range where concerns regarding such embrittlement are warranted and, second, cathodic polarization to potentials active to the reversible hydrogen value can result, in which case hydrogen is generated according to the reaction:

$$H_2O + e^- \rightarrow H_{ads} + OH^-, \tag{2}$$

where H_{ads} denotes atomic hydrogen adsorbed on the metal surface. This latter species (H_{ads}) has either of two subsequent reaction paths available as:

$$H_{ads} + H_{ads} \rightarrow H_2 \quad \text{or} \tag{3}$$

$$H_{ads} \rightarrow H_{dis}, \tag{4}$$

where H_{dis} denotes hydrogen dissolved in the metal. Interaction of this latter species with the stressed steel lattice can then lead to embrittlement by one or more of the classically proposed mechanisms. (24,25)

The rate of reaction 2 and, hence, the concentration of H_{dis} should be influenced by environment (temperature, electrolyte composition and pH), potential, metallurgical structure and surface condition of the steel. With regard to the last of these (metallurgical structure) Gilchrist et al. demonstrated that cold drawn, high carbon steels of a pearlitic microstructure are more resistant to environmental cracking than quenched and tempered

ones of the same strength; and it is upon this former material that the applicable standard is now based. (26,8)

A variety of test techniques have been employed historically to study environment and electrochemical potential (polarization) effects upon the fracture properties of prestressing steel. These have involved either constant or dynamic loading of smooth, notched or precracked specimens and in some cases test acceleration by either potential modification or by addition of a hydrogen recombination poison such as NH_4 CNS to the electrolyte. While each of these approaches has its own inherent advantages and disadvantages, constant extension rate testing or CERT (alternately, slow strain rate testing or SSRT) has been identified as being particularly appropriate. In this regard, figure 2 reports CERT results as plots of normalized fracture load (strength) versus potential (figure 2a) and normalized fracture area (specimen cross section area at the fracture location divided by the original area) versus potential (figure 2b) from testing of smooth prestressing steel wire in saturated $Ca(OH)_2$. (27) The former (figure 2a) indicates that the maximum strength reduction, even at excessively negative potentials, was only by about 10 percent. However, the corresponding change in ductility (figure 2b) at potentials negative to about -1.2 v amounted to an 85 to 90 percent reduction. This could potentially manifest itself as a reduced capacity by tendon to resist impact type loadings; however, it should not generally be of concern. Consequently, it is concluded based upon the above data and rationale that hydrogen embrittlement of smooth prestressing steel tendon should not be a factor which limits application of cathodic protection. Such a projection is at least partially substantiated by experiments of Scannell and Hartt who polarized uncorroded prestressing steel in slab type specimens to a current-off potential of -1.30 v (SCE) for 36 days with no failures being noted. (28)[2]

It has been reasoned that smooth prestressing steel polarization results may not be relevant to the questions at hand, however, since, first, tendons in structures and components that are candidates for cathodic protection are likely to be corroded and, as such, to no longer be smooth and, second, material with a locally reduced cross section, as could result from corrosion, is generally more susceptible to embrittlement than smooth. With this point in mind several research studies have reported results from CERT experiments upon notched prestressing steel specimens, also in saturated $Ca(OH)_2$, as a function of potential with results being as shown in figure 3. (27, 29-31) This reveals that normalized fracture load was relatively high and potential independent for $\phi \geq$ -1.00 v (SCE). Strength decreased, however, with cathodic polarization in the range -1.00 $\geq \phi \geq$ -1.20 v to a value approximately one-half that in air. A dominating influence of potential, compared to that of other variables, is inferred by the fact that the same general trend prevailed for the different data sets in figure 3 despite the fact that these represent four different investigations which employed different material stock and test conditions. Relatedly, Hartt et al. demonstrated that chloride ion concentration and electrolyte pH exhibited only a modest influence upon fracture load compared to potential. (27) The observation that fracture load in saturated

---

[2] This conclusion is based upon the state of knowledge which existed at the beginning of this project. The experiments and analyses performed as a part of this project have caused this opinion to be modified, as discussed subsequently.
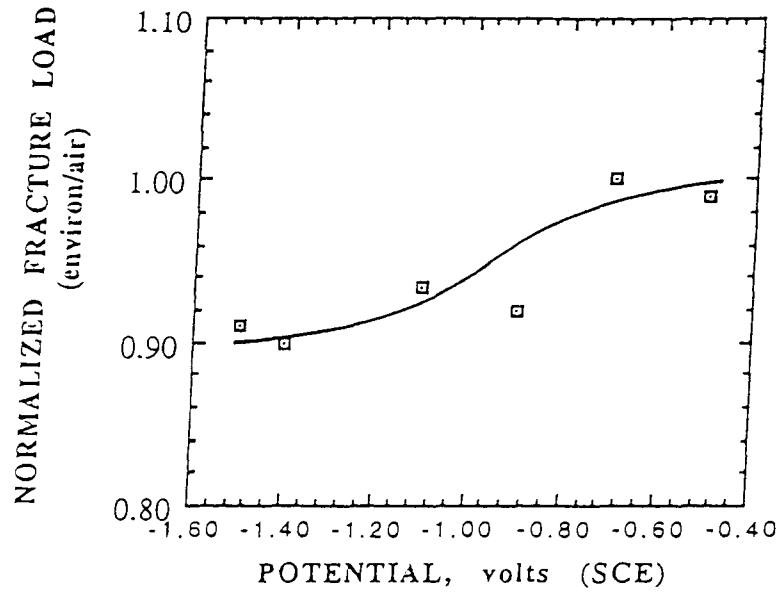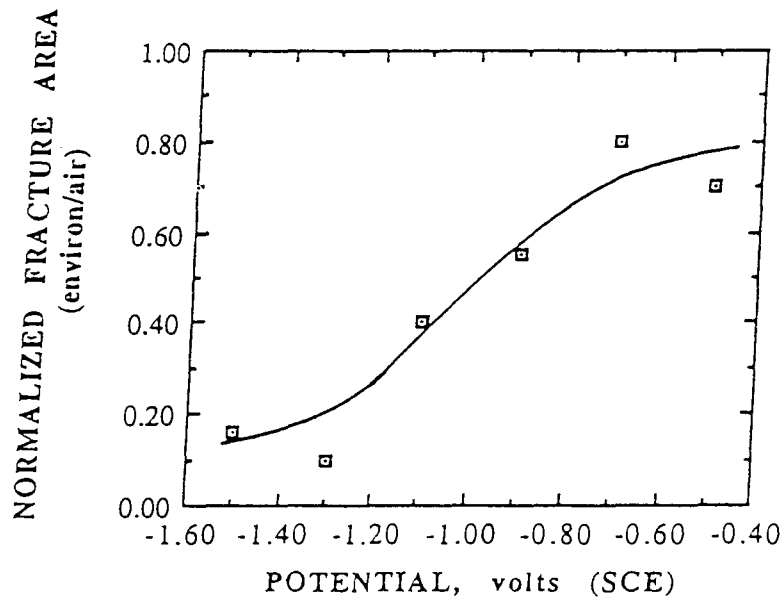
Figure 2: Previous CERT results as: (a) normalized fracture load
as a function of potential and (b) normalized reduction
in area as a function of potential. (27)
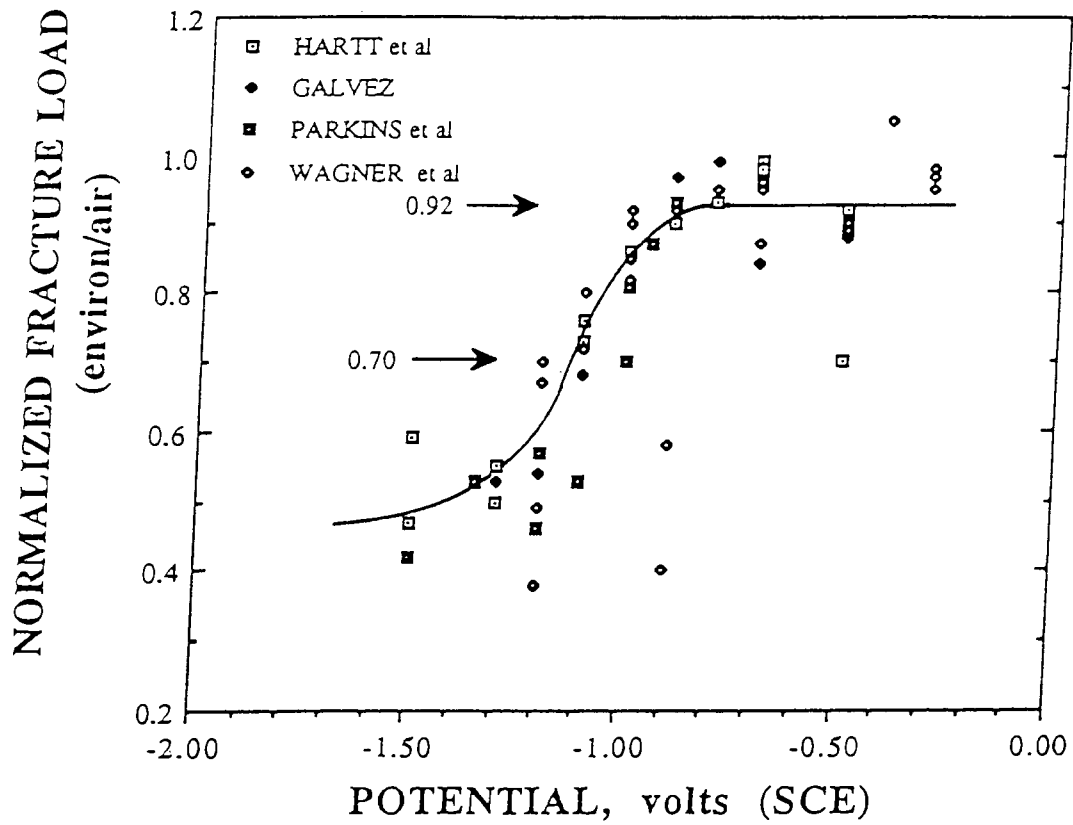
Figure 3: Normalized fracture load as a function of potential for notched Grade 270 prestressing steel specimens as reported from previous research. (27,29-31)

Ca(OH)$_2$ for $\phi \geq$ -1.00 v (figure 3) was below that in air has been attributed to water adsorption induced lattice decohesion. (27) By this process, water that is adsorbed at a potential fracture site or at a crack tip is projected to reduce interatomic bond strength between iron atoms at potential fracture sites and lower fracture strength accordingly. On the other hand, the more pronounced loss of strength for $\phi \leq$ -1.00 v is indicative of hydrogen embrittlement. This corresponds approximately to the reversible potential for the hydrogen reaction at the pH of a saturated Ca(OH)$_2$ solution ($\approx$ 12.45), which is -0.98 v, and has led to -0.90 v being proposed as an appropriate lower potential limit for cathodically protected prestressing steel, considering that a 100 mV (approximate) safety factor is sufficient. (27,31)

Structure/Component Qualification for Cathodic Protection

In a generalized sense a number of factors influence a decision regarding applicability of cathodic protection for a reinforced or prestressed concrete structure or component. These include the extent of existing corrosion induced concrete cracking and spalling and the anticipated remaining service life. The present discussion pertains to a consideration which is specific to prestressed, as contrasted with reinforced, concrete, however; and in this regard the data for notched, polarized specimens suggest that, if tendon wire is locally corroded such that notch-like pits exist, then susceptibility to hydrogen embrittlement and brittle fracture is greater than if corrosion damage is modest and uniform (compare figures 3 and 2a). In the former case (presence of notch-like pits) design of the cp system must be such that potentials below -1.00 v (SCE) do not occur. However, even at potentials positive to this, the data in figure 3 indicate that the average fracture load is reduced to about 92 percent of the value without cp. While this seems like a modest reduction, it must be assumed that the prestress is 70 percent of the fracture load; and on this basis the lowered strength reduces the safety margin by 27 percent ([(1.00-0.92)/(1.00-0.70)]x100, see figure 3). The situation is compounded further by the fact that the 70 percent prestress is referenced to the original wire and tendon cross section, but with occurrence of pitting cross section area is decreased and the prestress increased accordingly. Also, factors such as the level of prestress and remaining wire fracture strength are statistically distributed parameters such that occurrence of some failures is not unexpected upon application of cp even though consideration of the mean strength suggests integrity should be maintained.

A technology termed Electrochemical Proof Testing (ECPT) has been proposed for establishing the likelihood that tendon failures will not occur upon application of cathodic protection. (32) This involves 1) identification of a worst-case area of the candidate structure or component, 2) mounting of a temporary cp system and polarizing one or more tendons to a current-off potential of at least -1.20 v for a period of about 1 day, 3) monitoring for strand failure during the polarization by a procedure such as (a) electrical continuity, (b) acoustic emission or (c) component shape change. Qualification then is based upon no tendons failing, either during the polarization or within 1 to 2 days thereafter. Shortcomings of the procedure are the requirement for intentional excessive cathodic polarization and the possibility of inducing damage to the structure as a consequence.

12

Loss of Bond

Various investigations have reported a decrease in concrete-to-reinforcing steel bond strength as a result of prior cathodic polarization. (33-39) In two instances this bond strength reduction correlated best with the total charge transferred as opposed to applied voltage or current density. (33,34) If this is the case, then an accelerated experimental program which employs a relatively high current density in conjunction with an appropriate value for total charge density transfer should yield results that are directly applicable to and correlatable with practical cathodic protection circumstances where current density is relatively low but application periods are intended for many years. However, a subsequent investigation reported a dependence of loss of bond upon each of these two parameters (current density at constant total charge transfer and visa versa); and it was unclear which of the two was more influential. (37) In this same study, the reduction in ultimate bond stress (calculated from the maximum load which occurred during the pull-out test and the embedded steel surface area) for current densities upon the steel as high as 53,900 mA/m^2 and total charge transfer densities up to 2,200 A-h/m^2 were no greater than 15 percent, which is typical of what was reported in the earlier studies. (33-36)[3]

Two additional parameters, in addition to ultimate stress, have been considered historically for bond loss characterization. The first of these is the bond stress at which the loaded bar end has slipped 0.25 mm. This, in turn, has been projected to correspond to the slip that should accompany presence of a concrete crack of maximum tolerable width 0.5 mm. Relatedly, slip at the opposite or free bar end of 0.025 mm is considered indicative of bond being compromised along the entire embedded length. While in the study sited above the reduction in ultimate bond strength was by no more than 15 percent, the bond stress for a loaded-end slip of 0.25 mm was reduced by about 40 percent, and the bond stress at 0.025 mm free-end slip at either 53,900 mA/m^2 or 2,200 A-h/m^2 was 33 percent of that for the control specimens (no polarization). (37)

Rasheeduzzafar et al. reported a reduction in ultimate bond strength of up to 33 percent for specimens containing 4.5 kg/m^3 admixed chlorides at a charge density transfer of 5,400 A-h/m^2 . (38) The fact that this bond strength reduction was greater than for any of the other studies could be due to the relatively high charge density transfer or, alternately, to Rasheeduzzafar et al. having employed a newly developed experimental approach which better assured that the concrete was not compressed about the embedded steel during testing which could, in turn, unrealistically enhance bond strength. These same authors also presented load versus slip plots for their pull-out tests which indicated that maximum load occurred at about one mm loaded end slip. The fact that this exceeds the slip projected to cause significant concrete cracking suggests that the bond stress at 0.25 mm loaded end slip may be a more useful parameter than ultimate bond strength in assessing the influence of cathodic polarization upon this aspect of structure integrity.

---

[3] 2,200 A-h/m^2 is equivalent to a current density of 10.8 mA/m^2 applied for approximately 23 years.

Several more recent studies have involved either 1) both chloride admixed chloride and chloride free specimens or 2) specimens with two levels of admixed chloride, whereas earlier programs were based upon chloride free specimens only. (33-39) Interestingly, comparison of data from these two specimen types reveals that the bond strength of reinforcing steel in chloride admixed concrete was greater than for the non-admixed case and that bond loss in association with cathodic polarization was greater for the former (chloride admixed) than for the latter. Also, the magnitude of bond loss was greater for specimens with 4.76 kg/m^3 admixed chloride than for ones with 1.19 kg/m^3. However, the reduced bond strength of the polarized chloride admixed specimens was about the same as that of non-admixed controls (no polarization), thereby indicating that the degradation should not be of practical importance. The difference in bond strength between chloride admixed and non-admixed specimens may have resulted from corrosion product induced compressive stresses about the concrete-steel interface. (37,39) On this same basis, the relatively large bond strength lowering for chloride admixed specimens in association with cathodic polarization has been projected to arise from electrochemical reduction of corrosion products and alleviation of the compressive stresses. (39) No direct determination has been made if this was, in fact, the case; but the finding that the reduced bond of chloride admixed specimens was about the same as for chloride free controls is consistent with this having been the case. On the other hand, the chloride admixed specimens employed by Rasheeduzzafar et al. were polarized immediately upon completion of a submerged water cure such that minimal reinforcing steel corrosion should have occurred. (38) These authors, as well as others, have projected that bond strength reduction in association with cathodic polarization is a consequence of electromigration of soluble cations (Na^+ and K^+) toward and accumulation of these species near the embedded steel surface as has been experimentally measured. (36,38) This results in softening of the cement paste, probably as a consequence of alkali attack of the calcium silicate hydrate binder. Such softening has been reported, and Clear has projected that significant bond loss should be anticipated when the depth of softening approaches the height of the bar deformations. (40,41)

The magnitude of the bond reduction reported in the above studies has been judged to be of little significance with regard to integrity of reinforced concrete transportation structures, where span-to-depth ratios are relatively large. Two factors suggest, however, that the magnitude of bond strength reduction as a consequence of cathodic polarization should be larger and more important in the case of prestressing steel compared to ordinary reinforcement. (32,42) First, the fact that a stress gradient is present across the steel-concrete interface for pretensioned concrete, irrespective of dead weight or applied loadings, means that any softening or weakening of the cement phase in association with cathodic polarization induced electromigration could trigger a bond reduction event that would not occur in the case of reinforced concrete. Second, because bar deformations largely determine bond in the case of reinforcing steel in concrete and because prestressing steel tendon is smooth (no deformations), the concrete-steel bond for the latter material should be less than for the former. While no data is available regarding cathodic polarization induced bond reduction for pretensioned concrete, the study of Buenfeld and Broomfield employed smooth reinforcing bars and, as such, is relevant to the questions being raised here. (39) While the bond strength magnitude measured by these latter authors was lower than for reinforcing steel with deformations, as should be expected, the

reduction caused by cathodic polarization for the two material types (bars with and without deformations) is apparently about the same.

CHAPTER II: EXPERIMENTAL PROCEDURE

GENERAL

The research plan for the present program was formulated in terms of tests in two general categories: first, experiments directed toward characterizing relevant aspects of hydrogen embrittlement susceptibility of tendon and, second, experiments which addressed any tendon-to-concrete bond strength reduction, both in association with cathodic polarization. Experiments directed toward better defining the influence of cathodic polarization upon embrittlement susceptibility (category one) were formulated based upon, first, mechanical property characterization of prestressing wire per se (Constant Extension Rate Testing or CERT) under conditions relevant to cp and, second, exposure of cathodically polarized prestressed concrete beams. Those experiments directed toward characterizing the influence of cp upon tendon-to-concrete bond strength also employed prestressed concrete beam specimens, in addition to non-prestressed concrete block pull-out specimens which contained either embedded tendon or straight wire, neither of which were prestressed). The procedures employed for these are described below.

CERT EXPERIMENTS

Materials and Specimens: Seven wire, nominally 12.70 mm diameter tendons, which were stated to conform to ASTM Standard A416-90a, were acquired from four lots. (8) The composition of each of these is presented in table 1, where the two sets of elemental composition values for the different steel reflect results from samples taken at different locations along the same tendon. Two materials (270D and 250D) were from one supplier and the other two (270F and 270F') were from a second. Those materials with a "270" designation were stated to conform to the Grade 270 specification (minimum ultimate strength 270 ksi) and the one indicated as "250" to Grade 250 (minimum ultimate strength 250 ksi) . The mechanical properties listed in table 2 for each of the steels indicate that the requisite strength was met by each of the four materials.

Different types of specimens, including smooth, notched and pitted, were fabricated from the straight central strand of the various tendon stock, according to the geometries in figures 4 and 5. Notched specimens included six different geometries; and pitted specimens represented four depth/width (L/d) combinations as detailed in table 3. Each of these was intended to define a unique geometrical irregularity and stress concentration, as might arise from either mechanical damage or localized corrosion (or both). It was intended that CERT testing of these different geometries would provide quantitative characterization of how tendon wire fracture properties transition from smooth specimen (figure 5) to notched specimen (figure 3) behavior. The former (smooth specimens) were prepared by circumferential grinding followed by longitudinal polishing through 600 grit SiC paper. Notched specimen types N1 through N4 were prepared using circular surface grinding and N5 and N6 by electrochemical machining. While the latter procedure (electrochemical machining) was considered the more appropriate of the two since it avoided any grinding induced, deformed surface layer (residual stresses), the more severe notch geometries (N1-N4) were better controlled

17

Table 1: Chemical composition of the four different lots of prestressing steel.

Steel 270D

Element	C	Mn	Si	Cr	Ni	Mo	S	P	Cu	Al	Fe
Weight(%)	0.85	0.78	0.2	0.02	0.03	0.01	0.02	0.02	0.07	0	Bal
	0.7	0.7	0.18	0.02	0.02	0.01	0.02	0.02	0.06	0	Bal

Steel 270F

Element	C	Mn	Si	Cr	Ni	Mo	S	P	Cu	Al	Fe
Weight(%)	0.79	0.68	0.15	0.24	0.04	0.01	0.04	0.02	0.11	0.01	Bal
	0.85	0.65	0.16	0.24	0.05	0.01	0.03	0.02	0.11	0	Bal

Steel 270F'

Element	C	Mn	Si	Cr	Ni	Mo	S	P	Cu	Al	Fe
Weight(%)	1.05	0.63	0.16	0.24	0.05	0.01	0.03	0.02	0.11	0	Bal
	0.81	0.65	0.18	0.24	0.05	0.01	0.03	0.02	0.11	0	Bal

Steel 250D

Element	C	Mn	Si	Cr	Ni	Mo	S	P	Cu	Al	Fe
Weight(%)	0.85	0.74	0.22	0.02	0.03	0.01	0.02	0.02	0.09	0	Bal
	0.86	0.69	0.22	0.02	0.03	0.01	0.02	0.02	0.09	0	Bal

18

Table 2: Mechanical properties of the four steels.

Steel	Hardness, Rockwell C	Young's Mod., GPa	Breaking Load, kN	Nominal Area, mm2	UTS*, MPa	Elongation, percent
270D	51	199	196	98.7	1985	5.21
270F	52	194	191	98.7	1935	5.6
270F'	52	196	190	98.7	1925	5.2
250D	54	199	177	92.9	1905	5.31

*Ultimate tensile stress.

19

smooth
specimen

pitted
specimen

4.28

203

20

2.03

radius =20

L

D

d

d

L

All units in mm

P1: d=1
L=1.3
D=2.54

P3: d=0.5
L=0.45
D=2.03

P2: d=0.5
L=0.8
D=2.54

P4: d=0.35
L=0.2
D=2.03
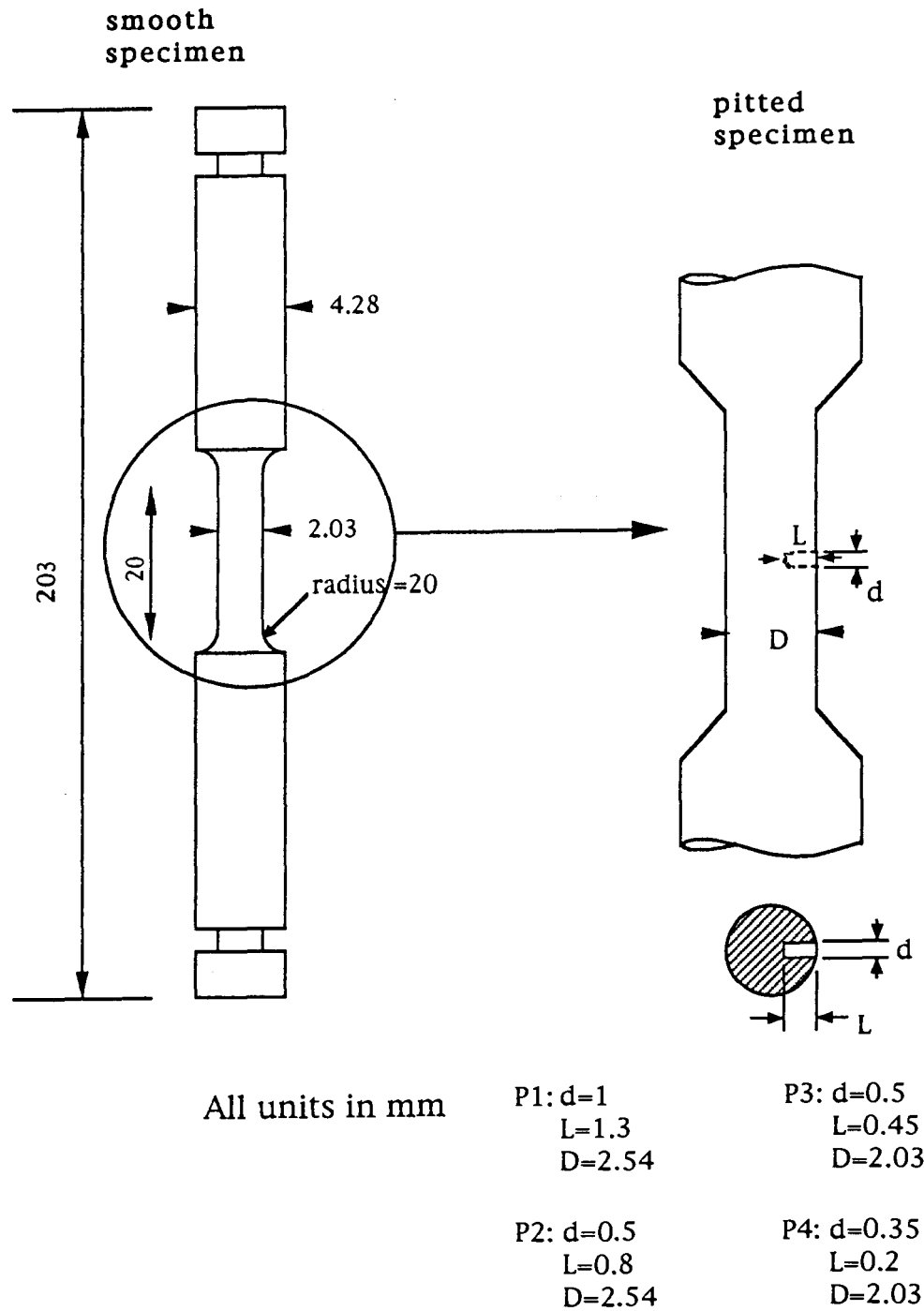
Figure 4: Geometry of smooth and pitted prestressing steel CERT specimens.

N1:	D=4.31	N3:	D=4.31
	d(N)=1.15		d(N)$_1$=2.54
	r=1.2		d(N)$_2$=1.52
			r=0.76
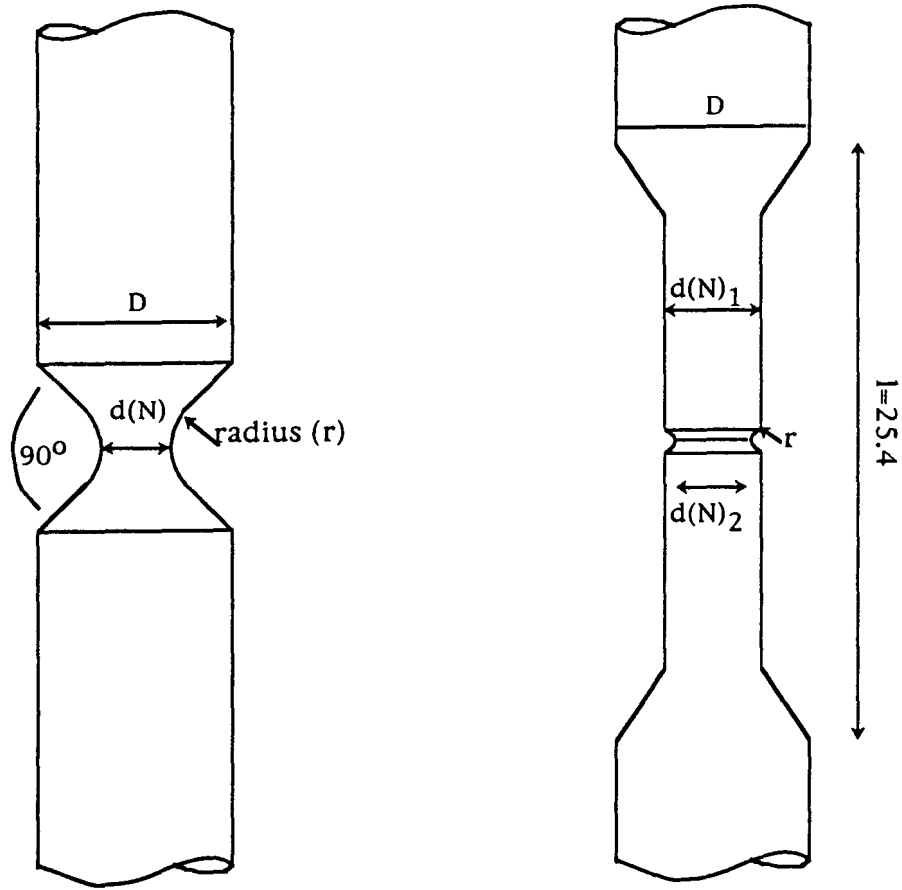
N5: D=4.31
d(N)$_1$=2.03
d(N)$_2$=1.88
r=0.30

N2: D=4.31
d(N)=1.65
r=1.2

N4: D=4.31
d(N)$_1$=2.54
d(N)$_2$=2.03
r=0.76

N6: D=4.31
d(N)$_1$=2.03
d(N)$_2$=1.94
r=0.72

all dimensions in mm

Figure 5: Geometry of notched prestressing steel CERT specimens.

Table 3: Dimension parameters of pits in CERT specimens.

PIT TYPE	PIT DEPTH (L), mm	PIT DIA (d), mm	DEPTH TO DIA. RATIO (L/d)	AREA FRACTION*
P1	1.3	1.0	1.3	0.74
P2	0.8	0.5	1.6	0.92
P3	0.45	0.5	0.9	0.93
P4	0.2	0.35	1.75	0.98

* Ratio of cross section area (reduced) in the plane of
  the pit to the nominal (unreduced) area.

and maintained by the mechanical technique (grinding). The electrochemical procedure involved masking all but the circumferential notch surface area with polytetrafluoroethylene (PTFE) tape and anodic polarization in a saturated $Ca(OH)_2$ solution at 0.1 A for 30 (N5) and 60 (N6) seconds. Preparation of pitted specimens began with a smooth specimen with pit types P1 and P2 being produced by electrochemical machining according to the same procedure as for notched specimens, but here a pinhole of diameter less than 0.2 mm in the PTFE tape was employed rather than a circumferential band to expose bare metal. Mechanical machining was employed for pit types P3 and P4.

Test System: The experimental set-up was essentially the same as described previously and consisted of 1) a four station constant extension rate unit, 2) electrochemical cells and 3) a data acquisition system. (27) The CERT machine, which was patterned after that of Nutter et al., was operated at an extension rate of $4.7 \cdot 10^{-6}$ cm/s, as was judged appropriate from earlier experiments. (27,43) The electrochemical cells were fabricated from PTFE and utilized platinum coated niobium counter and saturated calomel reference electrodes. Potentiostats were locally fabricated according to the circuit diagram proposed by Baboian et al. (44) The electrolyte was a saturated $Ca(OH)_2$ -water solution which was deaerated by nitrogen purging. The data acquisition system consisted of an eight channel signal amplification unit and a personal computer with software that permitted load versus time to be recorded during testing and for data to be subsequently analyzed.

Test Procedure: Prior to testing, the prestressing steel specimens were degreased with acetone; and the surface area which was not reduced by grinding was covered using PTFE tape. The pH of the test electrolyte (saturated $Ca(OH)_2$) was measured both before and after testing and was found to be nominally 12.5 with little or no change occurring with time. Nitrogen purging commenced about 90 min prior to testing and continued during the experiments. Potentials of either -0.90 or -1.30 v (SCE) were employed for the tests in solution, where the former was considered to provide a minimal and the latter a severe condition with regard to the tendency for environmental cracking. As such, these two potentials correspond to the upper and lower plateau fracture stress responses, respectively, in figures 2 and 3.

PRESTRESSED CONCRETE BEAM SPECIMENS

General: Fifty concrete beam specimens 3 m long by 0.25 m wide by 100 to 130 mm thick pretensioned were fabricated at Curry Industries in Miami, Florida with the assistance of project personnel using two symmetrically positioned seven wire, nominally 11.11 mm diameter Grade 270 tendons. Each of the two tendons was preloaded to 5,240± 20 N (23,300± 100 lb). The tendons were electrically isolated from one another, and no other steel was present in the prestressing bed forms. After pouring and finishing, but prior to concrete setting, a 60 mm high by 0.20 m wide by 2.1 m long rectangular polycarbonate frame ponding bath was positioned symmetrically upon the top surface of each specimen. Figure 6 presents a schematic illustration of the specimen and bath. Concrete mix design parameters are listed in table 4. Specimens for the hydrogen embrittlement phase of the experiments were locally admixed with chloride by adding 26 grams of solid $CaCl_2$ grains to the concrete at defined,

23

Top view

2.1 m

3.0 m

Cross section

200 mm

Sea water pond

Tendon (2)

100 to
130 mm

76 mm

70 mm

250 mm
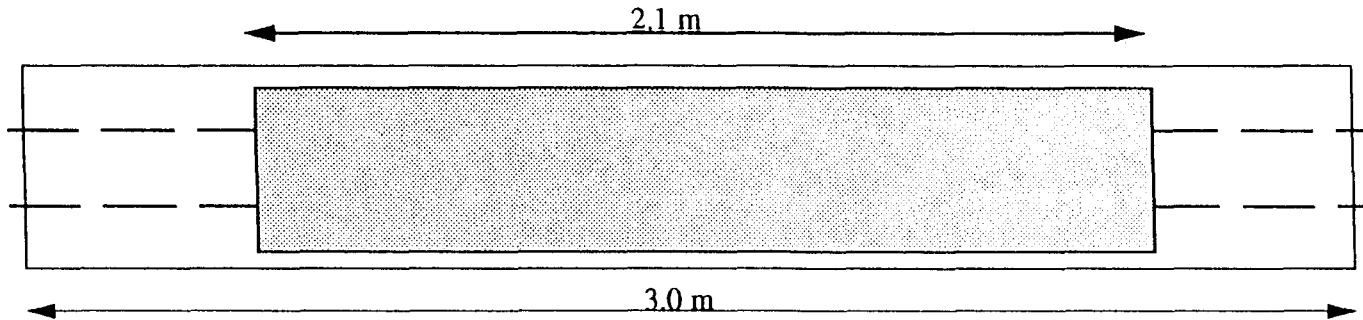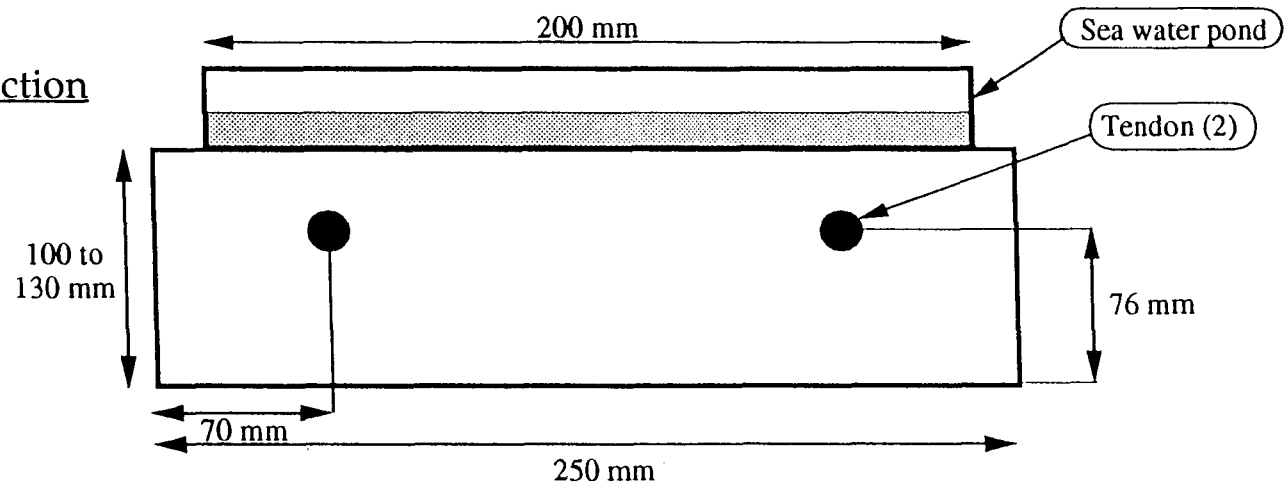
Figure 6: Schematic illustration of a prestressed concrete beam specimen and sea water electrolyte bath.

Table 4: Concrete mix design and concrete properties.

CEMENT (AASHTO M-85 Type I/II)	342.5 kg (755 lbs)
COARSE AGGREGATE (Grade 57 S. G. (SSO) 12.460) Crushed Limestone	771 kg (1700 lbs)
FINE AGGREGATE 2.86 S. G. (SSO)12.560 Limestone Screenings	463.6 kg (1022 lbs)
WATER REDUCING ADMIXTURE (WRDA 72/AASHTO M-194 Type D)	1.44 kg (3.2 lbs)
WATER	126.6 kg (279 lbs/33.5 gal)
SLUMP RANGE	0.0 to 8.9 cm (3.5 in)
AIR CONTENT	3 to 6 %
WATER CEMENT RATIO	0.37

60 to 90 mm wide positions along the beams in question during pouring. It was intended that a local Cl⁻ concentration of about 13 kg/m^3 would result from this.

Two types of strain gauges, which were obtained from TML, Texas Measurements, Inc., were incorporated into the pretensioned beams. These were intended to provide a means for measuring any specimen shape change that might occur during the subsequent exposure in association with either tendon fracture from hydrogen embrittlement or tendon-to-concrete bond strength reduction or loss. One type of strain gauge (PMLS 10) was embedded directly in the wet concrete after consolidation and initial finishing at a position approximately 5 mm below the top surface and either directly above one or midway between the two tendons. The second type of gauge (FLA 3) was bonded directly upon the tendon within polyvinylchloride (PVC) wells that were mounted about the steel and extended through the concrete cover to above the top surface of the specimen. Figure 7 schematically illustrates a PVC well in relation to a tendon and tendon mounted strain gauge. The purpose of these gauges was to, first, provide a measure of any tendon strain without interference from concrete which would otherwise contact and be bonded to the tendon mounted gauge and, second, provide access to gauges so that these could be replaced if necessary. Each tendon in the specimens was designated as either "N" or "S", depending upon its position in the pouring bed. Similarly, the location of all gauges (embedded and tendon mounted) was recorded relative to the nearest end of the surface mounted pond. Figure 8 presents a schematic illustration of a specimen and shows the location designation convention that was adapted for both of these gauge types, as well as for gauges that were subsequently mounted upon the external concrete surface as explained subsequently, and the locations of the zones of locally admixed CaCl$_2$ (see above). The procedure for mounting of tendon gauges employed an instant glue provided by the gauge manufacturer, and application was generally in accord with the specified procedure.

Three days after pouring the beams were removed from the bed, transported to the FAU Marine Corrosion Laboratory and arranged indoors in a stacked configuration as shown by the photograph in figure 9. A PVC piping system was installed which permitted natural sea water to circulate through the ponds.

Strain gauge monitoring during exposure and cathodic polarization of both the hydrogen embrittlement beams, which is yet to commence, and the loss-of-bond ones utilizes a Measurement Group Model P3500 strain indicator and a compensated quarter bridge, where the dummy gauge in this circuit was of the same type and was mounted upon a sample of the same material, either steel or concrete, as was being monitored. Preliminary tests indicated that a procedure which involved zeroing the strain indicator using a dummy gauge in place of the active one prior to actual data acquisition gave acceptable long-term reproducibility for a given gauge. The experimental rationale considered that either tendon fracture or tendon-to-concrete bond reduction or loss should result in extension of the beam in the longitudinal direction. Because sea water exposure also gives rise to expansion of concrete, detection of beam extension by strain gauges mounted in or on the concrete does not, by itself, necessarily mean that fracture or bond reduction/loss has taken place. If, however, the tendon mounted gauges indicate a contraction at the same

Side view

PVC tube

Strain gauge wire

Sea water

Side of the sea water pond

Strand

Concrete

PVC block

CL

Top view

3.8 cm dia. PVC fitting
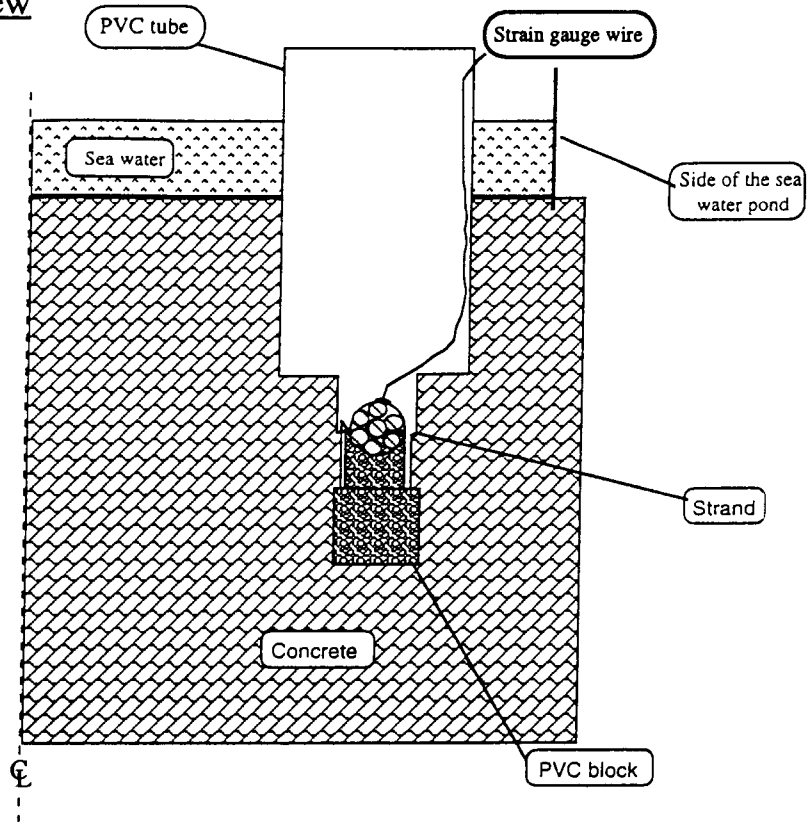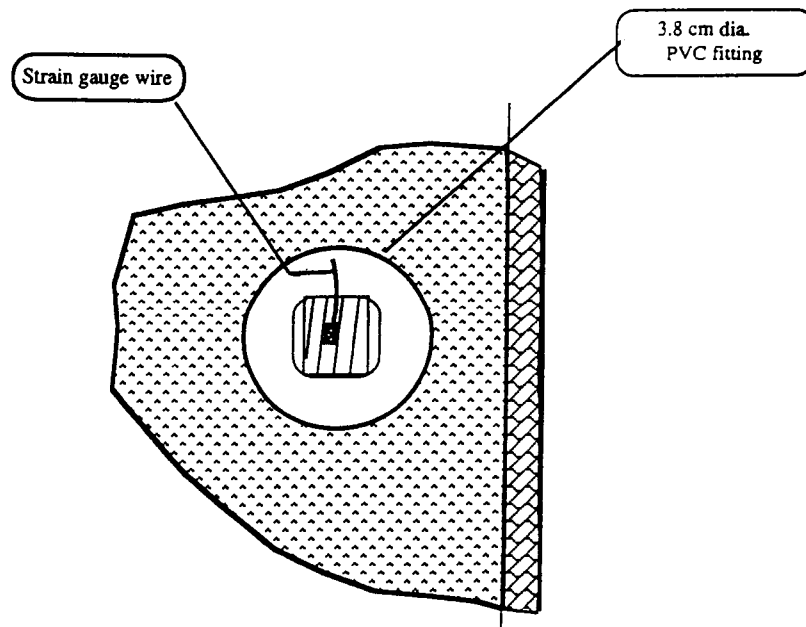
Strain gauge wire

Figure 7: Schematic illustration of PVC well, tendon and tendon mounted strain gauge.

Embedded gauge location designation:
[Beam designation], e/[Y coordinate], [X coordinate].
For example, B2cp2, e/m, E 30.5 cm is located on beam B2cp2,
in the middle of the pond, 30.5 cm from the center toward the
east.

The available gauge coordinates employed are:
for the X-axis: at the center (c) and 30.5 cm, 61 cm and 76.2 cm E or W of the center
for the Y-axis: above the tendon (N or S) and in the middle of the pond (m).

Y   North
      2' (61 cm)
      2.5' (76 cm)

West   East

                                                                    X
      1' (30 cm)
      South   e/m, E 1'

Top view

(a)
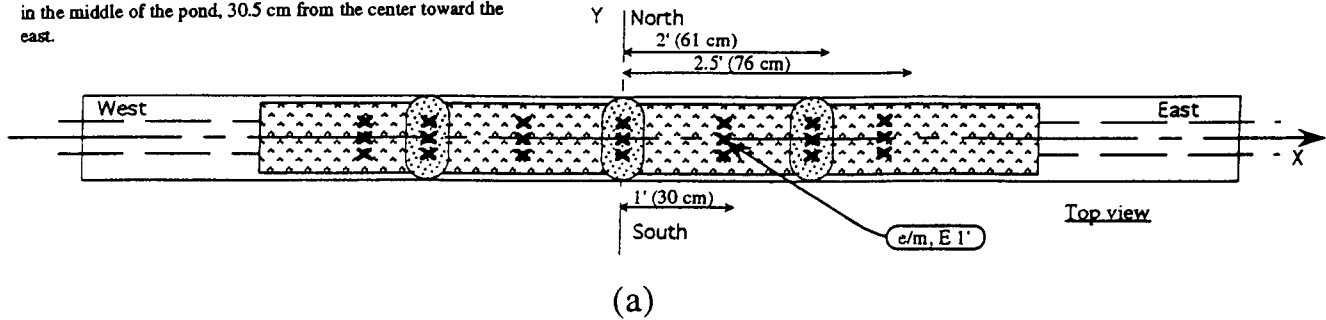
Tendon gauge location designation:
[Beam designation], t/[Y coordinate], [X coordinate].
For example, B2cp2, t/S, W 76.2 cm is located on beam B2cp2,
above the south tendon, 76.2 cm from the center toward the west.
The available gauge coordinates employed are:
for the X-axis: at the center (c) and 61 cm and 76.2 cm from the center
for the Y-axis: above the tendon (N or S).

Sea water ponding area
CaCl$_2$ admixture

Y   North
      2' (61 cm)
      2.5' (76 cm)

West   East

                                                                    X
      t/S, E 2.5'

Top view

South

(b)
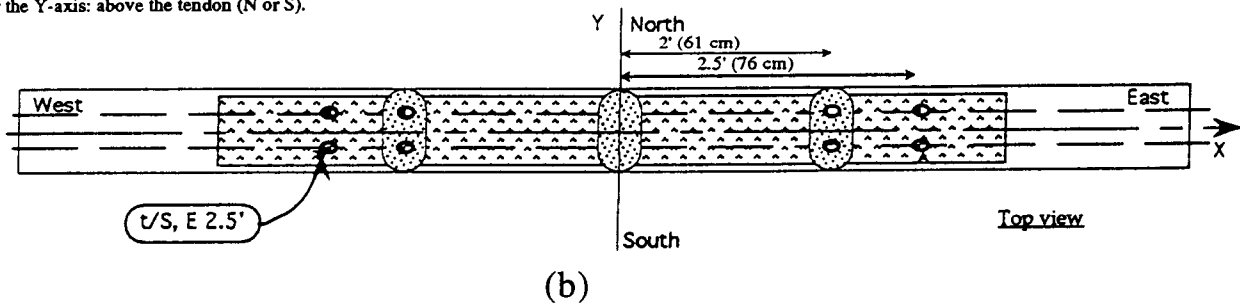
Surface gauge location designation:
for the gauges mounted on the underside of the beam:
u/[Y coordinate], [X coordinate],
for the gauges mounted on the side of the beam:
side, [X coordinate].
For example, u/S, E 76.2 cm is located below the south tendon
and 76.2 cm from the center toward the east.

The available gauge coordinates employed are:
for the X-axis: at the center (c) and East 76.2 cm
for the Y-axis: below the tendon (N or S).

Y   North
      2.5' (76 cm)   Bottom view

West   East

                                                                    X
      side, C   South   u/S, E 2.5'

(c)

Figure 8:   Schematic illustration of prestressed concrete beam specimen showing
             nomenclature for designating the location of (a) embedded strain gauges,
             (b) tendon mounted strain gauges and (c) surface mounted strain gauges.

28

Figure 9:   Photograph of prestressed concrete beam in position in the laboratory.

time the concrete is expanding, then this should be indicative of either tendon fracture or bond reduction/loss. In the case of concrete swelling from the sea water exposure, both the concrete and tendon gauges should indicate an expansion. Figure 10 illustrates schematically the response of both tendon mounted and concrete embedded strain gauges to both 1) concrete swelling in association with water absorption into the concrete and 2) a bond reduction or loss event. Where concrete expansion is accompanied by tendon contraction, post-test destruction may be required to discern if tendon fracture or bond reduction/loss was responsible.

Despite the fact that the procedure for strain gauge application upon the tendons was qualified based upon several months monitoring of sea water ponded but unpolarized prototype specimens, these gauges failed during the course of the experiments, as did the embedded gauges. Consequently, gauges designated as PL 60, which were obtained from the same manufacturer, were mounted upon a dry concrete specimen face, either directly to the side of or beneath one of the tendons, and were intended to provide the same function as the defunct embedded gauges. The same location designation nomenclature was employed for gagues mounted on the concrete surface as for the other gauge types (figure 8) except the "S" refers here to a side mounted gauge and "U" to a bottom (underside) mounted gauge. Replacement of failed tendon mounted gauges involved attachment of a new gauge of the same type at the same location on the steel. Several alternative glues and protective coatings have been employed, and an acceptable procedure seems to have now been defined. Unfortunately, it was necessary to develop this improved gauge attachment procedure while the experiments were ongoing; and, consequently, the tests experienced successive interruptions during the time that this was accomplished.

Hydrogen Embrittlement Experiments. The hydrogen embrittlement beam type experiments involve 23 specimens which are presently undergoing a one week wet - one week dry sea water ponding cycle. Table 5 lists the test matrix for these and indicates that it is intended that five di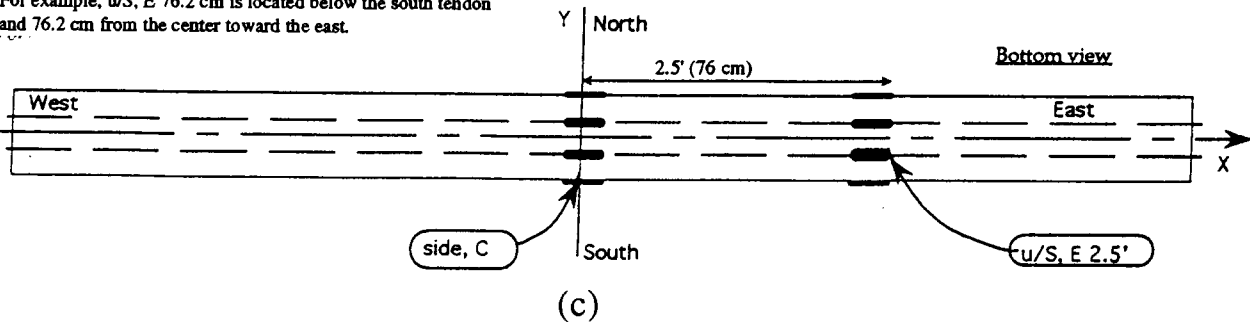fferent degrees of corrosion, which are intended to range from slight to severe, are to be developed for the prestressed tendon therein. While the table 5 matrix indicates that a total of 13 specimens are to be employed for these experiments, 23 are being exposed so to permit additional repetition where this might be deemed necessary. The more severe corrosion states are to occur either naturally at the locations of $CaCl_2$ admixing in association with the wet-dry cycling or by localized anodic polarization of tendons in these same zones. To-date potential measurements have been made routinely upon both tendons of each beam supplemented by a limited number of polarization resistance determinations. The former employed a saturated calomel reference electrode in conjunction with a moist sponge for measurements performed during the dry periods of the wet-dry cycle and simple immersion of the electrode tip in the sea water pond during the wet. The polarization resistance measurements utilized 3LP instrumentation manufactured by Kenneth C. Clear, Inc. Subsequently, it is intended that specimens be polarized to either -0.90 or -1.30 v (SCE) and monitored for any hydrogen induced tendon fracture. The more positive of these two potentials (-0.90 v) should be representative of cathodic protection within the acceptable range (upper plateau behavior in figure 3) and the more negative (-1.30 v) of extreme overprotection (lower plateau behavior). It is intended that the different degrees of corrosion (listed as 1-5

30
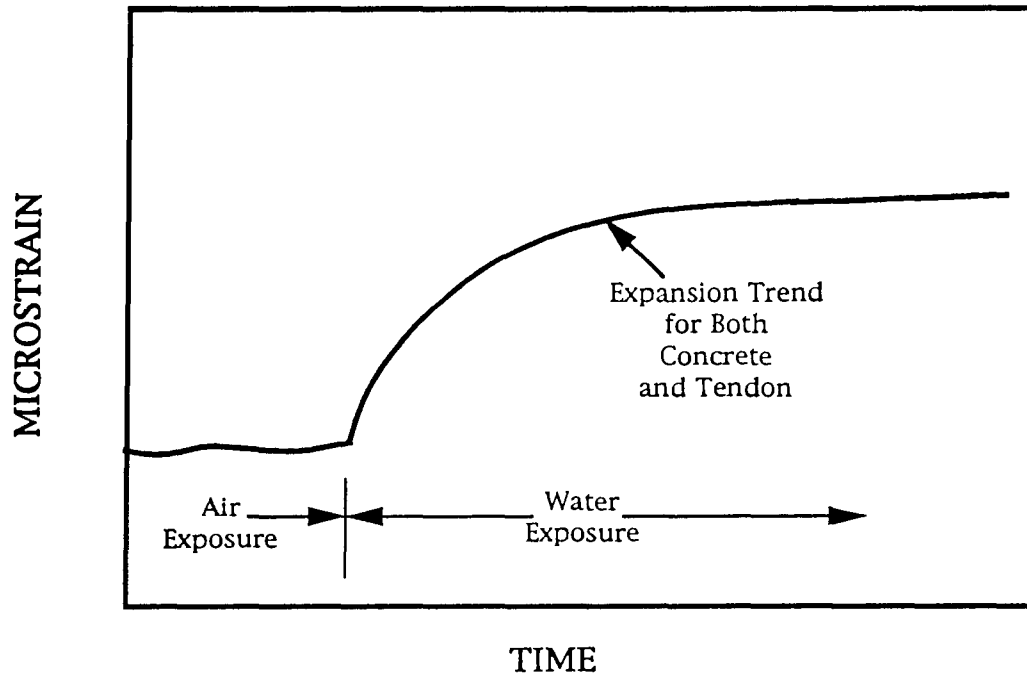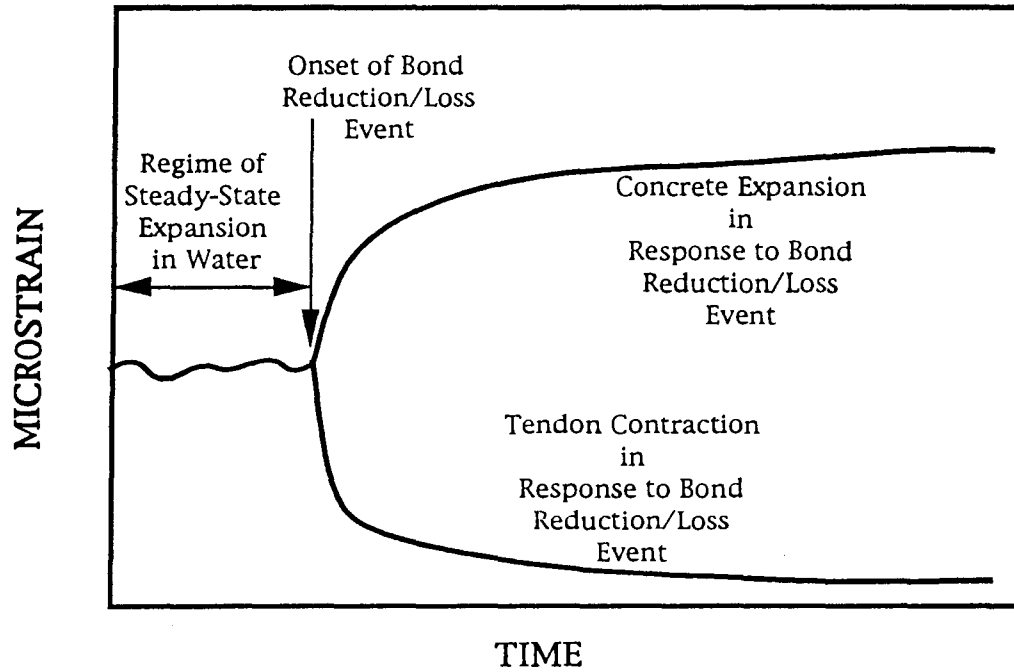
Figure 10: Schematic illustration of anticipated embedded and tendon mounted strain gauge response to a) wet exposure and b) hydrogen embrittlement induced tendon fracture or a bond reduction or loss event.

31

Table 5: Listing of test conditions for hydrogen embrittlement experiments upon cathodically polarized prestressed concrete beams.

CORROSION STATE*	POTENTIAL, v. (SCE)	
	-0.90	-1.30
1	-	1
2	1	2
3	1	2
4	1	2
5	1	2

Note: Number in each column under "potential" indicates the number of specimens for that particular test condition.

* Designates five levels of corrosion damage increasing in severity from 1 to 5.

32

in table 5) range from slight to severe, where the latter would involve occurrence of notch-like pitting corrosion upon the tendons.

Bond Strength Experiments: Fifteen prestressed concrete beam specimens are being employed in order to characterize and quantify any tendon relaxation brought about by cathodic polarization induced bond strength reduction or loss. The experimental plan involves polarization of eight of these (designated B2cp1 through B2cp8) according to a defined cathodic current density, as listed in table 6. Of the other seven specimens, one is being maintained in air and six with sea water ponding without polarization for comparison purposes. The experiment methodology involves monitoring of both tendon mounted and concrete embedded strain gauges as a function of time in order to disclose any change in length of the tendon and expansion/contraction of the concrete (see figure 10).

CONCRETE BLOCK (NO PRESTRESS) SPECIMENS

A second component of the loss-of-bond portion of the test program involved fabrication of 60 concrete block pull-out specimens 0.36 m by 0.20 m by 0.10 m, 30 with a 12.7-mm diameter seven-wire tendon and 30 with a straight central wire therefrom positioned symmetrically along the length direction. Figure 11 shows schematically the geometry of these two specimens types. In the case of specimens containing a tendon, a plastic sleeve encapsulated the steel to a depth of about 130 mm at what was to be the loaded end and 100 mm for the free end. Sleeves were not employed for the specimens which contained wire. Both type pull-out specimens were poured in plywood form molds using the same mix design as in table 4 and were moist cured outdoors under a plastic sheet. Table 7 presents the test matrix for these, and comparison with table 6 reveals that the current densities used here duplicated those for polarization of the beam specimens. The magnitude of applied current for the tendon compared to wire specimens was adjusted according to the embedded steel surface area such that current density was the same according to the values in table 7.

Specimens were placed within individual plastic baths which contained flowing natural sea water such that the lower 20 to 30 mm of the specimen were immersed. The desired polarization was affected by a DC power supply in conjunction with a parallel circuit which included balanced variable resistors and a strip of conductive rubber positioned at the bottom of each bath which served as an anode. (19) This setup probably results in higher current density upon the side of the tendon or wire that faced the anode than for the opposite side; however, such a situation is the same as for the polarized prestressed beams (see above) and also reflects what is likely to occur in service. Figure 12 shows a photograph of some of these specimens under this sea water exposure with cathodic polarization.

Once the requisite charge density transfer had accumulated for a particular specimen, it was removed from the sea water bath and positioned in a specially designed fixture mounted upon a MTS 100 metric ton (220 kips) universal testing machine. A photograph of the testing setup is shown in figure 13. The tendon or wire was gripped by a fixture attached to a load cell which, in turn, was mounted upon the hydraulic actuator. Adjustment bolts near the upper part of the specimen permitted vertica specimen

Table 6: Listing of prestressed beam specimens for bond loss determination.

BEAM NO.	TOTAL CURRENT, mA	CURRENT DENSITY, mA/m2 (concrete)	CURRENT DENSITY, mA/m2 (steel)	PLANNED TEST TIME, years	STATUS OF TEST
B2bas1	0 (laboratory air exposure)			4	ONGOING
B2bas2	0 (free corrosion in sea water)			4	ONGOING
B2bas3	0 (free corrosion in sea water)			4	ONGOING
B2bas4	0 (free corrosion in sea water)			4	ONGOING
B2bas5	0 (free corrosion in sea water)			4	ONGOING
B2bas6	0 (free corrosion in sea water)			4	ONGOING
B2bas7	0 (free corrosion in sea water)			4	ONGOING
B2cp1	10	21.5	50	4	ONGOING
B2cp2	10	21.5	50	4	ONGOING
B2cp3	10	21.5	50	4	ONGOING
B2cp4	100	215	500	1	ONGOING
B2cp5	100	215	500	1	ONGOING
B2cp6	100	215	500	1	ONGOING
B2cp7	1,000	2150	5,000	0.5	COMPLETED
B2cp8	500	1075	2,500	1	ONGOING

Note: For Specimen B2cp8 the initial 20 days of polarization (approximately 7 percent of the charge transfer) was at 1,000 mA.

34

100 mm

Concrete

Plastic sleeve
100 mm

355 mm

Block thickness
100 mm

Plastic sleeve
130 mm

200 mm

> 170 mm

Pull out block with central wire

Pull out block with complete tendon
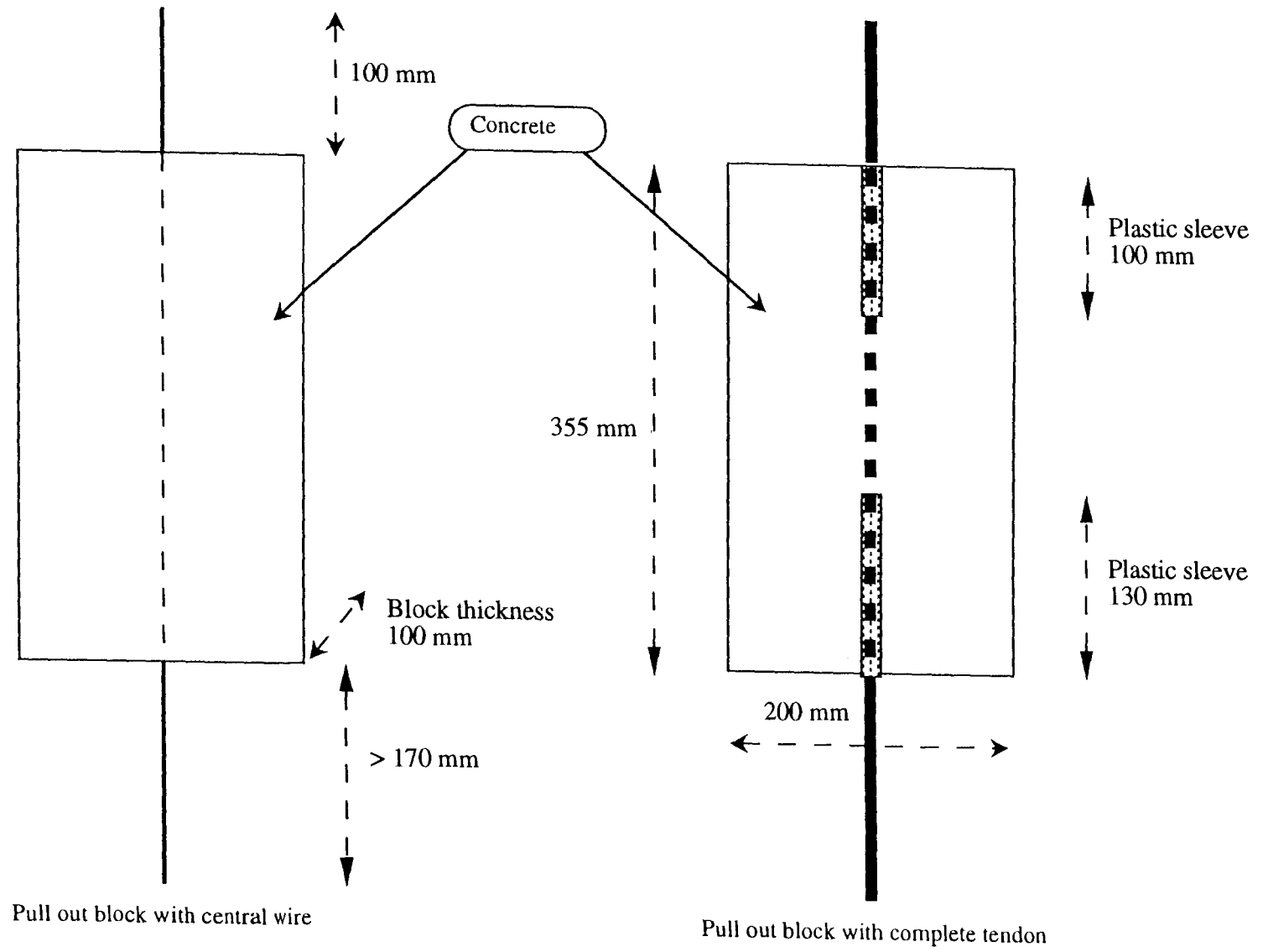
Figure 11: Schematic illustration of concrete block specimens for bond strength testing.

Table 7: Test parameters for concrete block pull-out specimens.

CATHODIC CURRENT DENSITY, mA/m2 of steel	CHARGE TRANSFER DENSITY, A-hr/m2 of steel	TIME OF POLARIZATION, days
50	1,400	1,169
500	14,000	1,169
500	7,000	589
500	4,400	368
500	1400	125
2500	14,000	232
2500	7,000	116
2500	4,400	72
2500	1,400	23

NOTE: Three specimens each of wire and tendon are to be tested
for each condition.
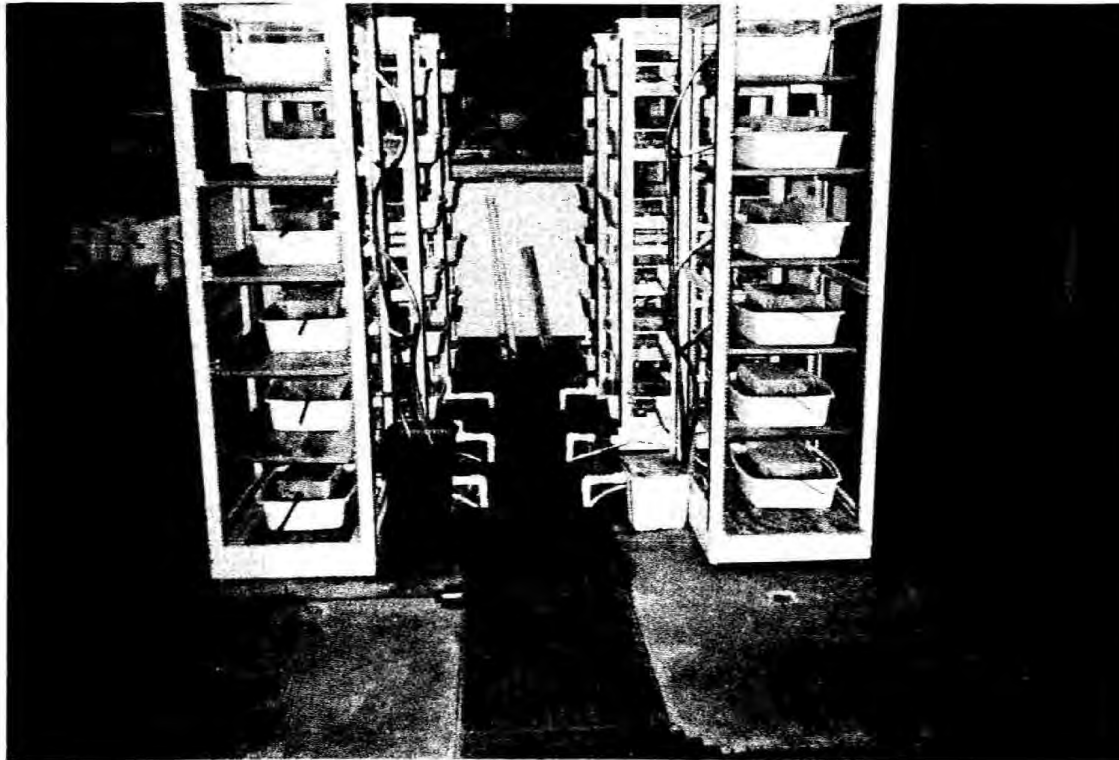
Figure 12: Photograph of concrete block pull-out specimens undergoing sea water exposure with cathodic polarization.

Free end L.V.D.T

Concrete Block

Loaded end L.V.D.T

38

Tendon anchor

Load cell

Actuator
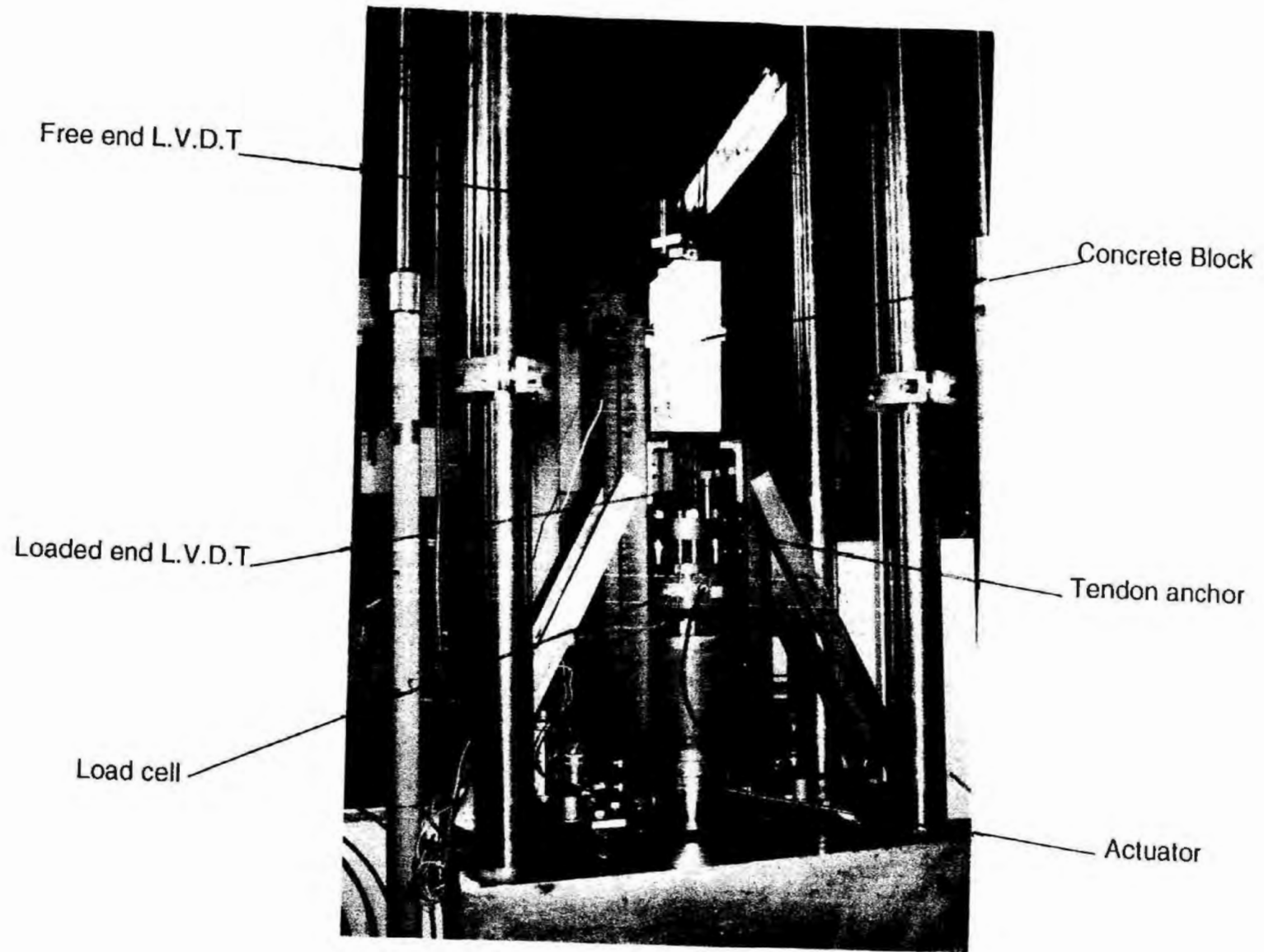
Figure 13: Photograph of the arrangement for tendon and wire pull-out tests.

alignment to be maintained during the test. A Trans-Tek, Inc. Series 240 LVDT was fixed to the tendon or wire at each of the two specimen ends with the sensing arm in each case contacting the respective concrete surface. The load was applied by moving the actuator down at a rate of 0.25 mm/min, and output from the load cell and from the two LVDTs was recorded as a function of displacement using a Measurement Group System 7000 data acquisition system. From this information the ultimate bond strength and the bond stress at 0.25 and 0.025 mm (see discussion above) were calculated.

CHAPTER III: RESULTS AND DISCUSSION

TENDON MATERIAL

Tendon for prestressed concrete construction consists of a center wire with six helically placed outer wires with overall nominal diameter ranging from 6.35 to 15.24 mm. (8) Two grades (250 and 270) are specified, where the number designates ultimate strength in ksi units (1725 and 1860 MPa, respectively). It is reasoned that, because brittle fracture tendency and susceptibility to environmentally assisted cracking normally vary inversely with steel strength, tendon fabricated from Grade 250 prestressing steel should be more resistant to such failure modes than that made from Grade 270. If this is the case, then it may be reasoned that the cathodic protection system for a prestressed component or structure which has been fabricated with Grade 250 tendon might be designed, constructed and operated in a less critical manner with regard to the likelihood of excessive cathodic polarization than would be the case with Grade 270. Accordingly, corrosion control costs should be reduced proportionally.

Table 2 listed the mechanical properties for the four wire materials, including both the Grade 250 and Grade 270 stock. These data indicate that there was no significant difference between the two grades and that the Grade 250 steel, in fact, met the Grade 270 specification. (8) From subsequent discussions with producers it became apparent that Grade 270 is routinely substituted for Grade 250 depending upon availability because the former invariably meets the specification for the latter. This follows since the specification lists a minimum strength but not a maximum. Thus, in order for a structure for which Grade 250 prestressing steel was specified to be qualified as being of relatively low cp induced embrittlement susceptibility, it is necessary that sampling and testing be performed to confirm that such material is actually in place throughout. Because this is likely to be an impractical task, this approach to corrosion control which considers that tendon embrittlement might be less significant for the lower strength steel than for high has been judged not feasible and has not been pursued further.

HYDROGEN EMBRITTLEMENT

Smooth Constant Extension Rate Testing Specimens

Values for various mechanical parameters, as determined by the CERT (constant extension rate testing) tests, are presented for each smooth specimen and test condition (air and $Ca(OH)_2$ solution with polarization to -0.90 v and to -1.30 v) in table 8a-c. The representation of ductility shown here is based upon the premise that the plastic elongation that transpired between the yield and ultimate stresses occurred uniformly along the specimen cross section and that between the ultimate and final fracture stresses the plastic deformation involved localized necking. (45) Figure 14 illustrates this schematically, where the former is designated as PEBN (plastic elongation before necking) and the latter as PEAN (plastic elongation after necking). Reduction-in-area data (ratio of the reduced specimen cross section area at the fracture location divided by the original area and expressed as a percent (designated RA)) for each specimen are also shown, and a general correlation between PEAN and RA is apparent. This latter observation is consistent with

Table 8: CERT results from smooth specimens of each of the four steels tested in
(a) in air, (b) in deaerated, saturated Ca(OH)2-distilled water while
polarized to -0.90 v (SCE) and (c) in deaerated, saturated Ca(OH)2-distilled
water while polarized to -1.30 v (SCE).

STEEL	Yield Stress, MPa	Max. Stress, MPa	Stress at Failure, MPa	PEBN, mm	PEAN, mm	Reduction in Area, %
270D	1809	2050	1736	0.83	0.23	28
	1663	1998	1677	0.7	0.25	--
	1813	2021	1731	0.63	0.22	--
	1785	2243	2047	0.93	0.15	21
	1733	2059	1728	0.81	0.19	26
	1734	2043	1719	0.99	0.22	32
Average	*1756*	*2069*	*1773*	*0.815*	*0.21*	*27*
250D	1786	2061	1553	0.92	0.32	36
	1723	2050	1670	0.82	0.31	37
	1720	1994	1511	0.84	0.33	--
Average	*1743*	*2034*	*1578*	*0.86*	*0.32*	*37*
270F	1717	2048	1565	0.8	0.29	--
	1698	2002	1558	0.79	0.31	33
	1700	2015	1559	0.75	0.26	33
Average	*1705*	*2022*	*1561*	*0.78*	*0.28*	*33*
270F'	1662	1979	1607	0.76	0.24	33
	1698	1995	1607	0.7	0.26	32
	1660	2004	1548	0.78	0.29	31
Average	*1673*	*1993*	*1587*	*0.75*	*0.26*	*32*

(a)

42

Table 8: CERT results from smooth specimens of each of the four steels tested in
(a) in air, (b) in deaerated, saturated Ca(OH)2-distilled water while
polarized to -0.90 v (SCE) and (c) in deaerated, saturated Ca(OH)2-distilled
water while polarized to -1.30 v (SCE) (continued).

STEEL	Yield Stress, MPa	Max. Stress, MPa	Stress at Failure, MPa	PEBN, m m	PEAN, m m	Reduction in Area, %
270D	1703	1938	1643	0.7	0.23	22
	1704	1955	1681	0.7	0.2	20
	1738	1977	1686	0.74	0.19	19
Average	*1715*	*1957*	*1670*	*0.71*	*0.21*	*20*
250D	1709	2074	1571	0.74	0.32	34
	1711	2076	1601	0.71	0.31	34
	1700	2079	1600	0.6	0.31	35
Average	*1707*	*2077*	*1591*	*0.68*	*0.31*	*34*
270F	1340	1514	1326	0.38	0.26	19
	1631	1973	1690	0.55	0.25	18
	1432	1601	1365	0.41	0.26	--
	1386	1515	1310	0.35	0.26	--
	1358	1526	1338	0.34	0.25	20
Average	*1429*	*1620*	*1405*	*0.4*	*0.25*	*19*
270F'	1471	1546	1353	0.4	0.16	16
	1367	1500	1280	0.4	0.27	20
	1744	2094	1643	0.76	0.26	20
Average	*1527*	*1713*	*1425*	*0.52*	*0.23*	*19*

(b)

Table 8: CERT results from smooth specimens of each of the four steels tested in
(a) in air, (b) in deaerated, saturated Ca(OH)2-distilled water while
polarized to -0.90 v (SCE) and (c) in deaerated, saturated Ca(OH)2-distilled
water while polarized to -1.30 v (SCE) (continued).

| STEEL	Yield Stress, MPa	Max. Stress, MPa	Stress at Failure, MPa	PEBN, m m	PEAN, m m	Reduction in Area, %
270D	1406	1612	1612	0.28	0	less
	1609	1956	1956	0.38	0	than
	1738	1997	1997	0.39	0	4%
Average	*1584*	*1855*	*1855*	*0.35*	*0*	
250D	1260	1386	1355	0.28	0.01	less
	1469	1663	1649	0.36	0.01	than
	1606	1852	1852	0.42	0	4%
Average	*1445*	*1634*	*1619*	*0.35*	*0.01*	
270F	1326	1460	1460	0.34	0	less
	1588	1905	1905	0.53	0	than
	1546	1717	1717	0.33	0	4%
	1744	1980	1980	0.55	0	
	1366	1532	1532	0.32	0	
Average	*1514*	*1720*	*1720*	*0.41*	*0*	
270F'	1375	1574	1574	0.35	0	less
	1675	1981	1981	0.48	0	than
	1699	1884	1884	0.3	0	4%
Average	*1583*	*1813*	*1813*	*0.38*	*0*	

(c)

44
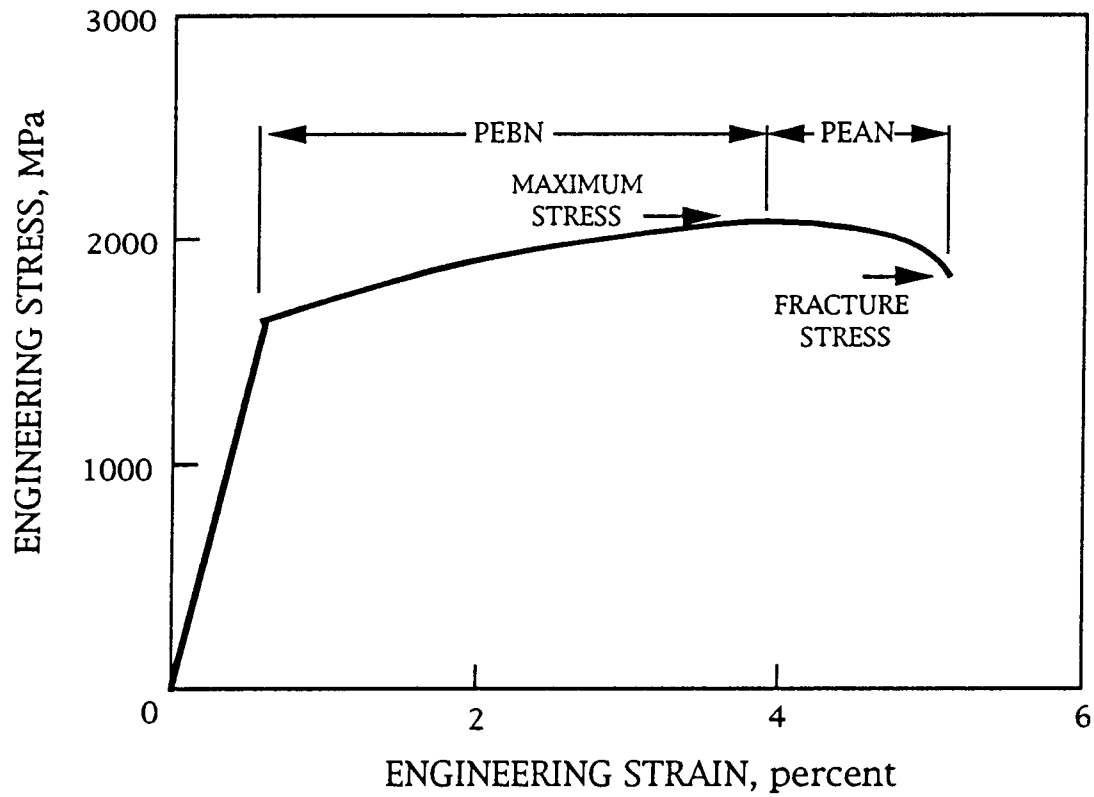
Figure 14: Schematic illustration of CERT stress-strain curve
and the relative regimes of Plastic Elongation Before
Necking (PEBN) and Plastic Elongation After Necking
(PEAN).

the projection above that the deformation subsequent to the ultimate stress being reached involves predominantly localized necking. Figures 15 and 16 illustrate graphically the maximum stress and ductility results, respectively, as reported in the above table for each of the four steels and three exposure conditions.

Previous research has projected that hydrogen embrittlement is responsible for the observed decrease in strength and ductility at relatively negative potentials; however, at the pH of the present test solution (~12.45) the reversible potential for the hydrogen reaction is active to -0.90 v (SCE) and so an alternative mechanism (water induced lattice decohesion) has been cited as possibly important here (see discussion of this topic in the Introduction section of this report). Comparison of the data in figure 15 with that from figure 2 makes it apparent, however, that the magnitude of prestressing steel strength reduction as a consequence of polarization was greater for some of the present smooth specimens than previously reported in the literature. In this regard figure 17 represents the data in question relative to the trend line from figure 2 and shows an envelope encompassing the present results. Thus, for some specimens tested at -0.90 v the normalized maximum stress was near unity (indicative of little or no strength reduction), whereas for others the value for this parameter approached 0.7, the anticipated prestress for in-place tendon. This variability was for the most part material specific with all 270D and 250D specimens exhibiting a relatively high maximum stress at this potential (-0.90 v) but with 270F and 270F' showing low. Thus, for the "D" materials the maximum stress for all six tests at -0.90 v was in the range 1938 to 2079 MPa (281 to 301 ksi); but for the "F" two of the eight specimens exhibited a maximum stress near 2000 MPa (290 ksi) and the remaining six in the range 1500 to 1600 MPa (217 to 232 ksi). The fact that scatter for tests in air was modest by comparison (see table 8) suggests that the variations seen here under conditions of polarization were an inherent feature of the material behavior in the environment employed for testing.

Reference to table 1 indicates that elemental composition was nominally the same for all four steels with the exception of an order of magnitude higher chromium concentration for 270F and 270F' (0.24 w/o) compared to 270D and 250D (0.02 w/o). Presence of chromium at this higher level is consistent with the F and F' materials having been microalloyed, and apparently presence of this element in even this relatively small amount had a significant detrimental affect upon embrittlement susceptibility at -0.90 v. On the other hand, the scatter in the present data at -1.30 v does not appear to be material specific. However, the embrittlement susceptibility at -1.30 v, as reflected by a reduction in maximum stress, was more pronounced than suggested by the limited amount of earlier smooth specimen data (see figure 2). Statistical considerations, in conjunction with the relatively small material volume in the specimen test section, may have been responsible for the average maximum stress for the F and F' materials being greater at -1.30 v than for -0.90 v.

The finding from the present experiments that the maximum stress at -0.90 v for the microalloyed material approached 0.7 of the ultimate tensile stress in air indicates that appropriateness of this potential (-0.90 v) as a lower limit for cathodic protection of prestressing steel should be reevaluated. Additional experiments are required upon microalloyed tendon before an appropriate lower potential limit for this material can be defined. It may be

46
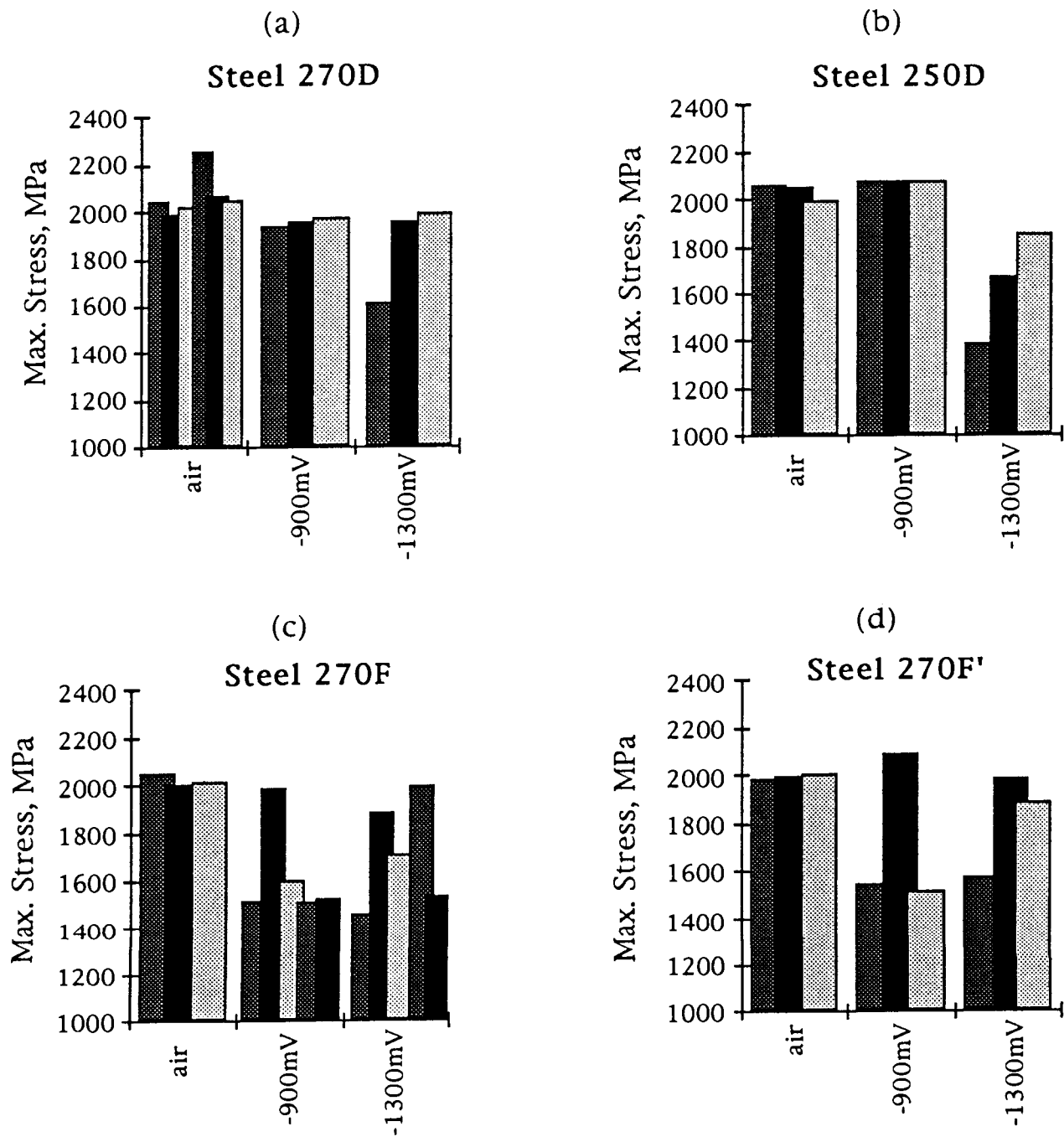
Figure 15: Ultimate tensile strength for individual CERT tests in air and deaerated saturated calcium hydroxide at -0.90 and -1.30 v (SCE) for (a) 270D, (b) 250D, (c) 270F and (d) 270F'.
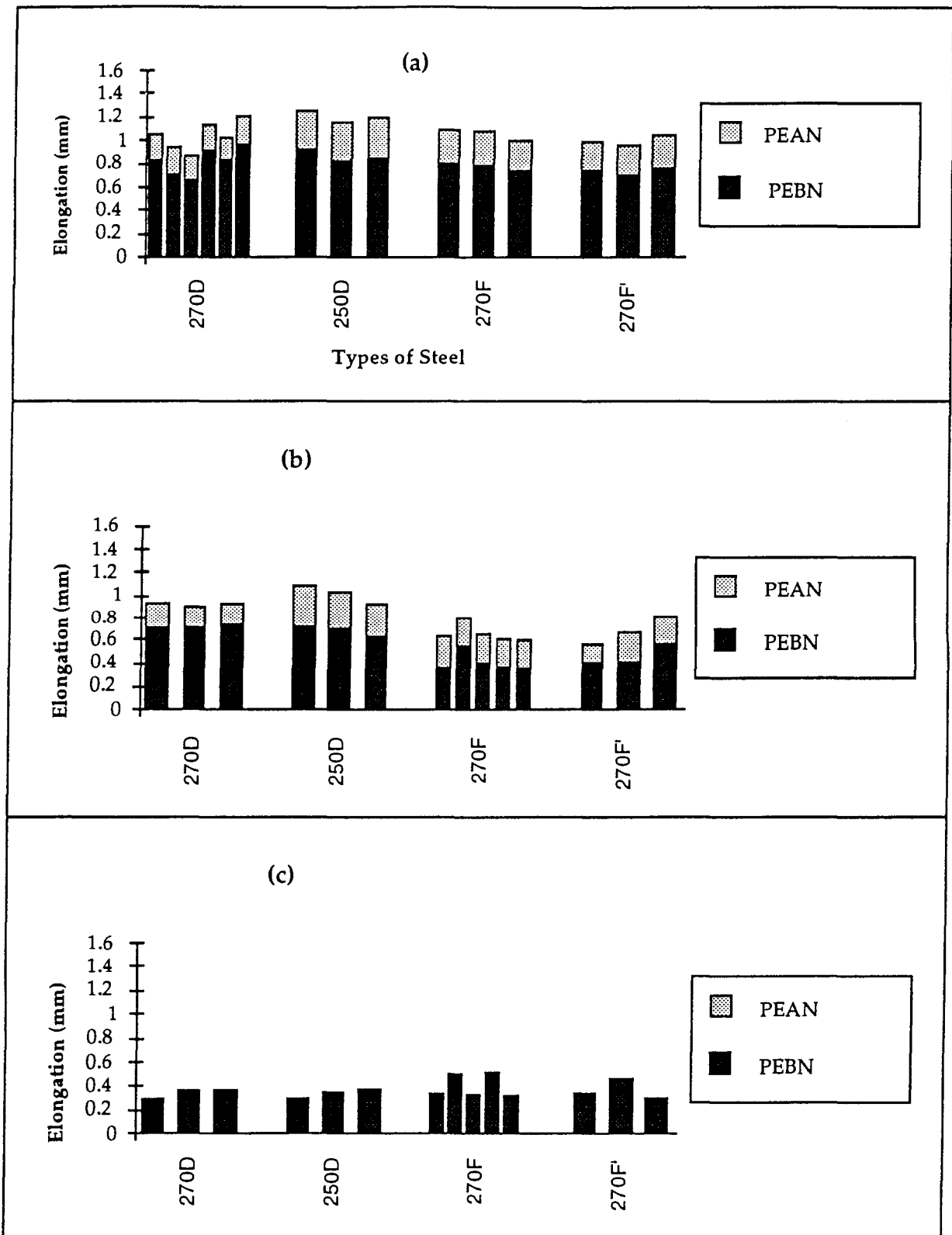
Figure 16: CERT elongation data from table 8 for each of the four steels in (a) air, and deaerated synthetic pore water (DSPW) at (b) -0.90 v and (c) -1.30 v (SCE).

48
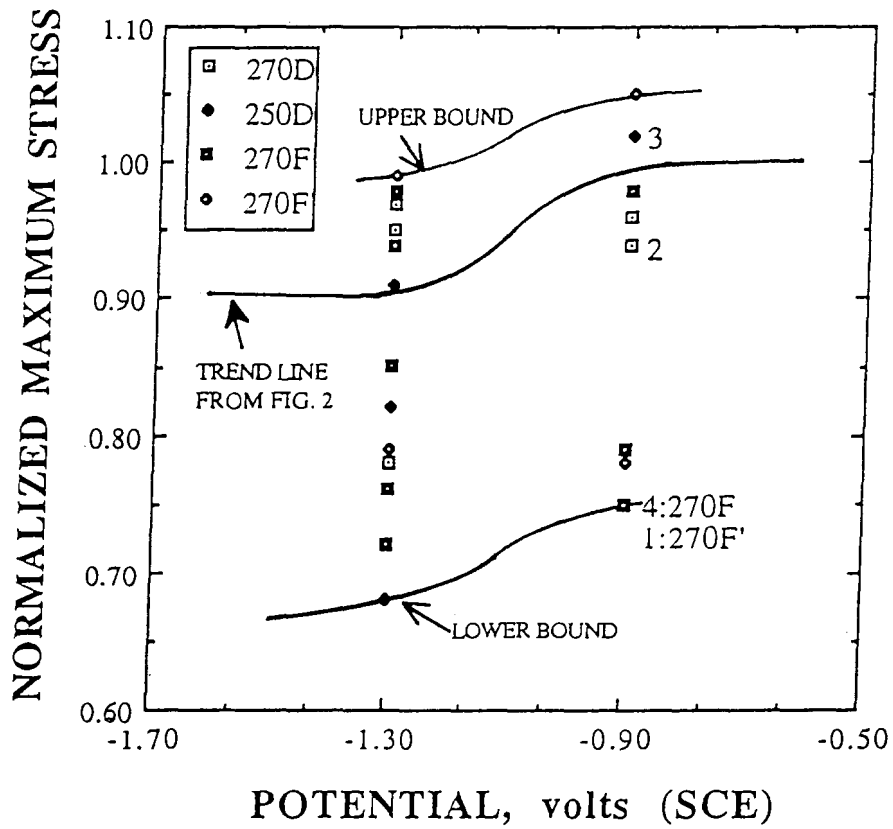
Figure 17: Normalized maximum stress results for smooth specimens polarized to -0.90 and -1.30 v (SCE). Both the trend line from figure 2a and upper and lower bound curves are illustrated.

impractical, however, at least for some applications, to specify a cathodic protection lower potential limit that is sufficiently positive to -0.90 v to preclude embrittlement of microalloyed prestressing steel which contains chromium in a concentration near the upper limit for this material (~0.24 percent). It is important also that a determination be made regarding how embrittlement varies with chromium concentration since the amount of this element in prestressing steel can range from 0.05 to 0.25 weight percent. In this regard the embrittlement question for chromium based microalloyed prestressing steel can be approached from the standpoint of either defining an appropriate lower potential threshold (more positive than -0.90 v as discussed above) or in terms of an upper chromium concentration limit to which the -0.90 v threshold value applies. It is concluded based upon present knowledge that prestressed structures and components utilizing high chromium microalloyed tendon should not be cathodically protected. Also. further experimentation is necessary to determine if microalloyed prestressing steel containing vanadium or vanadium plus chromium exhibits embrittlement at potentials positive to -0.90 v.

The specification for prestressing steel focuses upon minimum mechanical property values, stress relaxation treatment, dimensional tolerances, workmanship, finish and appearance with the choice of material composition being left to the producer. (8) With confirmation of the negative influence of chromium upon embrittlement tendency of cathodically polarized prestressing steel and definition of the requisite parameters whereby these and other microalloy composition can be cathodically protected, it may be appropriate that relevant standards be modified such that material composition is addressed.

The data in table 8a-c and figure 16 indicate that ductility of specimens decreased in proportion to the magnitude of polarization. Thus, comparison of the air (table 8a) and -0.90 v data (table 8b) indicates that the extent of uniform elongation prior to necking (PEBN) was from 13 to 49 percent less for the latter compared to the former. Figure 18 shows that this elongation at -0.90 v correlated generally with the maximum tensile stress in that a low value for one resulted in a low value for the other. This suggests that polarization to this potential (-0.90 v) caused for some specimens a premature onset of localized plastic deformation (necking) compared to testing in air such that a reduced value of maximum stress resulted. The relatively small specimen size coupled with statistical considerations regarding presence of some yet undefined compositional or microstructural feature which reduced the PEBN is thought to have been responsible. The resultant localized plasticity (necking) occurred to about the same extent as in air, as revealed from comparison of PEAN values for air and -0.90 v tests in table 8 and figure 16. At -1.30 v the reduction in PEBN was by from 47 to 59 percent of that in air. Figure 19 presents a maximum stress versus PEBN plot analogous to what was shown in figure 18 and indicates here also a relationship between these two parameters. In contrast to the situation at -0.90 v, however, the PEAN at -1.30 v was essentially nil (see table 8c and figure 16).

Figure 20 illustrates the range of CERT stress-strain behavior for each of the three test conditions (air and both -0.90v and -1.30 v in saturated Ca(OH)$_2$). Data scatter for tests in air was sufficiently modest that results for this environment are represented by a single curve. However, scatter

Figure 18: Normalized maximum stress as a function of plastic elongation before
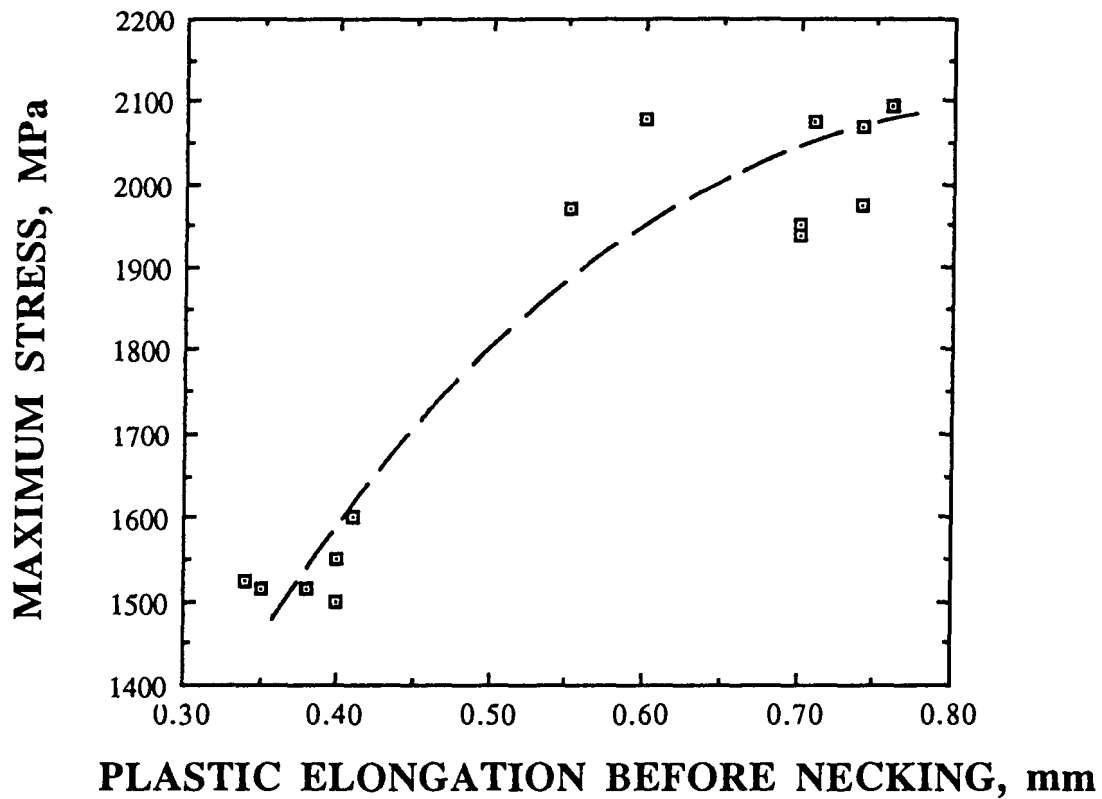necking (PEBN) for smooth specimens polarized to -0.90 v (SCE).
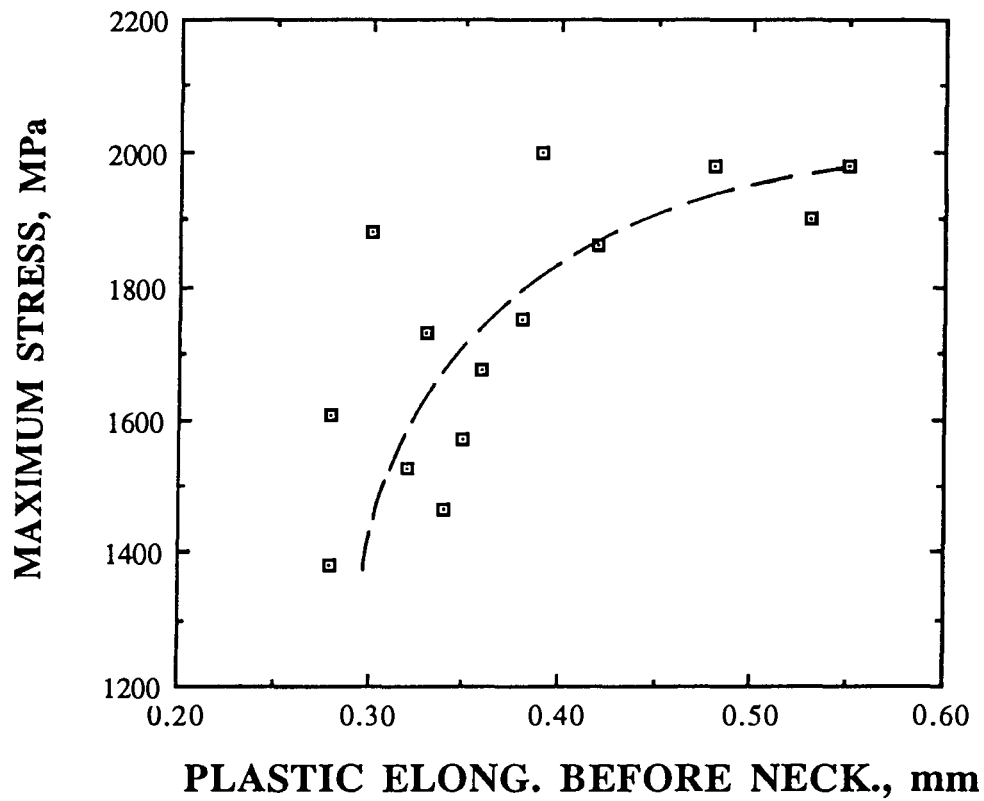
51

Figure 19:   Normalized maximum stress as a function of plastic
elongation before necking (PEBN) for smooth specimens
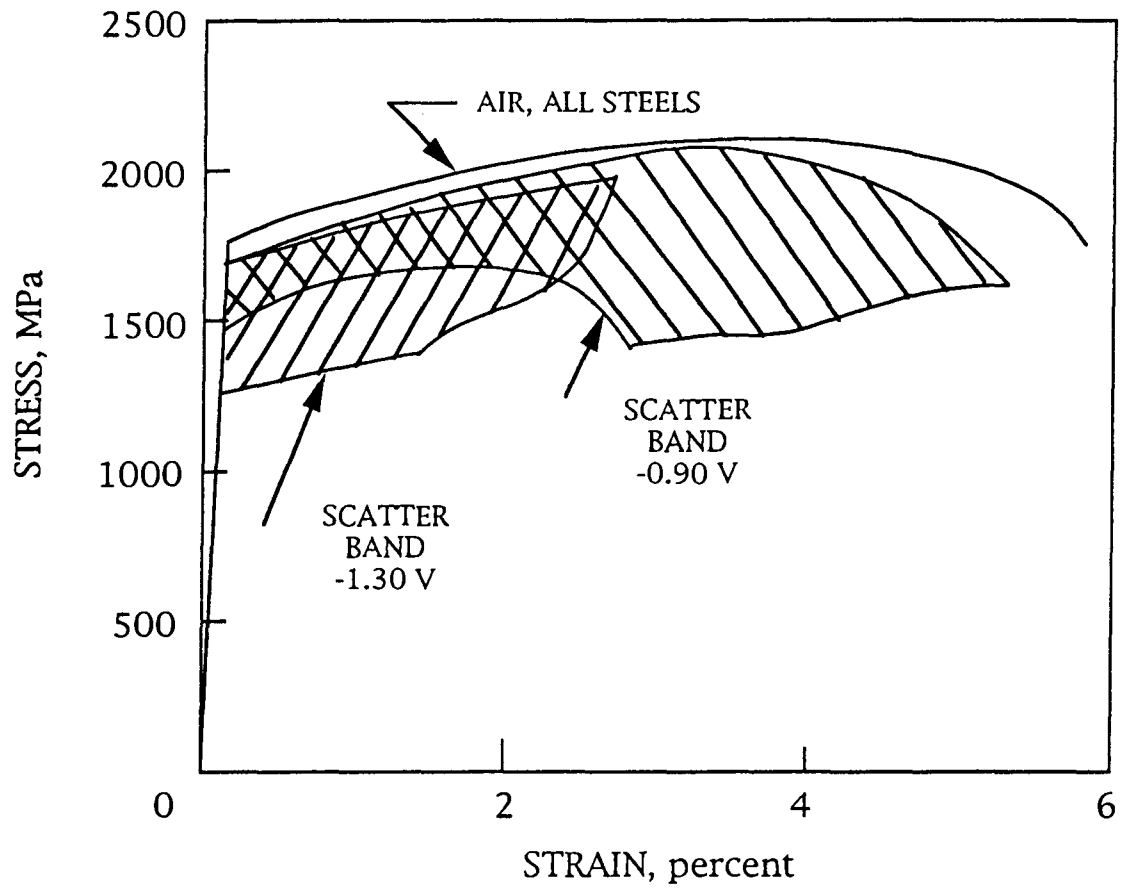polarized to -1.30 v (SCE).

Figure 20: Schematic illustration of the range of CERT stress-strain data for each of the four steels in the three test environments.

increased progressively with increasing cathodic polarization; and so results for -0.90 and -1.30 v are shown as a scatter band. Statistical effects in conjunction with the relatively small specimen size may have contributed to this scatter. Yield stress varied inversely with the magnitude of polarization. Water related lattice decohesion and not hydrogen is thought to have been responsible at -0.90 v, as discussed above; but hydrogen was probably also influential at -1.30 v. Irrespective of the responsible mechanism per se, yielding was facilitated by cathodic polarization, moreso at the more negative potential. On the other hand, analysis of the plastic portion of the stress-strain curves showed that the Holloman strain hardening coefficient, n, (slope of the true stress-strain curve in log-log coordinates), as defined by the expression:

$$\sigma = K\varepsilon^n, \qquad\qquad\qquad (5)$$

where σ and ε are true stress and strain, respectively, and K is a material constant defined as the true stress at a true strain of 1.0, was the same for the three test conditions. (46) This, in turn, indicates that work hardening properties of the steels were the same for each of the three test conditions (air and two levels of polarization). In general, specimens with a low yield stress also exhibited low ultimate stress and strain-to-fracture, suggesting that the same process which facilitated yielding also promoted embrittlement.

Notched Constant Extension Rate Testing Specimens

This specimen type was included in the experiments so that the fracture properties of prestressing steel could be characterized under conditions where a stress concentration was present. It was considered that the fracture behavior in the presence of a notch might, in turn, be indicative of tendon wire that has undergone localized pitting corrosion, as is often observed in service. All experiments in this category were limited to the 270D material. Table 9 presents air test results for notched specimens of the six different geometries (figure 5); and figure 21 plots average normalized maximum stress in air versus notch cross section, where the latter is expressed as a percentage of the smooth specimen area. This indicates that maximum stress was greatest for the N1 geometry, that maximum stress generally decreased as the specimen cross section increased and that this parameter merged with the smooth specimen data as the notch size approached zero (stress computed based upon the reduced cross sectional area).

Table 10 and figure 22 present companion data for specimens polarized to -1.30 v with the previous air data (figure 21) also shown for comparison. In this case the normalized maximum stress for the notched specimens was invariably less than for the smooth. The two curves (air and -1.30 v) exhibit a similar trend for the relatively severe N1-N4 geometries but differ for N5 and N6, the latter being necessitated since the two data sets must merge at the smooth specimen extreme.

Ductility of the notched specimens was less than for the smooth as noted by comparison of PEBN and PEAN data in tables 9 and 10 with values for these same parameters in table 8. This point is also illustrated schematically by figure 23 for both air (a) and -1.30 v (b) tests. For notch types N2 and N3 in air and N1-N4 at -1.30 v both PEBN and PEAN were nil, and fracture occurred in the elastic range.

54

Table 9: CERT results for notched 270D specimens tested in air. Smooth specimen data are included for comparison.

Specimen Geometry	A/Ao* (%)	Yield Stress, MPa	Max. Stress, MPa	Stress to Fail., MPa	PEBN, m m	PEAN, m m
N1	7.5	2560	2624	2624	0.03	0
	7.5	2621	2638	2621	0.015	0.015
	7.5	2621	2621	2592	0	0.01
N2	15	2390	2390	2390	0	0
	15	2328	2328	2328	0	0
	15	2722	2722	2722	0	0
N3	36	2405	2405	2405	0	0
	36	2398	2398	2398	0	0
N4	64	2060	2310	2310	0.12	0
	64	2285	2395	2395	0.04	0
N5	86	1810	2155	2155	0.25	0
		1865	2130	2130	0.32	0
N6	92	1790	2031	2001	0.3	0.038
		1957	2140	1911	0.37	0.118
Smooth	100	1750	2040	1700	0.8	0.2

* A/Ao is area of the notched versus smooth specimen cross section based upon the parameters d and D (figure 5).

55

Figure 21: Normalized maximum stress CERT results as a function of normalized specimen cross section area for each of the six notch geometry specimens and for smooth specimens of 270D tendon material tested in air.

Table 10: CERT results for notched specimens tested in deaerated, saturated Ca(OH)2-distilled water and polarized to -1.30 v. Smooth specimen data are included for comparison.

Specimen Geometry	A/Ao*, %	Yield Stress, MPa	Max. Stress, MPa	Stress to Fail., MPa	PEBN, mm	PEAN, mm
N1	7.5	1680	1680	1680	0	0
	7.5	1782	1782	1782	0	0
	7.5	1524	1524	1524	0	0
N2	15	1628	1628	1628	0	0
	15	1580	1580	1580	0	0
	15	1160	1160	1160	0	0
N3	36	1340	1340	1340	0	0
	36	1414	1414	1414	0	0
N4	64	1400	1400	1400	0	0
	64	1330	1330	1330	0	0
N5	86	1615	1740	1740	0.111	0
	86	1552	1647	1647	0.085	0
N6	92	1608	1804	1804	0.15	0
	92	1800	1848	1848	0.08	0
Smooth	100	1700	1850	1850	0.3	0

* A/Ao is area ratio of the notched versus smooth specimen cross section based upon the parameters d and D (figure 5).
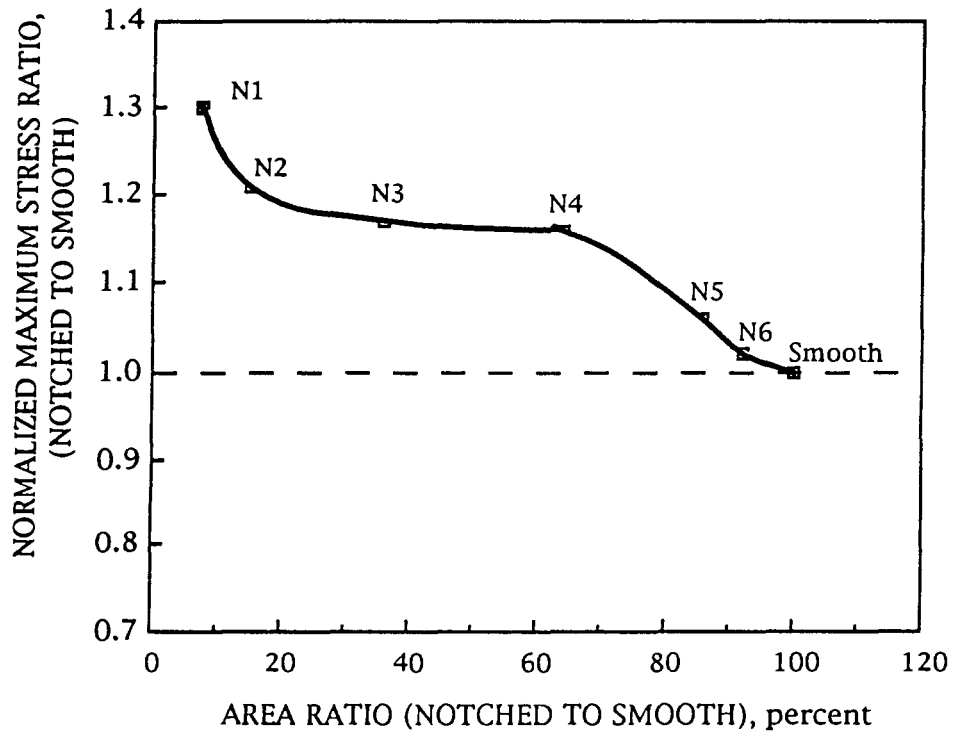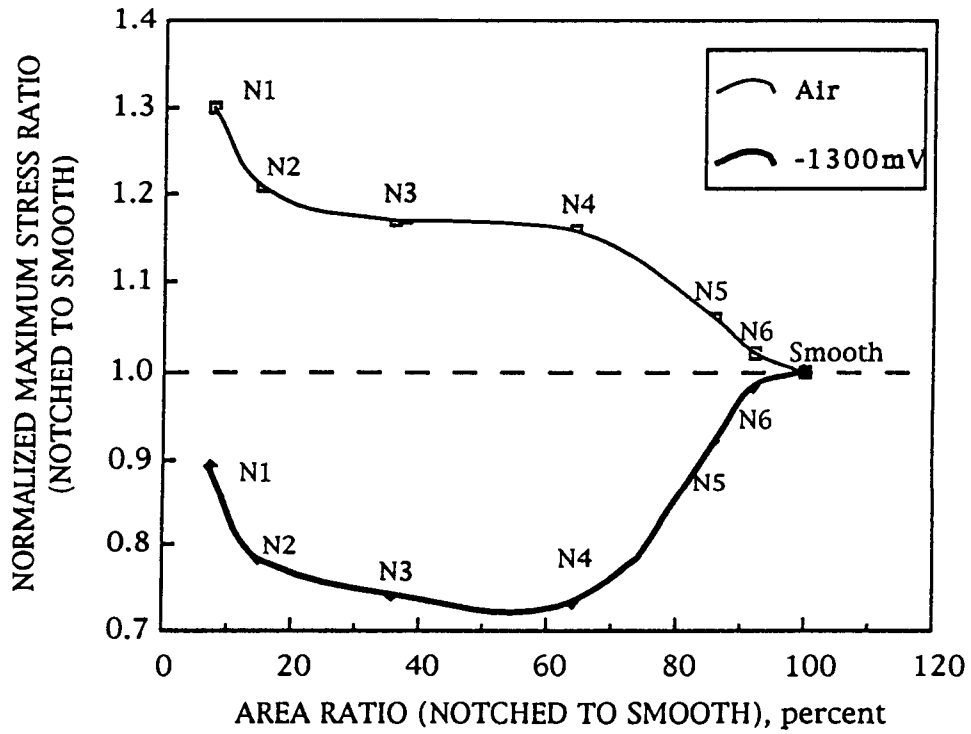
Figure 22: Normalized maximum stress CERT results as a function of normalized specimen cross section area for each of the six notch geometry specimens and for smooth specimens of 270D tendon material tested in deaerated, saturated calcium hydroxide-distilled water while polarized to -1.30 v (SCE). Air data from figure 21 are included for comparison.
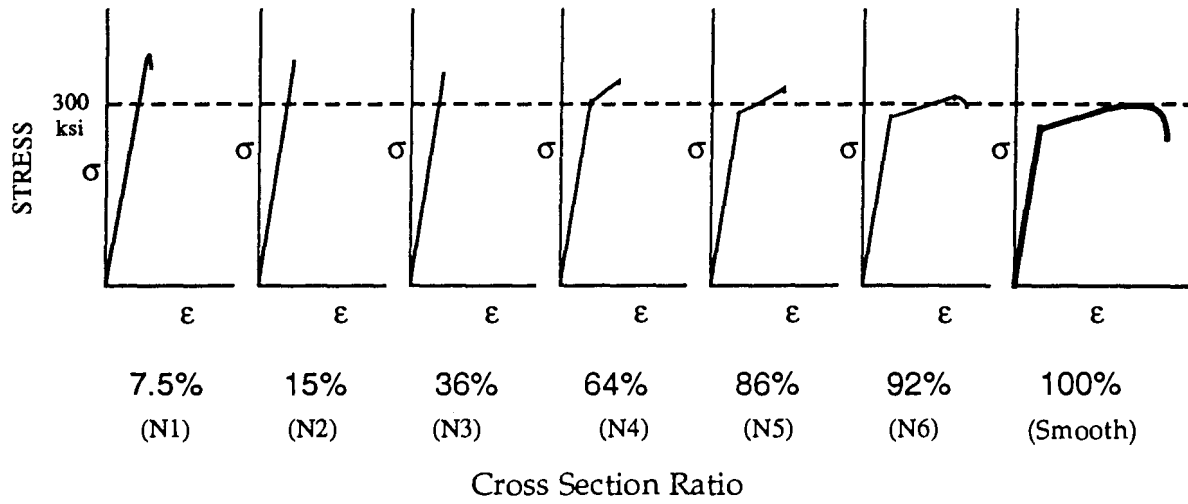
(a)
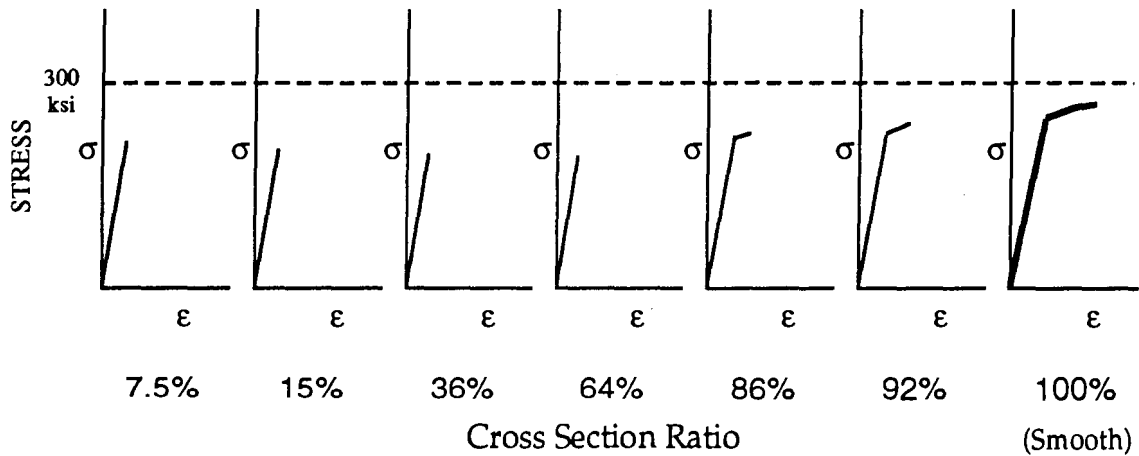
(b)

Figure 23: Schematic representation of the stress (σ) - strain (ε) curves for each of the six notch geometry specimens and for smooth specimens of 270D tendon material tested in (a) air and (b) deaerated, saturated calcium hydroxide-distilled water while polarized to -1.30 v (SCE).

59

Two factors are considered to have influenced specimen strength in the presence of a notch. The first is the magnitude of the stress concentration factor which, in and of itself, had a negative influence upon strength. Table 11 lists calculated stress concentration factors for the present notch geometries and indicates that this parameter increased from N1 to N4 and then decreased for N5 and N6. (47) This, in perspective of the data trend in figure 21, indicates that there is not a simple relationship between stress concentration factor alone and mechanical response of the notched specimens. The second influential factor is plastic constraint, whereby the geometrical irregularity associated with the notch limits lateral or transverse ductility and, as a consequence, renders the material stronger on an actual cross section area basis than if the geometrical irregularity were not present. This is referred to as notch strengthening. (48) For the representation in figure 21 (air tests) the latter factor (notch strengthening) dominated over the former (stress concentration factor), particularly for geometries where the notch was relatively severe. Values for r/d (ratio of notch root radius to reduced specimen diameter, see figure 5) are also listed in table 11, since the magnitude of triaxiality and, hence, notch strengthening has been projected to increase in proportion to this parameter. (49) Consistent with this a correlation is generally apparent between maximum stress for specimens tested in air and at -1.30 v. For the -1.30 v results the stress concentration in conjunction with an embrittling influence of the excessive polarization apparently outweighed any notch strengthening contribution.

An attempt was made to determine if the notched specimen behavior was conducive to a fracture mechanics representation, where the notch was assumed to be the same as a sharp crack. Figure 24 tabulates fracture toughness, as computed from the stress intensity factor (K) value at fracture using a classical expression for a circumferential crack in a cylindrical member, for each of the six notch types and for the two test conditions. (50)[1] Of particular significance is that the calculated fracture toughnesses for both air and -1.30 v, respectively, are approximately constant for geometries N1-N4, for which ductility was minimal or nil (see tables 9 and 10). The observation that fracture toughness for specimen types N5 and N6 was lower than for N1-N4 is attributed to the small 'crack' size for these former geometries (~0.10-0.15 mm) and to the fact that cross section yielding was more extensive (see PEBN data in tables 9 and 10), both of which compromise applicability of linear elastic fracture mechanics.

If the normalized maximum stress versus normalized cross section area data from figure 21 for the notch specimen types N4-N6 and smooth specimen geometries are replotted as shown in figure 25, then it is apparent that these conform to a linear interdependence with a slope of -0.0043. Application of this same rational to the -1.30 v data based also upon a linear representation of the N4-smooth specimen results, as replotted in figure 26 from figure 22, indicates a slope of -0.0075. Figure 27 provides an alternative representation of the data in figures 25 and 26 in terms of normalized maximum load rather than stress. This alternative parameter (applied load) is considered to be more revealing with regard to integrity of locally reduced cross section tendon wire

---

[1] Fracture toughness is, for conditions of plain strain, a material property which reflects that combination of applied stress and crack size at which fracture occurs. It is analogous to fracture stress in the case of uncracked materials.

Table 11: Calculated values for the stress concentration factor for each of the six notch geometries along with average maximum stress data in the two test environments (air and deaerated, saturated Ca(OH)2- distilled water while polarized to -1.30 v (SCE)).

Specimen Type	A/Ao %	Stress Conc. Factor	r / d	Average Max.Stress in Air, MPa	Average Max.Stress at -1.30 V, MPa	Ratio	Normalized Max. Stress in Air	Normalized Max. Stress at -1.30 V
N1	7.5	<1.2	1.04	2628	1662	0.63	1.29	0.9
N2	15	1.3	0.73	2480	1456	0.59	1.22	0.79
N3	36	1.8	0.5	2401	1377	0.57	1.18	0.745
N4	64	2.3	0.37	2352	1365	0.58	1.15	0.74
N5	86	2.1	0.16	2150	1694	0.79	1.05	0.915
N6	92	1.6	0.37	2085	1804	0.86	1.02	0.975
SMOOTH	100	1	--	2040	1850	0.91	1	1
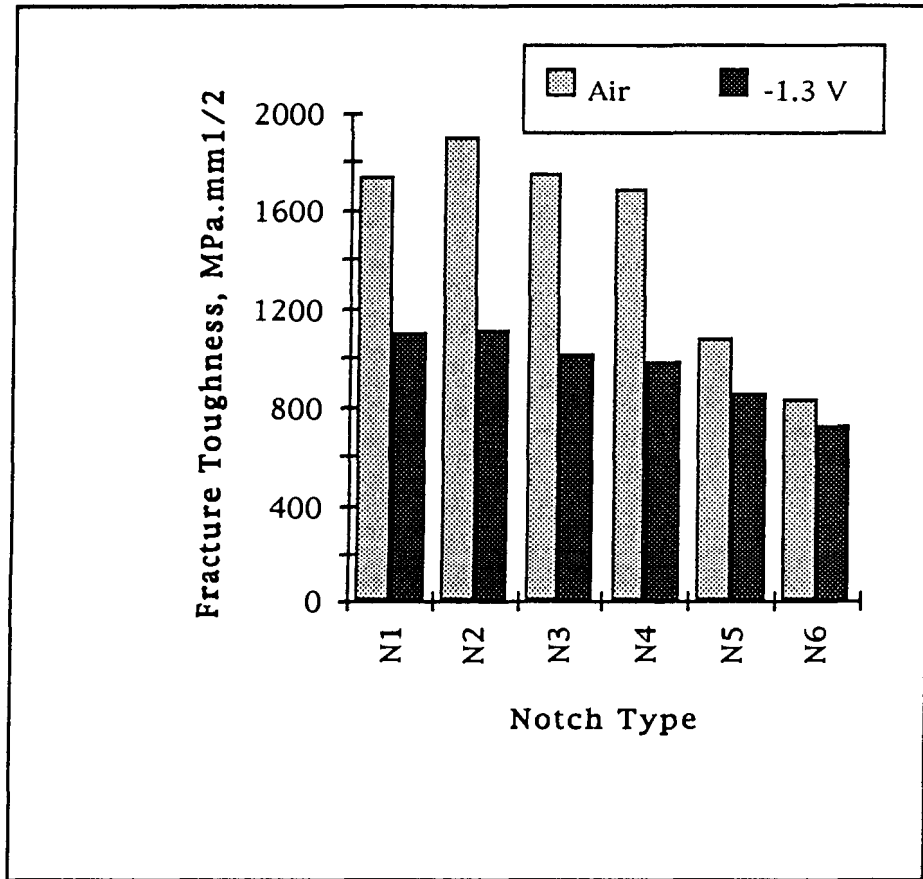
Figure 24: Fracture toughness of the six notched specimen types as calculated from CERT results in air and in deaerated, saturated calcium hydroxide-distilled water while polarized to -1.30 v (SCE). The analysis assumed that the notch was equivalent to a sharp crack of the same depth.
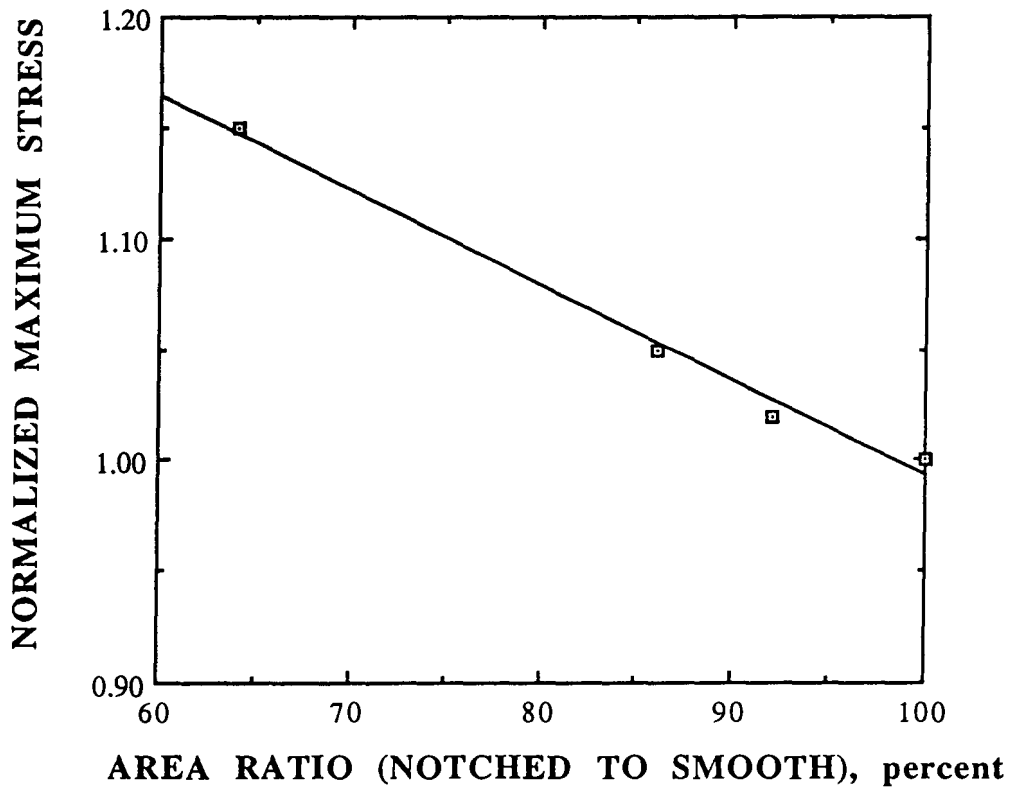
Figure 25: Replot from figure 21 of the normalized maximum stress versus normalized cross section area for smooth and N4-N6 notch type specimens tested in air.

Figure 26: Replot from figure 22 of the normalized maximum stress versus
normalized cross section for smooth and N4-N6 notched type
specimens polarized to -1.30 v (SCE).

Figure 27: Normalized maximum load versus normalized cross section area for N4-N6 notched and smooth specimens tested in air and polarized to -1.30 v (SCE).

than is wire strength based upon remaining cross section, since in service it is load bearing capacity that is ultimately important. Thus, the latter representation (figure 27) shows that for exposure of notch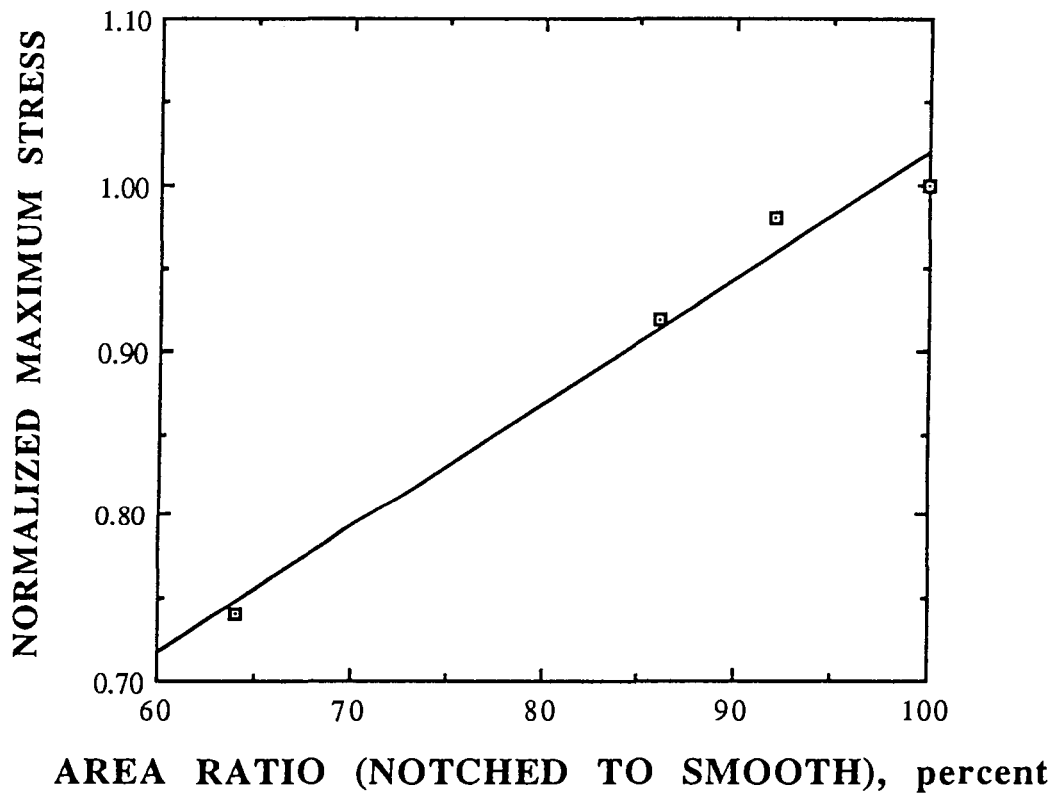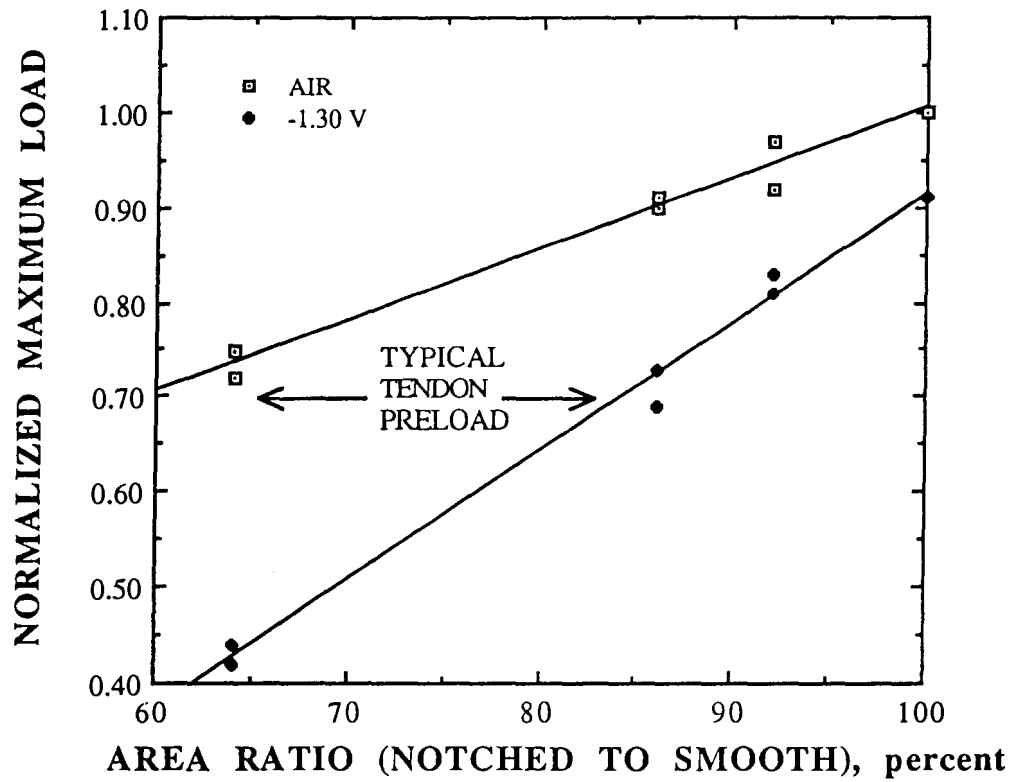ed tendon in air (alternately, in an environment that does not result in embrittlement) it is projected that an area reduction of 40 percent is required to reduce the load bearing capacity to that which is typical of the applied prestress (70 percent of the ultimate stress based upon the original tendon cross section). At -1.30 v the corresponding area reduction is about 15 percent.

Pitted Constant Extension Rate Testing Specimens

Experimental results for pitted specimens tested in air are listed in table 12. As for the notched specimen experiments, these tests also were limited to the 270D material. Plasticity of pitted specimens was restricted with fracture occurring in the elastic region in the most severe geometry case (P1). Some PEBN was apparent for specimen types P2 and P3 but with necking and PEAN also for P4. Specimen types P2 and P3 had essentially identical area ratios (extent to which the cross section was locally reduced); however, the pit geometry for P2 was relatively deep and narrow (L/d = 1.6, see figure 4) while for P3 it was more shallow and wide (L/d = 0.9). In contrast to the notched specimen case, presence of a pit lowered the maximum stress (reduced cross sectional area basis) in air for all four of the geometries investigated. This indicates that, irrespective of the extent of plasticity, little or no notch strengthening resulted from presence of the pits. Correspondingly, table 13 presents results at -1.30 v. These exhibited the same trend as for the air results, but maximum stress for a particular pit geometry was lower and ductility less.

Figure 28 illustrates the above results graphically in perspective to the -1.30 v notched specimen data and according to the same format as in figures 21 and 22 but with all data normalized with respect to the smooth specimen maximum stress in air. This makes it apparent that the average maximum stress of pitted specimens in both air and solution with polarization to -1.30 v decreased with decreasing cross section area according to the same general trend as for similarly polarized notched specimens. A close correspondence is apparent for the notched and pitted specimen data at -1.30 v with data for the latter in air lying at a slightly higher stress. Of particular significance here is that, first, cross section area is further confirmed as a parameter with which maximum stress is simply dependent and, second, the relative pit dimensions (depth and breath) exhibited little influence upon maximum stress compared to the magnitude of area reduction, as least to the extent that these factors were represented by the present geometries.

Figure 29 reproduces the maximum load representation in figure 27 for the notched specimens at -1.30 v and adds to this the data for pitted specimens both in air and at -1.30 v. These data indicate that a pit encompassing about 20 percent of the cross section area should be required to reduce the load bearing capacity to the 0.7 value upon stressing in air or under environmental exposure conditions that do not alter the fracture properties. Alternately, for the -1.30 v case this area reduction magnitude is by 13 percent. The relatively modest wire cross section area reduction to reduce the load bearing capacity of notched and pitted specimens to the prestress amount (13 to 15 percent) is within the range where fracture mechanics cannot be relied upon to provide a geometry independent assessment of fracture strength (see figure 24).

66

Table 12: CERT results for 270D specimens of each of the four pit
geometries tested in air. Smooth specimen data are
included for comparison.

Specimen Geometry	A/Ao, %	Yield Stress, MPa	Max. Stress, MPa	Stress to Fail. MPa	PEBN, mm	PEAN, mm
P1	74	1680	1680	1680	0	0
		1755	1755	1755	0	0
P2	92	1830	2005	2005	0.2	0
		1850	1976	1976	0.14	0
P3	93	1784	1962	1962	0.26	0
		1750	1990	1990	0.32	0
P4	98	1734	2030	1860	0.67	0.095
		1680	1990	1800	0.63	0.11
Smooth	*100*	*1750*	*2040*	*1700*	*0.8*	*0.2*

Table 13: CERT results for 270D specimens of each of the
four pit geometries tested in deaerated, saturated
Ca(OH)2-distilled water and polarized to -1.30 v
(SCE). Smooth specimen data are included for
comparison.

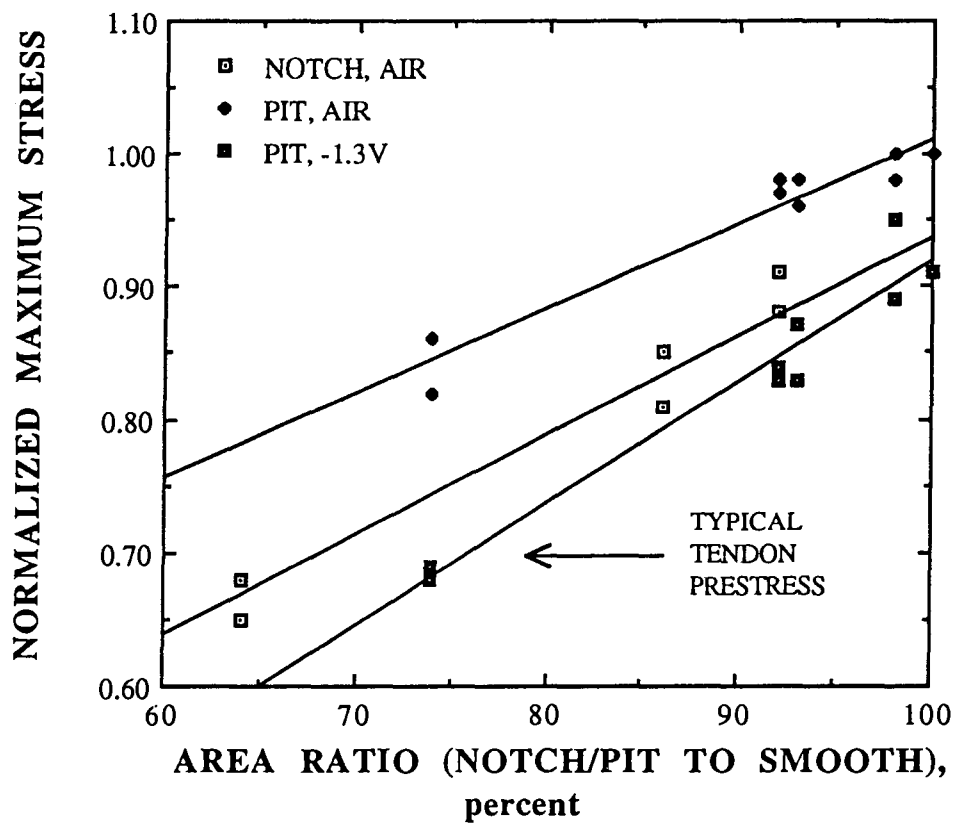| Specimen Geometry	A/Ao, %	Yield Stress, MPa	Max. Stress, MPa	Stress to Fail., MPa	PEBN, m m	PEAN, m m
P1	74	1390	1390	1390	0	0
		1402	1402	1402	0	0
P2	92	1688	1688	1688	0	0
		1715	1715	1715	0	0
P3	93	1690	1690	1690	0	0
		1780	1780	1780	0	0
P4	98	1730	1928	1928	0.24	0
		1650	1820	1820	0.21	0
Smooth	100	1700	1850	1850	0.3	0

Figure 28: Normalized maximum stress versus normalized cross section area for pitted and smooth specimens in air and at -1.30 v (SCE). Notched specimen data at -1.30 v is included for comparison.
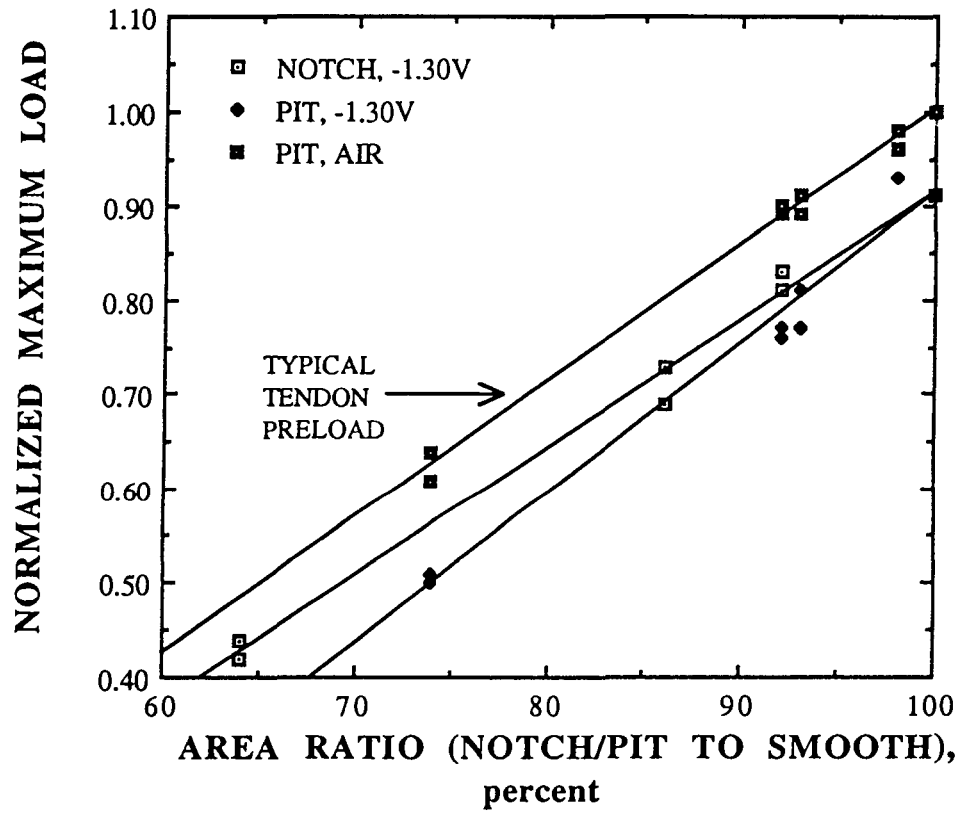
69

Figure 29: Normalized maximum load versus normalized cross section area
for pitted and smooth specimens in air and at -1.30 v (SCE). Notched
specimen data at -1.30 v is included for comparison.

Hence, the fracture mechanics approach to evaluation of residual strength of tendon with a locally reduced cross section is not considered to be of any practical significance.

Structure Qualification for Cathodic Protection

The fact that maximum load of the notched and pitted specimens correlated with remaining specimen cross section area lends itself to a new approach whereby a particular pretensioned concrete component or structure can be qualified for cathodic protection. This proposed protocol involves the following steps:

1. If no corrosion induced concrete cracking and spalling are evident, then the structure is automatically qualified.

2. In cases where cracking and spalling are evident, remove cracked and spalled concrete from corrosion damaged areas thereby allowing visual inspection of the already exposed tendon. Such concrete removal should be performed under the direction of a structural engineer. It is assumed that the concrete being removed is in such a deteriorated state that load bearing capacity is not compromised any further than might already be the case.

3. Identify locations on the exposed steel tendon where corrosion is uniform and where it is localized. Attack at such sites is expected to represent the worse cases. For locations where uniform corrosion has occurred, residual strength should be proportional to the remaining cross section. Thus, a 30 percent loss in cross section for a wire whose tensile strength corresponds to the specification minimum (270 ksi or 1863 MPa for Grade 270 material, see reference 8) should result in a residual strength equal to the assumed prestress (70 percent of ultimate). Where corrosion is localized, measure the diameter (d) of the largest pit. From this and assuming a semi-circular pit cross section determine the normalized remaining cross section area, A, of the wire from the expression

$$A = \left[1 - \left(\frac{d}{D}\right)^2\right] \cdot 100, \qquad (6)$$

where D is the original wire diameter (see figure 4) as illustrated by figure 30 (recall from figure 29 that a 13 percent cross section reduction should reduce residual strength to that of the same assumed prestress). Corrosion of tendon in sound (uncracked, non-spalled) areas of the concrete is expected to be modest by comparison to that which has undergone corrosion induced damage, and residual strength for tendon here should be essentially unchanged from what it was originally.

4. Qualify the structural member for cathodic protection based upon the following criteria:

   A. The remaining wire cross section at locations of uniform corrosion is no less than 85 percent of the original (uncorroded) area.
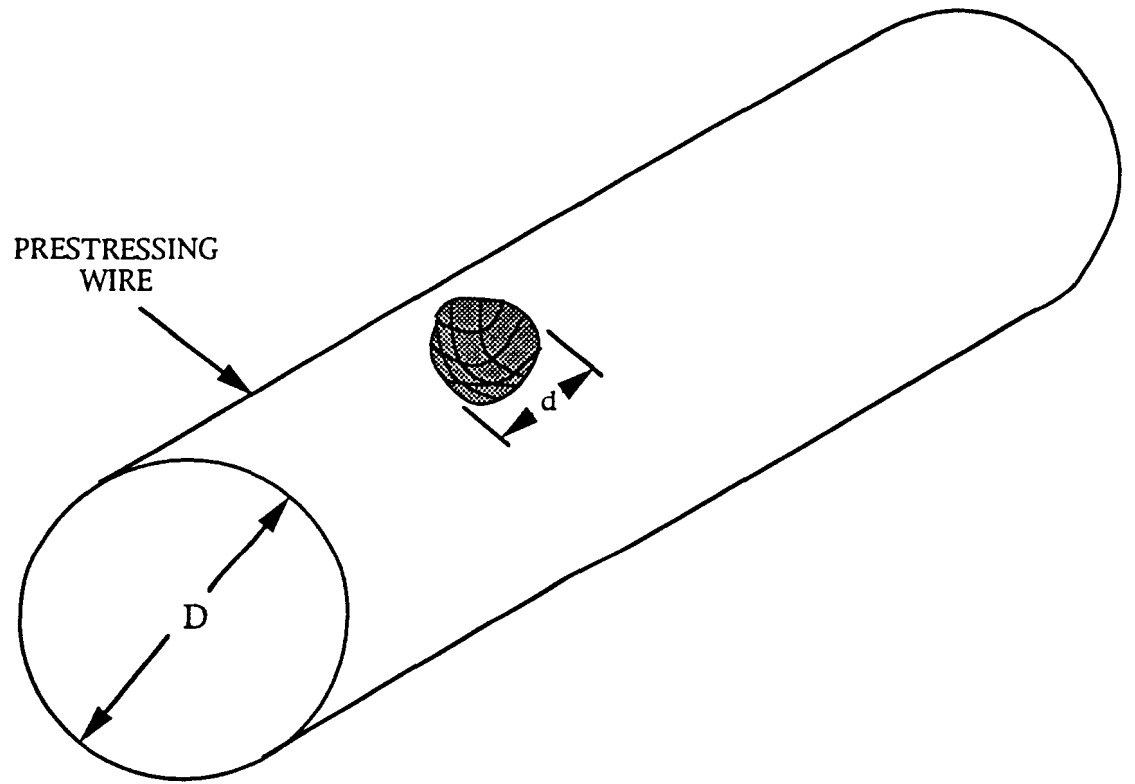
Figure 30: Schematic illustration of the procedure for field estimation of remaining wire cross section determination.

B. Diameter of the largest pit is such that the remaining localized area is ≥ 90 percent of what it was originally. For locations were there is both uniform and localized corrosion this same 90 percent net remaining wire cross section should apply.

These proposed qualification criteria incorporate a factor of safety from several sources. First, the maximum allowable localized area reduction (10 percent) is less than the 13 percent indicated from the experimental data (figure 29). Second, the data upon which the local corrosion penetration criterion is based were acquired at a potential of -1.30 v, whereas a cathodic protection system for prestressing steel in concrete should be designed for a lower potential limit of -0.90 v or more positive. Third, the assumed wire strength is the specified minimum and in actuality is likely to be higher.

The above procedure for qualification is simpler and more straightforward than Electrochemical Proof Testing. (32) However, the evaluation of fracture response for notched and pitted prestressing wire in the present program was based solely upon the 270D material which, according to the data in table 8 and figure 17, exhibited relatively low sensitivity to embrittlement at -0.90 v. Additional experiments are required upon a more susceptible material (270F or 270F' or chromium microalloyed, for example) to determine if the above results for 270D are conservative compared to what might otherwise be encountered. In the meantime the procedure is intended for normal prestressing steel only and not for microalloyed.

Prestressed Concrete Beam Specimens

As explained in chapter II, 23 prestressed concrete beams are undergoing wet-dry sea water ponding for the purpose of developing various extents of corrosion upon the embedded tendon (see table 5). Figures 31 and 32 present plots of potential for different measurement locations along each of the two embedded tendons (designated 'N' and 'S') of specimen number C3bas2 as a function of time during the initial 110 days of exposure. The horizontal bar data points and the interconnecting line which range predominantly between 0 and -45 mV identify the respective time periods when the slab was wet and when it was dry.[2] Also, the potential measurement position in feet relative to one end of the bath is indicated as 1', 1.5' and so forth; and positions of locally admixed chloride are designated as 'Cl'. The S tendon, for which data are shown in figure 32, exhibited the most negative potentials of any of the beams during this initial exposure period, whereas the N tendon data typified behavior of tendons that were not yet indicating active corrosion. As should be expected, potential was independent of position along the tendon length during the ponding portion of the cycle but exhibited a range of values when dry. Subsequent to 110 days of exposure the data acquisition protocol was relaxed such that a single potential measurement only was made for each location at the end of the dry portion of the cycle. Figure 33 presents a three-dimensional plot of the potential-position-time results to date for a typical beam (specimen number C35). Here, the right horizontal scale designates position within the ponding bath (in feet) from one end to the other for

---

[2] Data points at potentials intermediate to 0 and -45 mV reflect an attempt to quantify an intermediate stage of drying as existed at the particular time that a set of measurements were made.
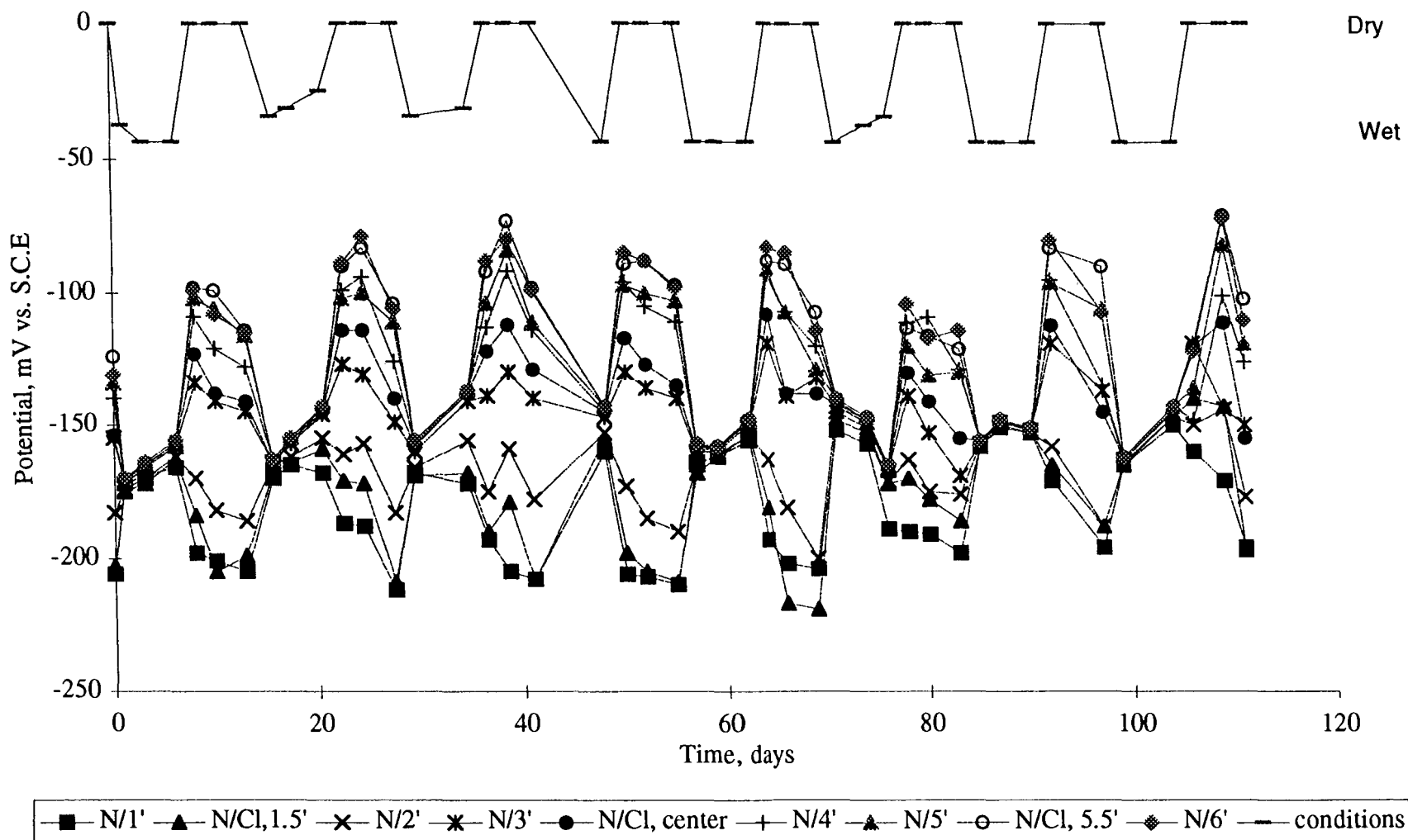
Figure 31: Potential as a function of time for different positions during the initial exposure for the N tendon of specimen C3bas2.
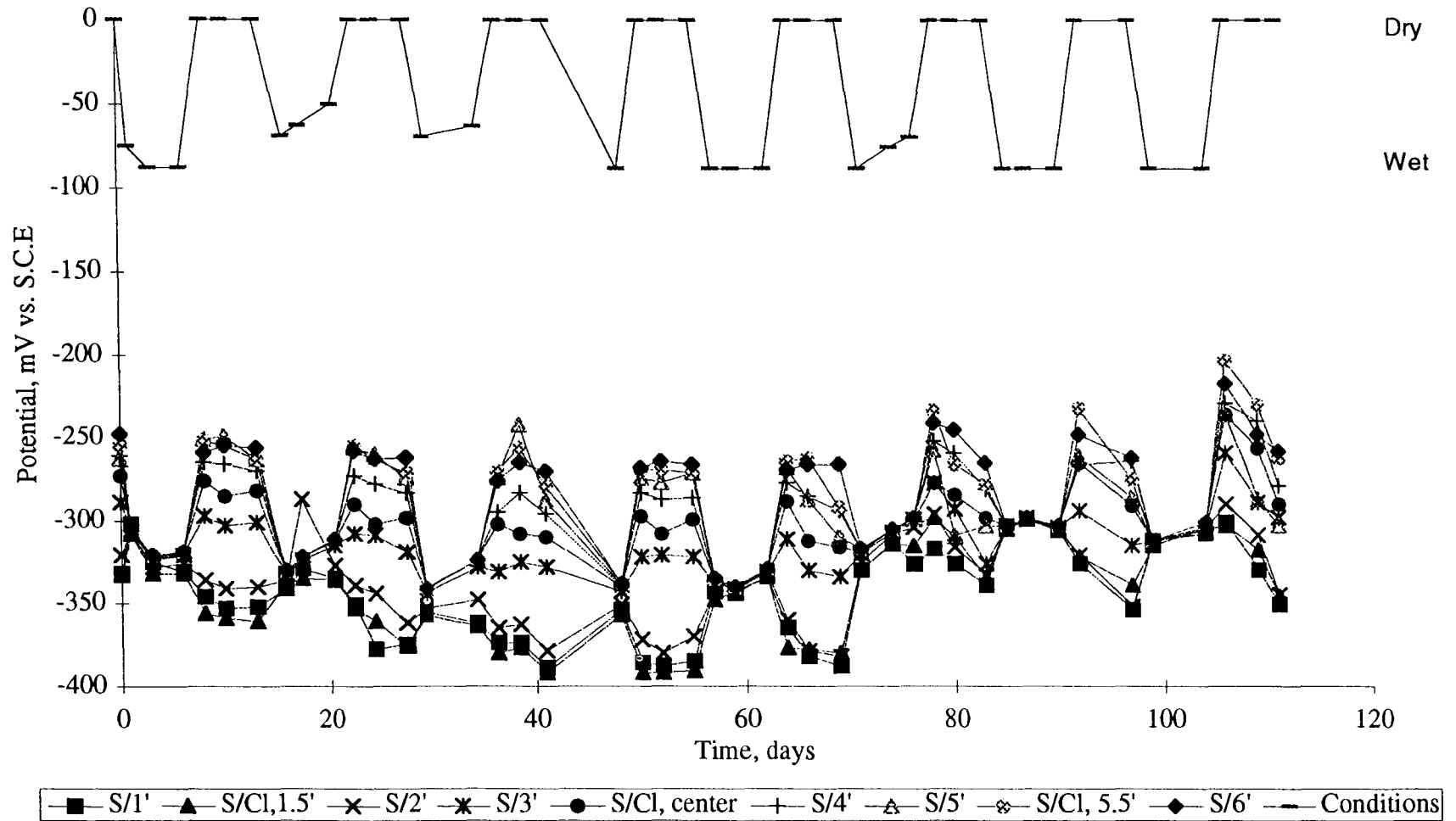
Figure 32: Potential as a function of time for different positions during the initial exposure for the S tendon of specimen C3bas2.
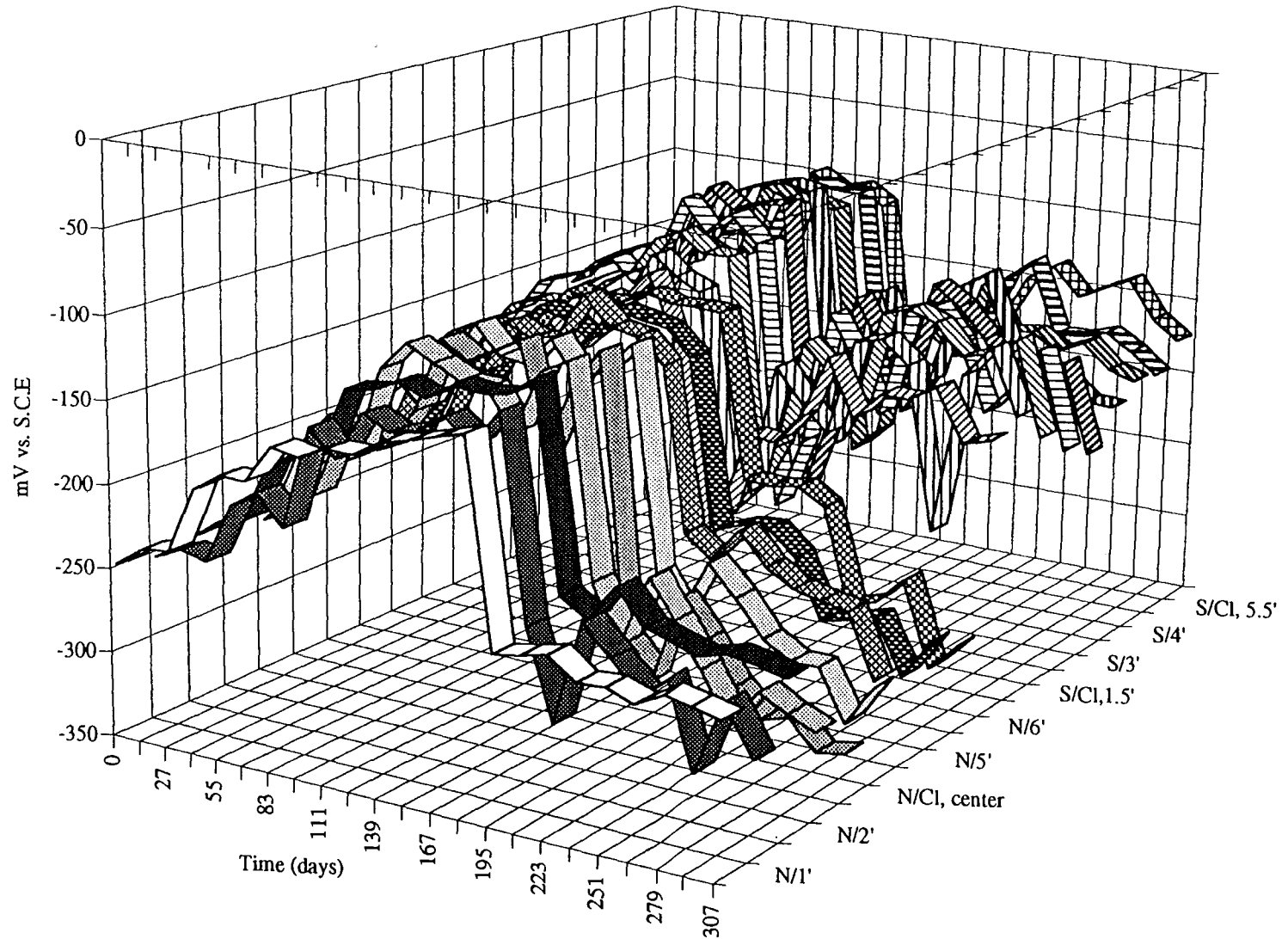
Figure 33: Potential-time-position data for N and S tendons of specimen C35 during cyclic sea water ponding.

each of the two tendons (S and N) and where this corresponded to a location of admixed chlorides (labled 'Cl' in caption). This representation is intended to provide a perspective of corrosion state evolution for each measurement position along each tendon. Thus, the N tendon for this beam became active (potential ≤ -0.28 v (SCE)) after 195 days, whereas potential for the S tendon for this same specimen has remained more positive. Table 14 summarizes the potential data for each of the two tendons in the 23 slabs that are under test in this phase of the program. To date, 26 tendons have become active, whereas potential for the remaining 20 has remained positive to -0.28 v.

A limited number of polarization resistance measurements and corrosion rate calculations based upon these were made after 143 and 266 days of wet-dry cycling. Figures 34a and 34b presents the results from these for specific locations upon both the N and S tendon (depth axis) of six different beams (width axis) after these two times, respectively, and indicates that corrosion rate ranged from 6 to 86 μ m per year. Thus, in some cases corrosion rate is sufficiently high to, in time, cause concrete cracking and spalling. A general correlation between corrosion rate and potential was found to exist for these same data as shown by figure 35. While this may be fortuitous, none the less it suggests that for the present specimens it may be possible to estimate the extent of ongoing corrosion activity from potential data alone.

LOSS OF BOND IN ASSOCIATION WITH CATHODIC PROTECTION

General

As noted above, loss of tendon-to-concrete bond is one of two potential degradation processes which has been projected to potentially transpire in pretensioned concrete in response to cathodic polarization, the other being hydrogen embrittlement. Two general types of experiments, one involving pull-out tests upon cathodically polarized non-pretensioned tendon or wire concrete block specimens and the second dimensional monitoring of cathodically polarized pretensioned concrete beam specimens, were performed to characterize the extent to which loss of bond might be important.

Tendon and Wire Pull-Out Tests

As described in chapter II, exposure and polarization of the 60 bond strength pull-out specimens (30 with a centrally positioned tendon and 30 with a straight wire) has been under way for about 11 months, and so only a limited number of specimens have accumulated the intended charge density transfer and been mechanically tested. Table 15 presents a listing of these along with test results for 1) ultimate bond strength, 2) bond stress at 0.25 mm loaded end slip and 3) bond stress at 0.025 mm free end slip. The current density applied for the test period (500 mA/m^2 of steel) is equivalent to the same net charge transfer density (14,000 A·h/m^2) that occurs in 15.1 years of cathodic polarization with a current density of 10.8 mA/m^2 of steel. The results are in general accord with what has been reported previously in that, first, the ultimate bond strength was not appreciably influenced by cathodic charging, while the bond stress at 0.25 mm loaded end slip was (compare data for specimens 1 and 2 with those from specimens 4 and 5), and, second, the magnitude of the bond strength and reduction thereof was approximately the same as reported by Buenfeld and Broomfield who performed pull-out tests

Table 14: Listing of the time at which an active potential was noted for each of the 23 wet-dry cycle beams.

| Beam Designation	Northern Tendon			Southern Tendon		
	Time to Active Potential, (days)	Location of Most Active Potential	Most Active Potential (mV vs. SCE)	Time to Active Potential, (days)	Location of Most Active Potential	Most Active Potential (mV vs. SCE)
C 35	195	N/Cl, 1.1 m	- 386	> 307		
C 34	0	N/Cl, 1.1 m	- 295	0	S/Cl, 1.1 m	- 378
C 32	13	N, 1.8 m	- 283	0	S, 1.8 m	- 322
C 33	> 307			> 307		
C 31	> 307			> 307		
C 38	237	N, 0.3 m	- 359	153	S, 1.8 m	- 306
C 3bas4	307	N/Cl, 0.5 m	- 330	41	S/Cl, 1.1 m	- 315
C 39	64	N/Cl, 1.7 m	- 308	209	S, 1.8 m	- 363
E 1	0	N/Cl, 1.1 m	- 283	0	S/Cl, 1.1 m	- 290
C 36	167	N/Cl, 1.7 m	- 359	293	S/Cl, 1.7 m	- 285
C 311	> 307			> 307		
C 3bas2	> 307			0	S/Cl, 0.5 m	- 333
C 313	> 307			> 307		
C 3bas3	> 307			> 307		
C 3bas1	> 307			> 307		
E 4	> 307			> 307		
E 3	> 307			293	S/Cl, 1.1 m	- 318
E 6	> 307			> 307		
E 5	181	S, 1.8 m	- 306	0	S/Cl, 1.7 m	- 360
E 7	0	N, 1.8 m	- 373	0	S, 1.8 m	- 323
E 8	0	N/Cl, 1.7 m	- 369	0	S, 1.8 m	- 335
E 10	125	N/Cl, 1.7 m	- 306	83	S/Cl, 1.7 m	- 291
E 9	0	N/Cl, 1.7 m	- 337	> 307		
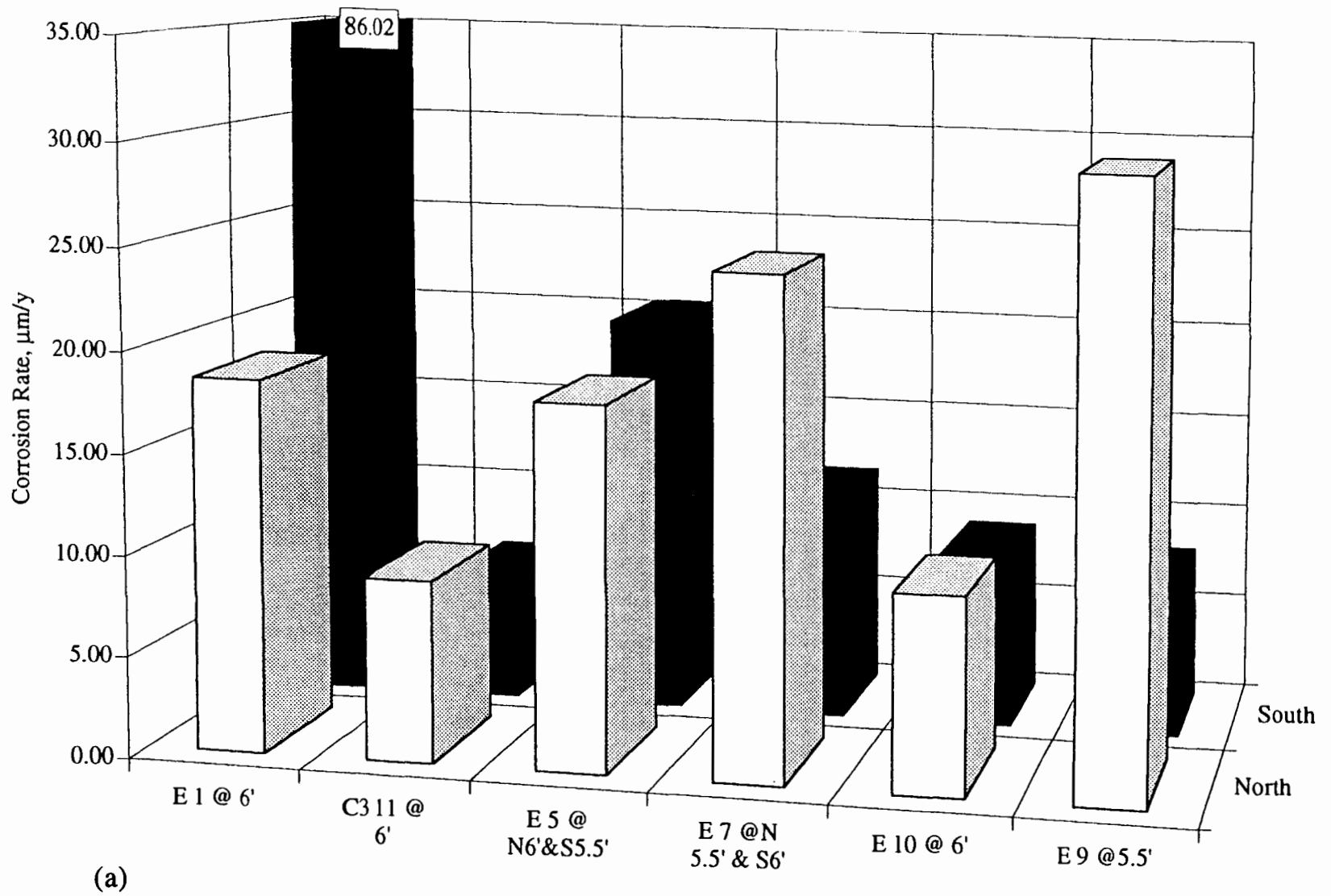
Figure 34: Corrosion rate data for selected beams after (a) 143 days of wet-dry cycling and (b) 266 days of wet-dry cycling.
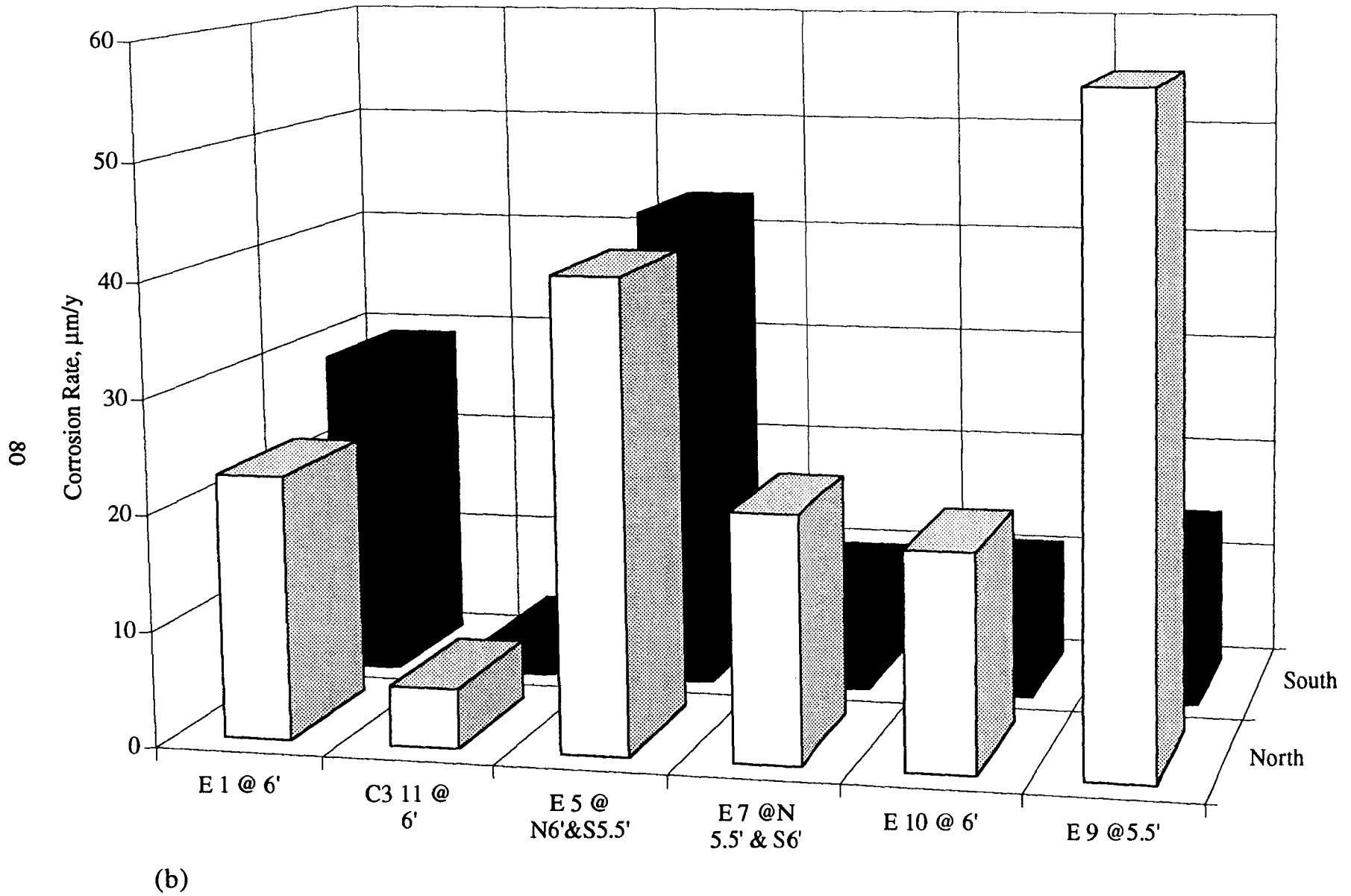
Figure 34:   Corrosion rate data for selected beams after (a) 143 days of wet-dry cycling
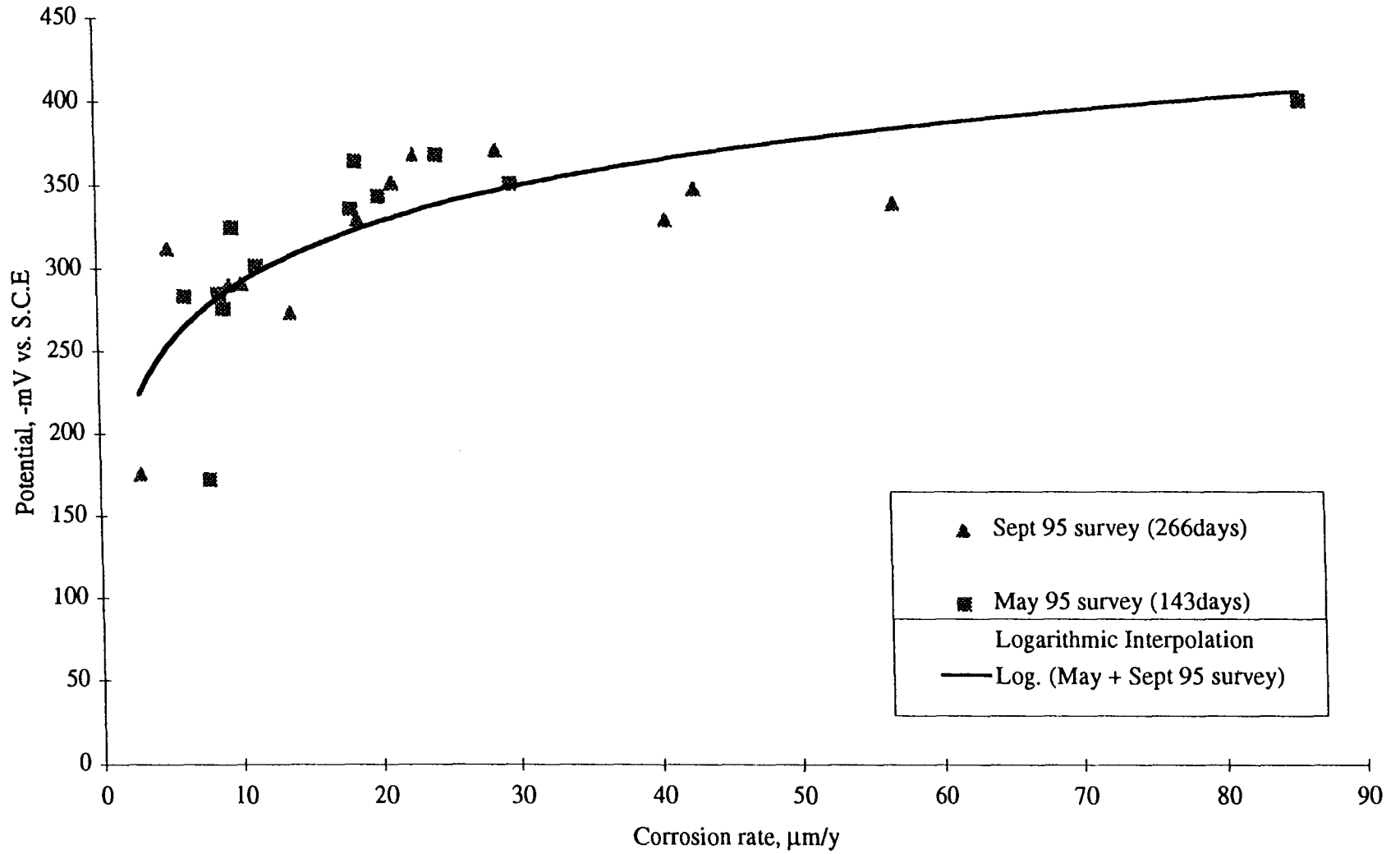   and (b) 266 days of wet-dry cycling (continued).

Figure 35: Plot of potential versus corrosion rate for beams undergoing wet-dry cycling.

Table 15: Bond strength and slip results for pull-out specimens
which have been tested to date.

SPECIMEN NUMBER	SPECIMEN TYPE	CURRENT DENSITY, mA/m2 (steel)	TOTAL CHARGE, A-hr/m2 (steel)	ULT. BOND STRENGTH, MPa	BOND STRESS @0.25 mm LOADED END SLIP, MPa	BOND STRESS @0.025mm FREE END SLIP, MPa
1	TENDON	FC	0	2.33	2.15	2.12
2	TENDON	FC	0	2.72	1.69	2.65
3*	TENDON	500	1,400	-	-	-
4	TENDON	500	1,400	3.66	0.74	3.66
5	TENDON	500	1,400	2.43	0.52	2.39
6	WIRE	500	1,400	1.66	0.69	1.65
7	WIRE	500	1,400	1.54	1.08	1.47
8	WIRE	500	1,400	1.79	**	1.79

* Power surge during mechanical test failed the specimen without data
acquisition.
** Loaded end LVDT shifted during test.

upon smooth reinforcing bars in concrete that had been cathodically polarized. (34,38) Rasheeduzzafar et al. also reported that the load at 0.025 mm free end slip was greater in polarized specimens than controls; however, the limited data for the present specimens does not confirm this. (34) An analysis is forthcoming in conjunction with additional testing to determine if the reduced bond stress at 0.25 mm loaded end slip for polarized specimens compared to the controls has any negative structural implications.

Pretensioned Beam Specimens

General. This component of the experiments involved monitoring of both 1) tendon mounted and 2) concrete embedded and surface mounted strain gauges as a function of exposure duration for both control (unpolarized) and cathodically polarized specimens. The experimental approach was based upon the premise that any reduction or loss of prestress due to degradation of the concrete-tendon bond should result in a contraction of the tendon (strain gauge output decrease) and an expansion of the concrete in the length direction (strain gauge output increase), as illustrated previously by figure 10.

Dimensional Monitoring of Unpolarized Specimens. One pretensioned concrete beam (specimen B2bas1) was exposed to laboratory air and six to continuously flowing sea water (unpolarized, see table 6) via the ponds mounted upon the top surface to provide baseline information to which results from polarized specimens could be compared. Figure 36 shows strain measurements from two tendon mounted and three embedded strain gauges over the course of approximately 500 days exposure to laboratory air for specimen B2bas1. The gauge designation nomenclature that has been used here and for the other specimens was explained in figure 8. It was concluded from these data that the long-term gauge output stability was in the range $\pm$ 200 $\mu\varepsilon$. Such variations are thought to reflect seasonal temperature changes in the laboratory and long term gauge and measurement procedure variables.

Tendon mounted strain gauges were limited to a single free corrosion specimen (B2bas4), whereas embedded gauges were present for all six beams that were in this exposure category. Figure 37 plots the microstrain recorded for the five tendon mounted strain gauges upon B2bas4 as a function of exposure time. Output from three of the gauges (t/S,W1', t/N,E1' and t/N,E2.5') indicated a progressive extension of the tendons with time at a rate that was relatively rapid subsequent to initial exposure but which progressively moderated. Gauge t/S,W2.5' failed within 100 days of exposure, and the data from it should be considered suspect. The extension indicated by gauge t/N,W1' was within the range of the other gauges for the initial 55 days of exposure, but subsequently output from it decreased and remained approximately constant at a relatively small value. While the post 55 day behavior of this gauge could be indicative of slippage between the tendon and concrete, it is more probable that gauge debonding was responsible since no abnormal concrete expansion accompanied this, as explained below (see also figure 10. On this basis it is considered that response of the three gauges which indicated relatively large tendon extension (gauges t/S,W1', t/N,E1' and t/N,E2.5') probably reflects the actual behavior of the tendon upon sea water exposure of the beam.
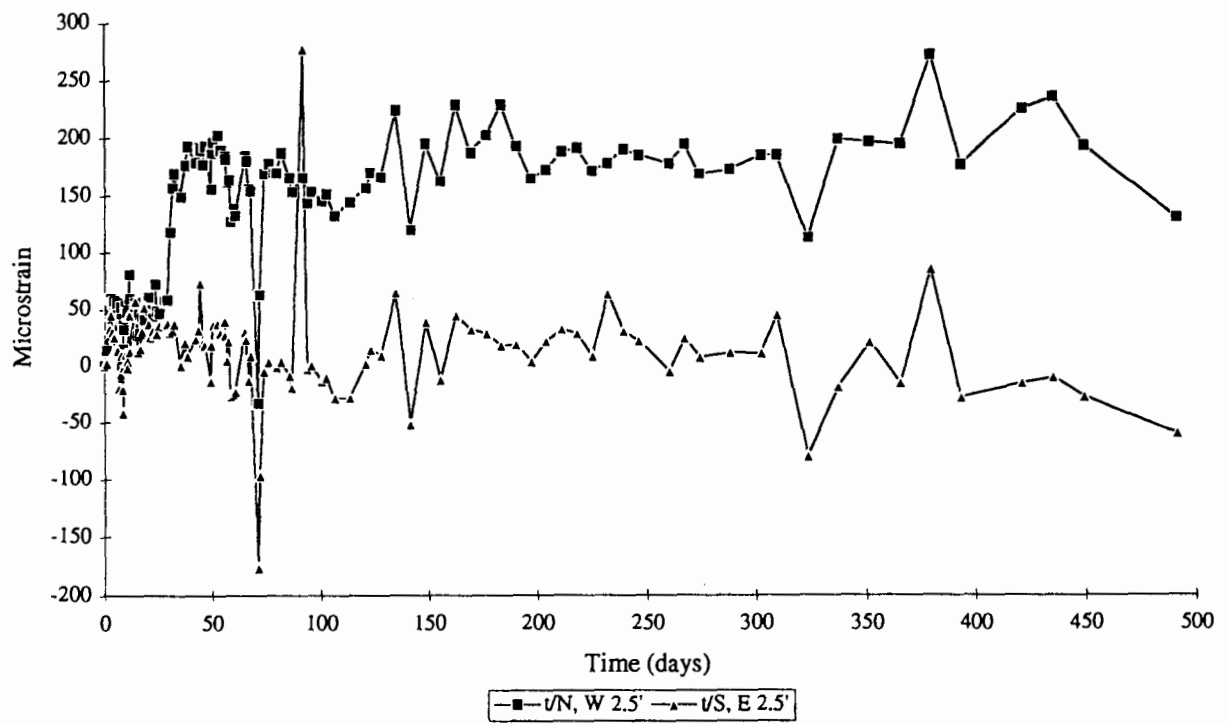
(a)
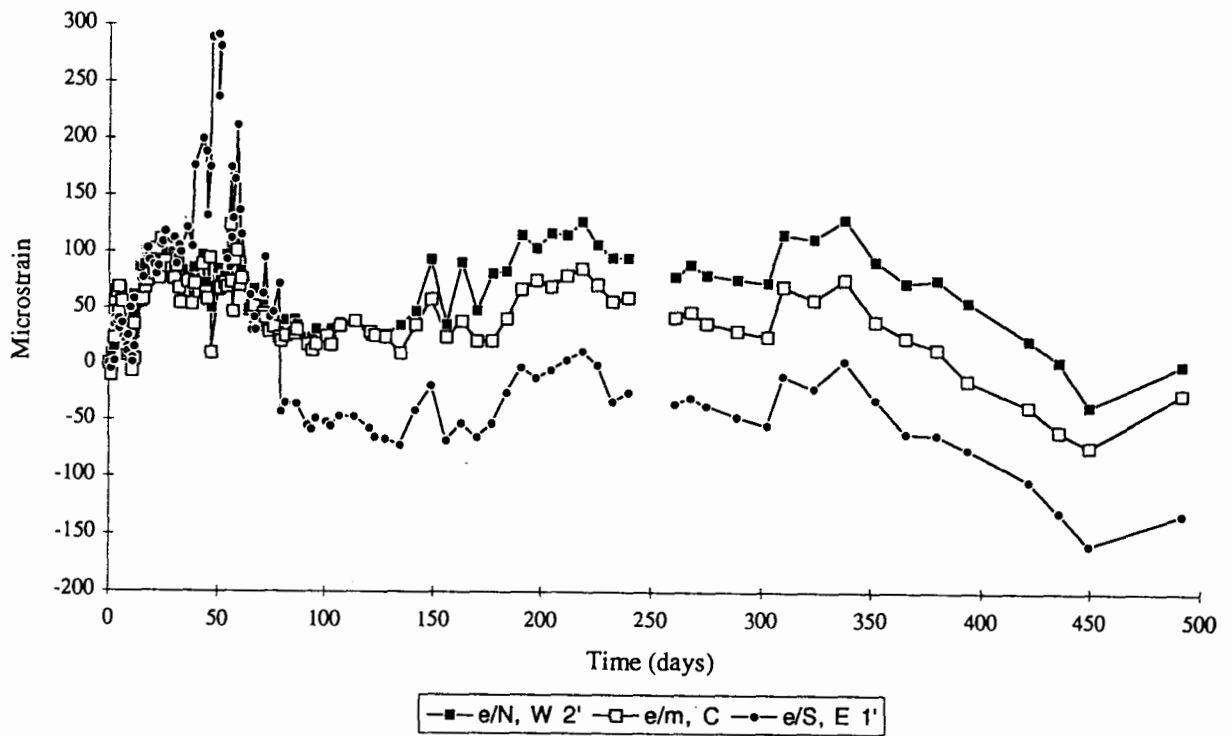
(b)

Figure 36: Output data for (a) tendon mounted and (b) embedded strain gauges for specimen B2bas1 as a function of time under laboratory air exposure.
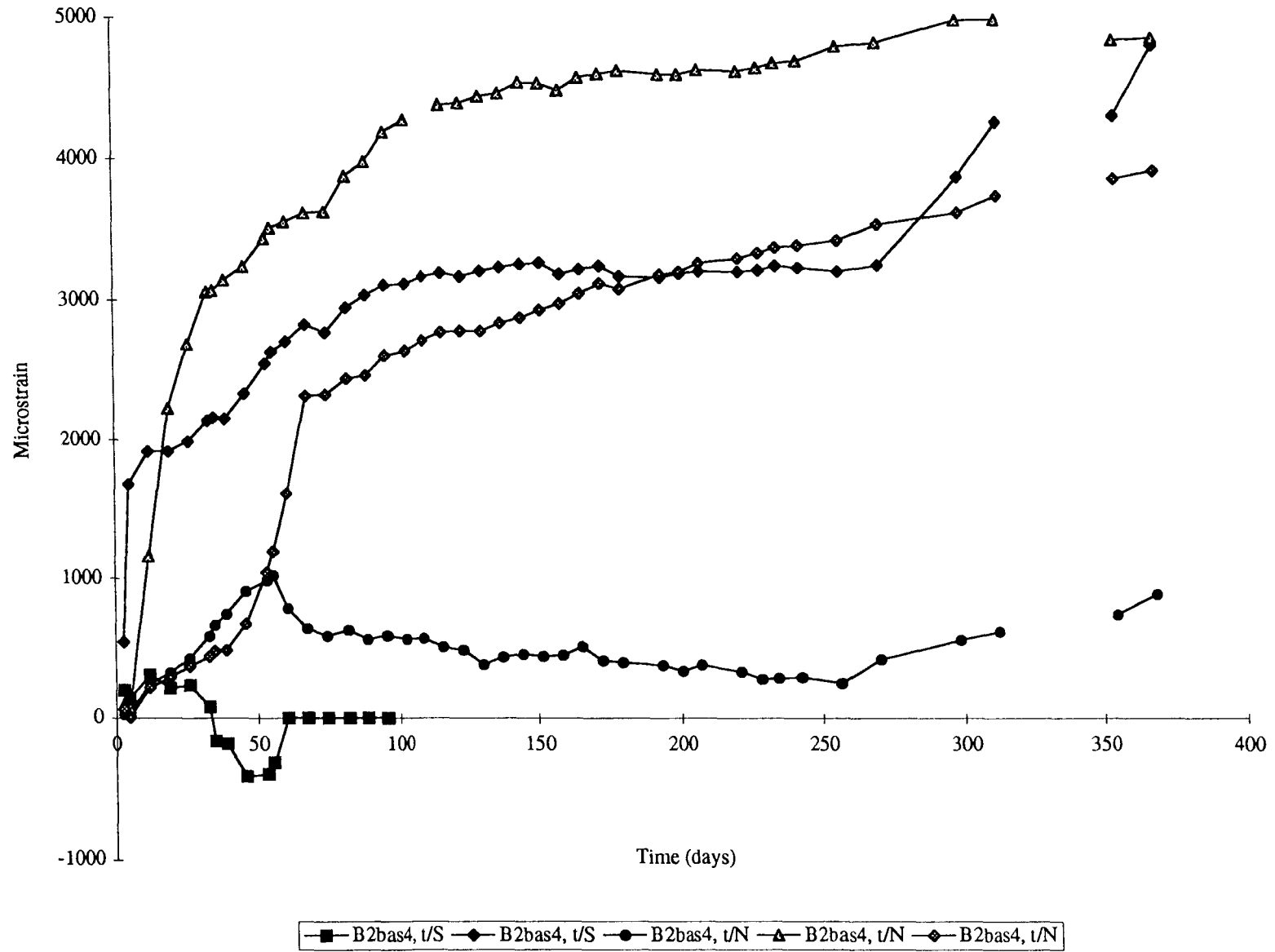
Figure 37: Output data for tendon mounted strain gauges for specimen B2bas4 as a function of time with sea water ponding without polarization.

Correspondingly, figure 38 reports strain data versus time for the nineteen gauges embedded in the six specimens, where the number of gauges per beam ranged from 2 to 4. While there is considerable scatter in the data, still the general trend parallels that for the tendon mounted gauges (figure 37) and is in accord with the historically reported behavior for a cementiteous material exposed to water which involves progressive expansion with time to an asymptotically approached value. (50-53) That the scatter was largely from one gauge to the next, whereas output from the individual gauges varied monotonically with time, suggests that locally variable conditions (heterogeneities) in the concrete were influential. The average tendon extension after 1 year was 4,353 $\mu\varepsilon$ based upon three gauges, as described above (figure 37), whereas for the concrete the corresponding value based upon the embedded gauges (figure 38) was 2,320 $\mu\varepsilon$. Results of previous research that have addressed cement, mortar and concrete expansion in either sea water or artificial sea water are presented in table 16. (50-53) While results from cement and mortar specimens bound the present results, the data from the single study which involved concrete per se indicated a lesser expansion. (50-53) Exposure of the strain gauges to moist and wet conditions for extended periods and swelling of the polymeric gauge encapsulating film resulting therefrom may have made expansion of the present prestressed beams appear greater than it actually was.

Dimensional Monitoring of Polarized Specimens. Figures 39 to 46 present data for both the embedded and tendon mounted strain gauge output data as a function of exposure time for the eight polarized specimens. The magnitude of cathodic current for each specimen was listed previously in table 6. For each of the microstrain versus time plots the exposure history is indicated by the horizontal line segments which are designated as "dry", "wet" and "polarized", respectively. Thus, specimen B2cp1 was initially exposed to sea water for 35 days without polarization. This was followed by polarization until day 112, after which the specimen was dry until day 126 for gauge replacement and so on. For each specimen the strain gauge data have been normalized to 0 $\mu\varepsilon$ at the beginning of exposure (time zero).[3] As an example of the data representation protocol consider the embedded gauges for Specimen B2cp5 (Figure III-30a). In this case polarization was interrupted in order to replace tendon mounted strain gauges that failed during the exposure (90-120, 145-160 days and so on), since doing this required draining the sea water pond and allowing the concrete surface to dry. The enhanced scatter for some embedded gauge data at long exposure times appeared to be a prelude to gauge failure. As such failures occurred, replacement surface mounted gauges were installed; and output from these was subsequently referenced to detect any concrete expansion.

Of particular importance is the accumulation of total charge transfer with time during cathodic polarization of the prestressed beam specimens. In this regard figure 47 shows the relationship between the magnitude of charge density transferred at a constant current density of 10.8 mA/m^2 and time. By the graphical relationship shown here 9,460 A·h/m^2 are accumulated in 100

---

[3] The time scale for specimen B2cp8 begins at 100 days exposure and these data are not normalizes to 0 $\mu\varepsilon$ because of the prior polarization of this beam using 1 A and the preceding free corrosion exposure.
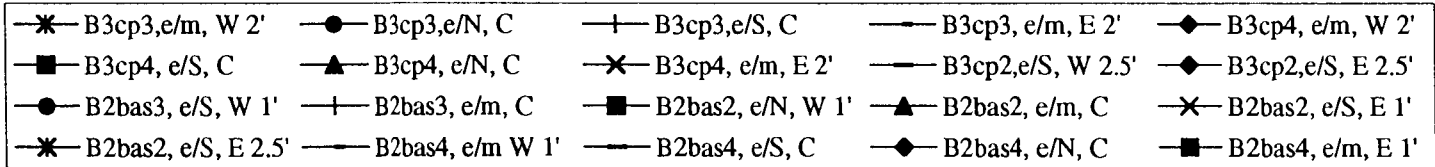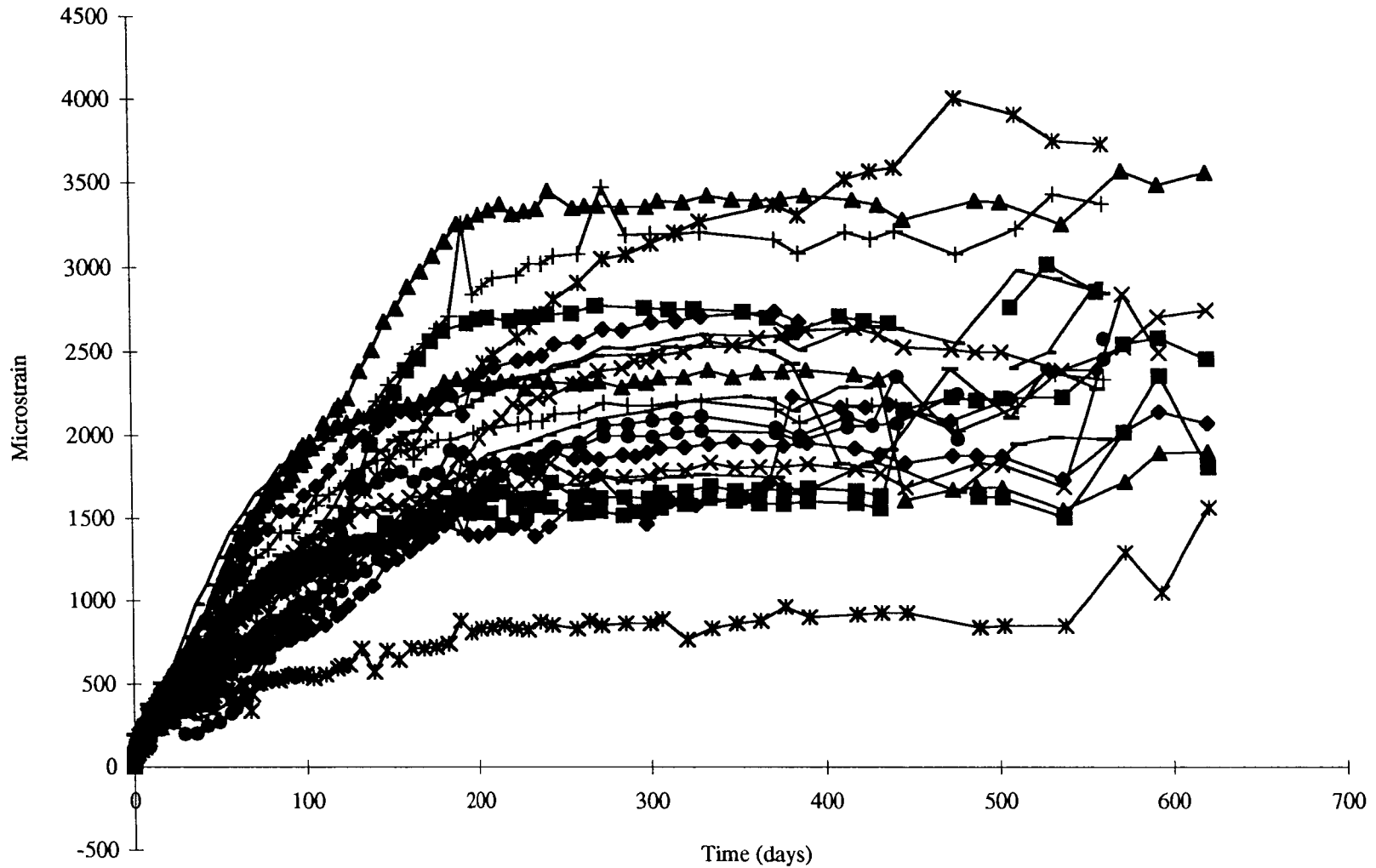
Figure 38: Output data for 19 embedded strain gauges for specimen B2bas4 as a function of time with sea water ponding without polarization.

Table 16: Expansions for cements and concrete in sea water.

Source	Specimen Geometry and Materials	Exposure	Exposure Duration	Expansion, $\mu m/m$
Regourd [51]	L.C.P.C[1] accelerated expansion tests on Portland cement mortars with variable contents of C_3A, slag and pozzolanic cements.	Artificial sea water or Mediterranean or Atlantic Ocean waters, complete immersion.	1 year 3 years	750 - 1220 1750 - 1940
Paillere and Raverdy [52]	L.C.P.C tests on Portland cement with variable contents of C_3A, slag, fly ash and 10 or 20 % of sulfur.	Artificial sea water, complete immersion	1 year	≥ 6600
Paillere and Raverdy and Millet [53]	L.C.P.C tests on Portland cement with variable contents of C_3A and SO_3.	Artificial sea water, complete immersion	1, 3 and 7 years	420 - 2150 1000 - 3300 1550 - 15000
Mijnsbergen and Reinhardt [54]	Hollow cylinders $\phi 20$ cm, 80 cm high of concrete using Portland cement, Portland blast furnace cement or Portland fly ash cement with w/c (0.45, 0.6).	Artificial sea water without $Mg(OH)_2$.	1 year w/c: 0.45 w/c: 0.60	140 - 700 400 - 600

1 L.C.P.C stands for 'Laboratoire Central des Ponts el Chaussées.' This French agency is in charge of testing all materials used in construction of public roadways in France. This laboratory has designed and standardized a test procedure on the expansion of hydraulic binders using parallelepiped specimens of 2x2x16 cm immersed in the exposure media of interest. References 51 - 53 used this procedure.
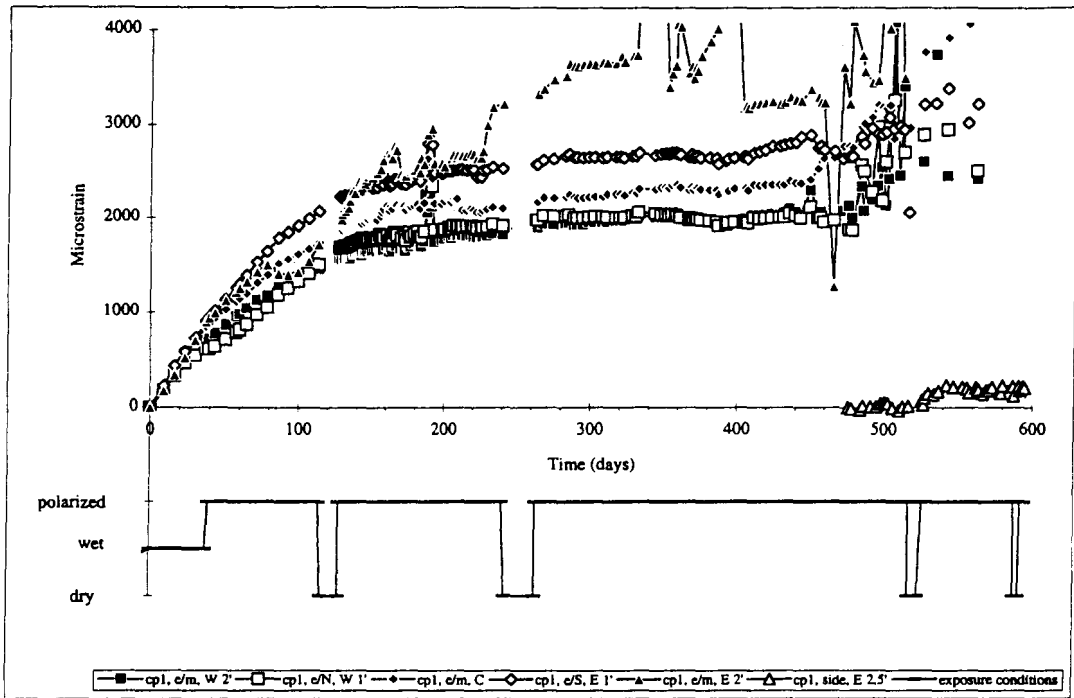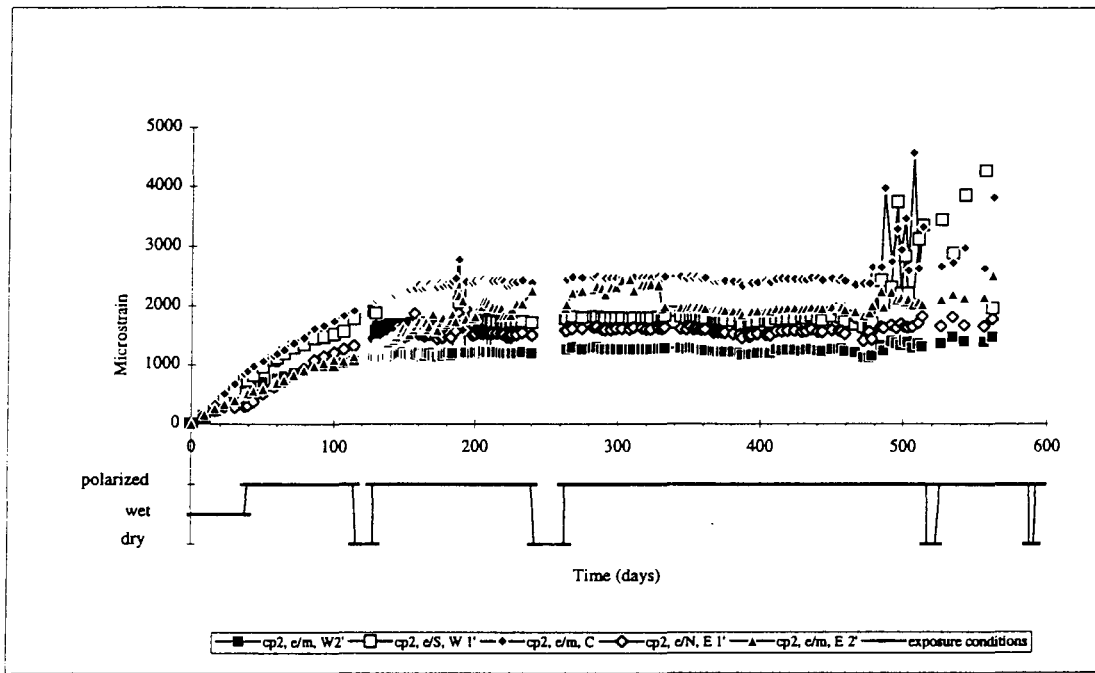
(a)
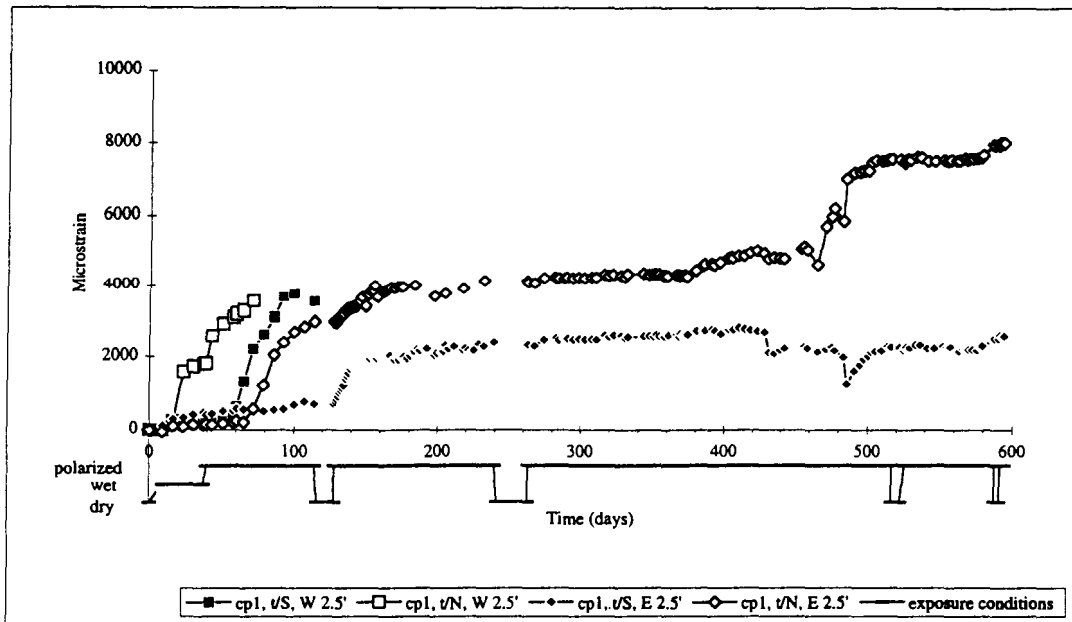
(b)

Figure 39:   Output of (a) embedded strain gauges and (b) tendon strain gauges as a
             function of time for specimen B2cp1 with sea water ponding and cathodic
             current density of 50 mA/m² of steel.

(a)

(b)

Figure 40:   Output of (a) embedded strain gauges and (b) tendon strain gauges as a function of time for specimen B2cp2 with sea water ponding and cathodic current density of 50 mA/m² of steel.

90

(a)

(b)

Figure 41: Output of (a) embedded strain gauges and (b) tendon strain gauges as a function of time for specimen B2cp3 with sea water ponding and cathodic current density of 50 mA/m² of steel.
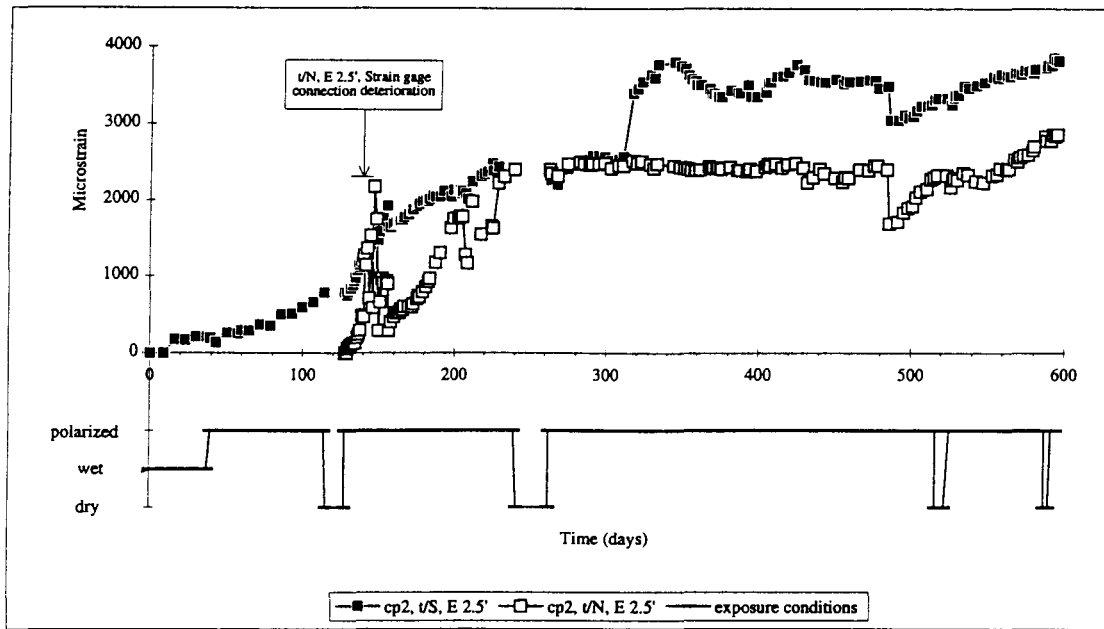
(a)

(b)

Figure 42: Output of (a) embedded strain gauges and (b) tendon strain gauges as a function of time for specimen B2cp4 with sea water ponding and cathodic current density of 500 mA/m² of steel.

(a)

(b)

Figure 43: Output of (a) embedded strain gauges and (b) tendon strain gauges as a function of time for specimen B2cp5 with sea water ponding and cathodic current density of 500 mA/m^2 of steel.
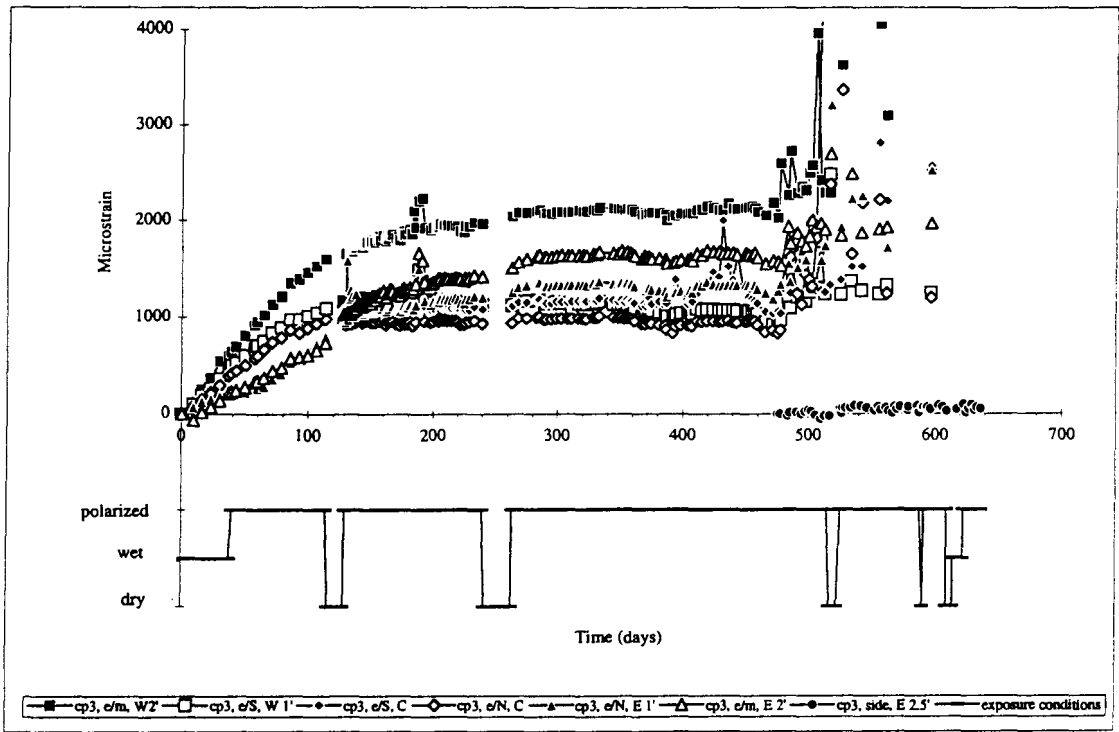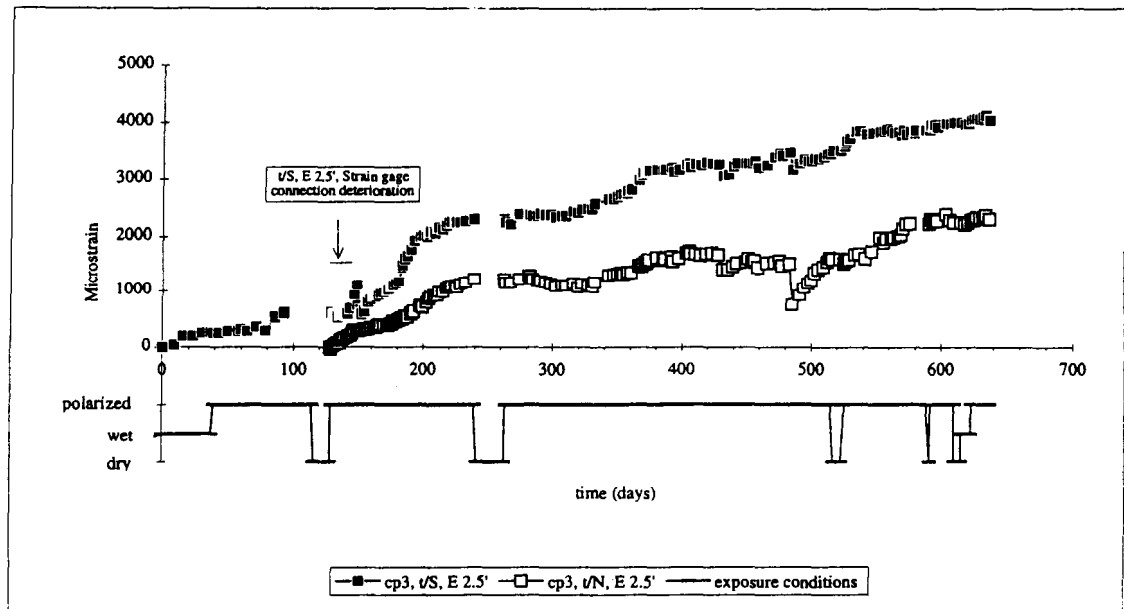
(a)

(b)

Figure 44:   Output of (a) embedded strain gauges and (b) tendon strain gauges as a function of time for specimen B2cp6 with sea water ponding and cathodic current density of 500 mA/m^2 of steel.

94

(a)

(b)

Figure 45: Output of (a) embedded strain gauges and (b) tendon strain gauges as a function of time for specimen B2cp7 with sea water ponding and cathodic current density of 5000 mA/m^2 of steel.
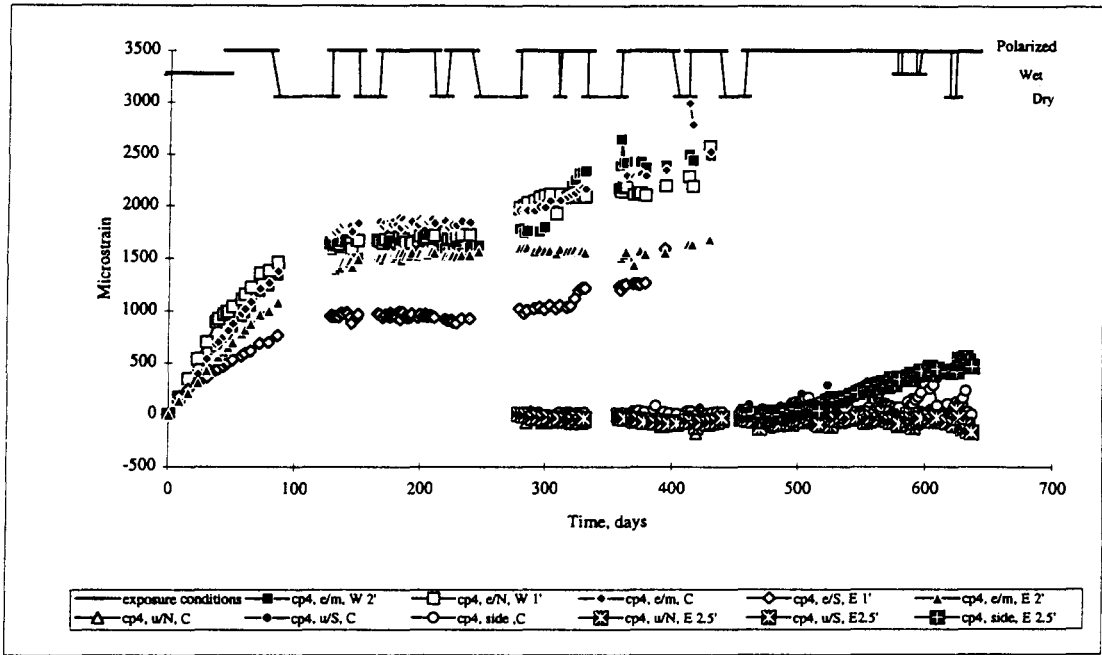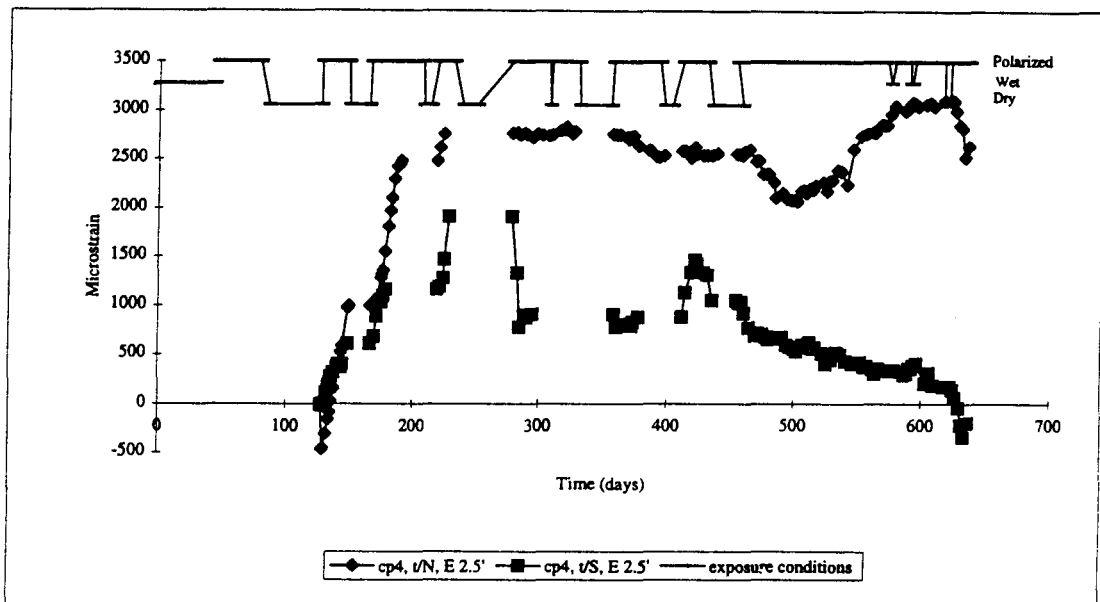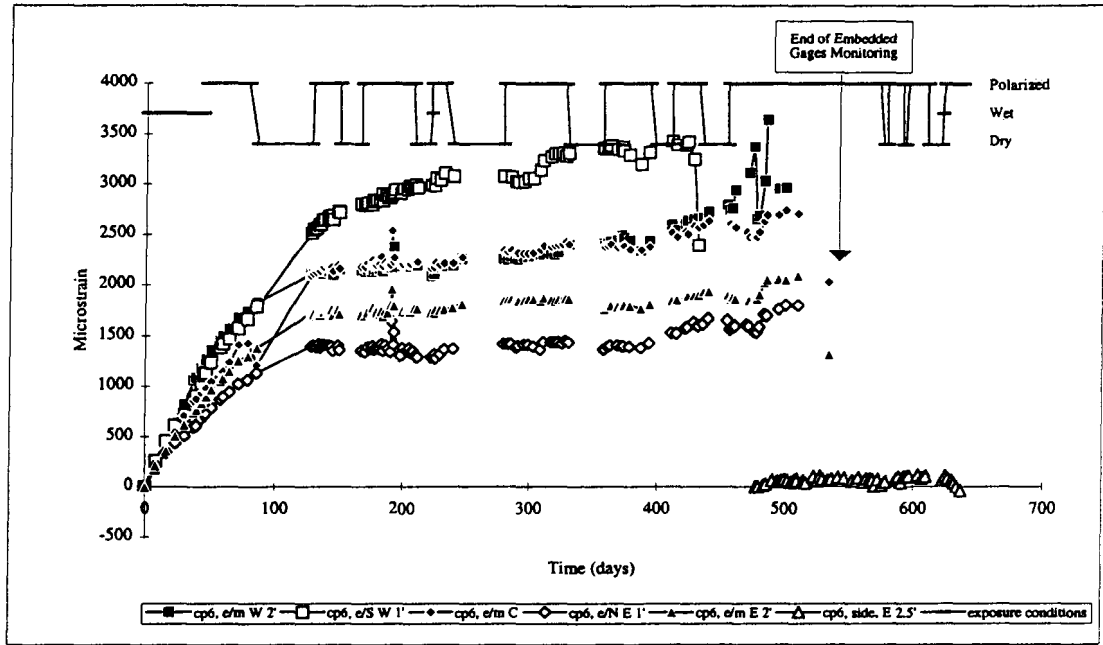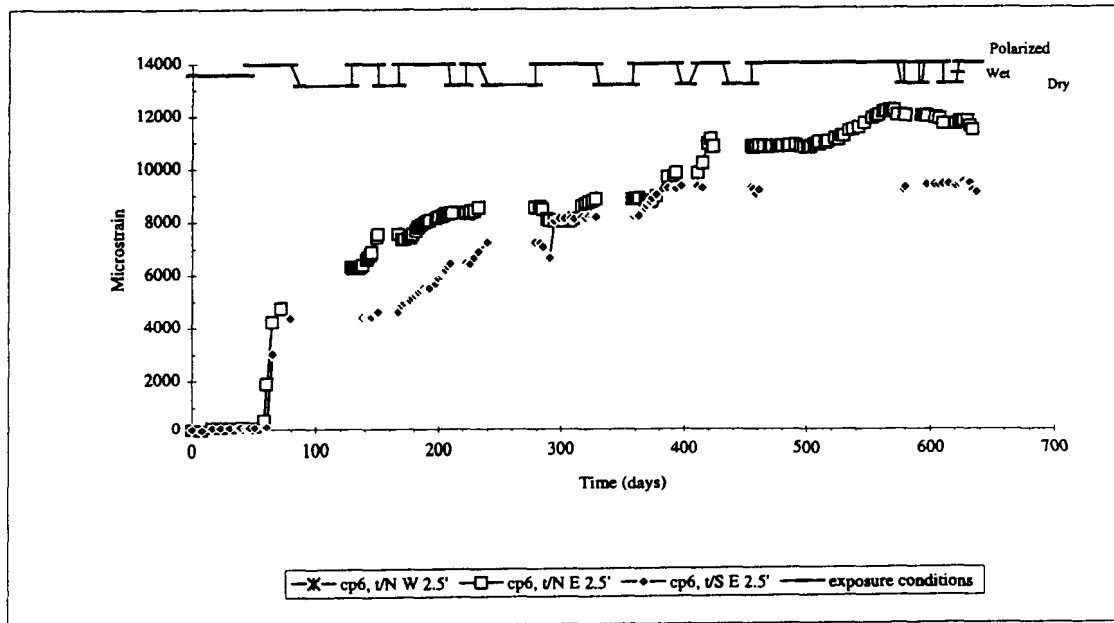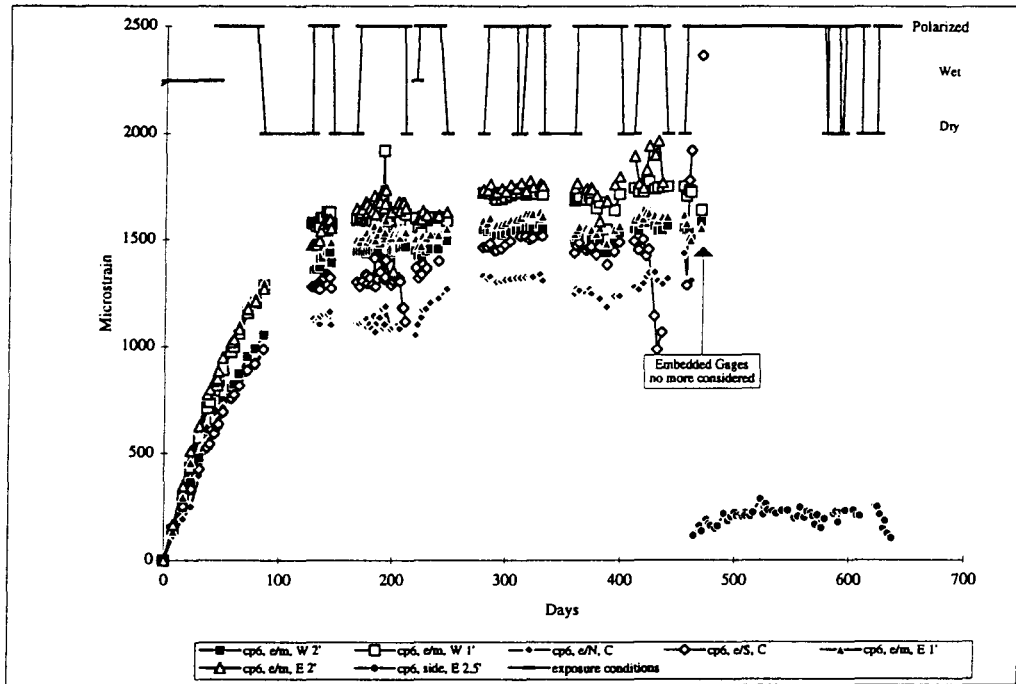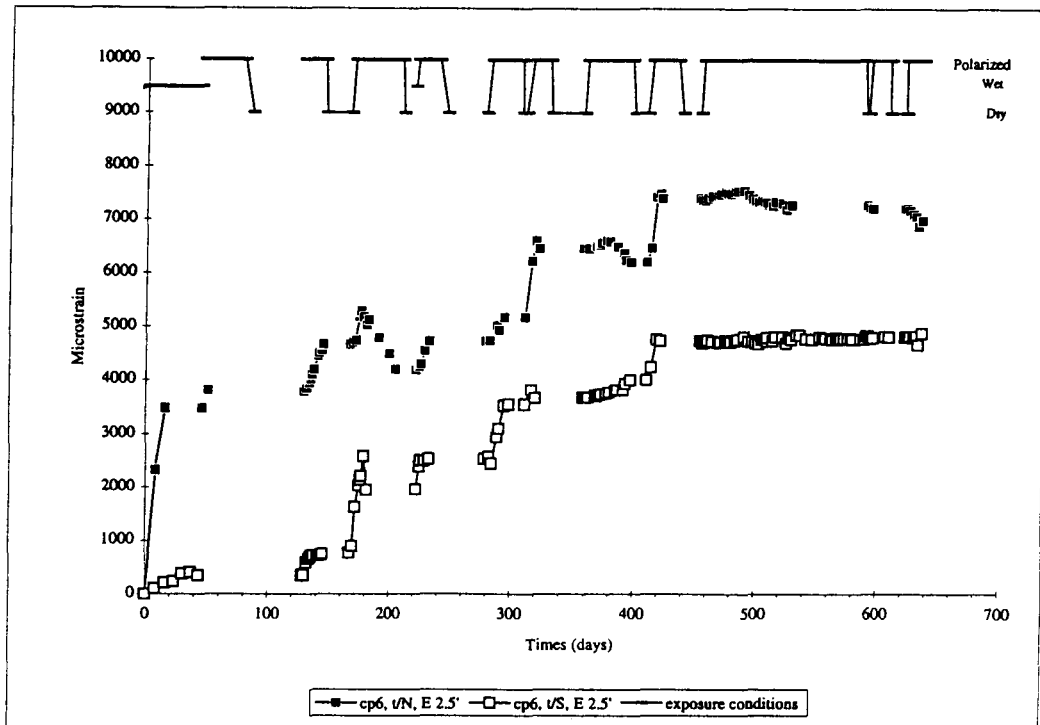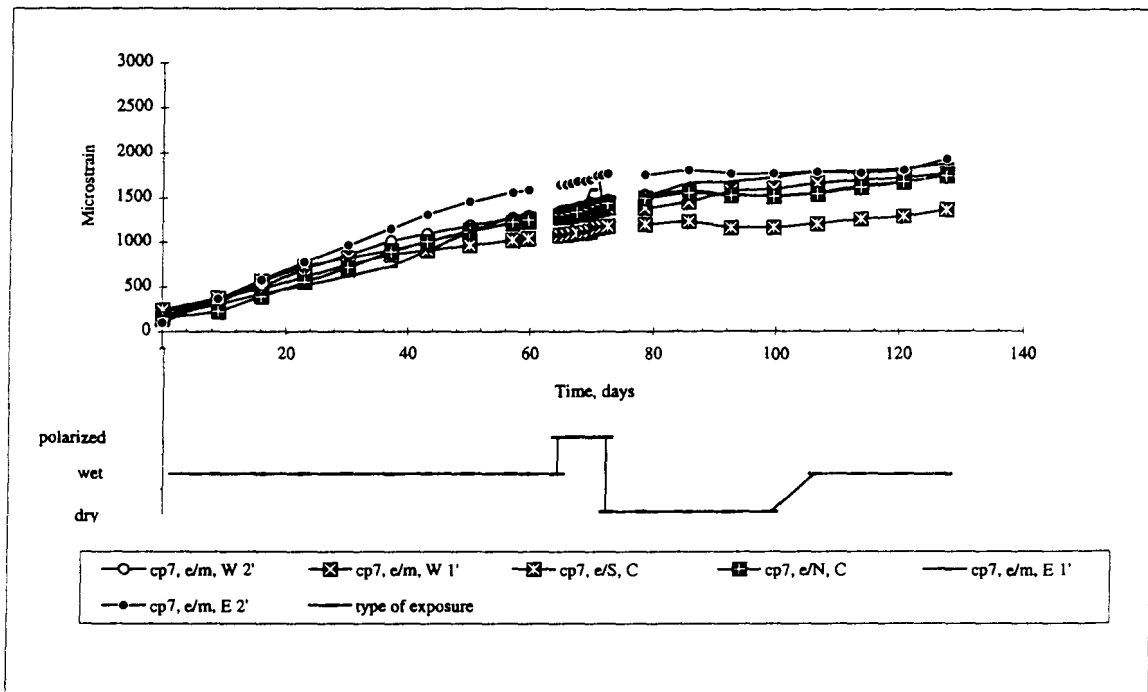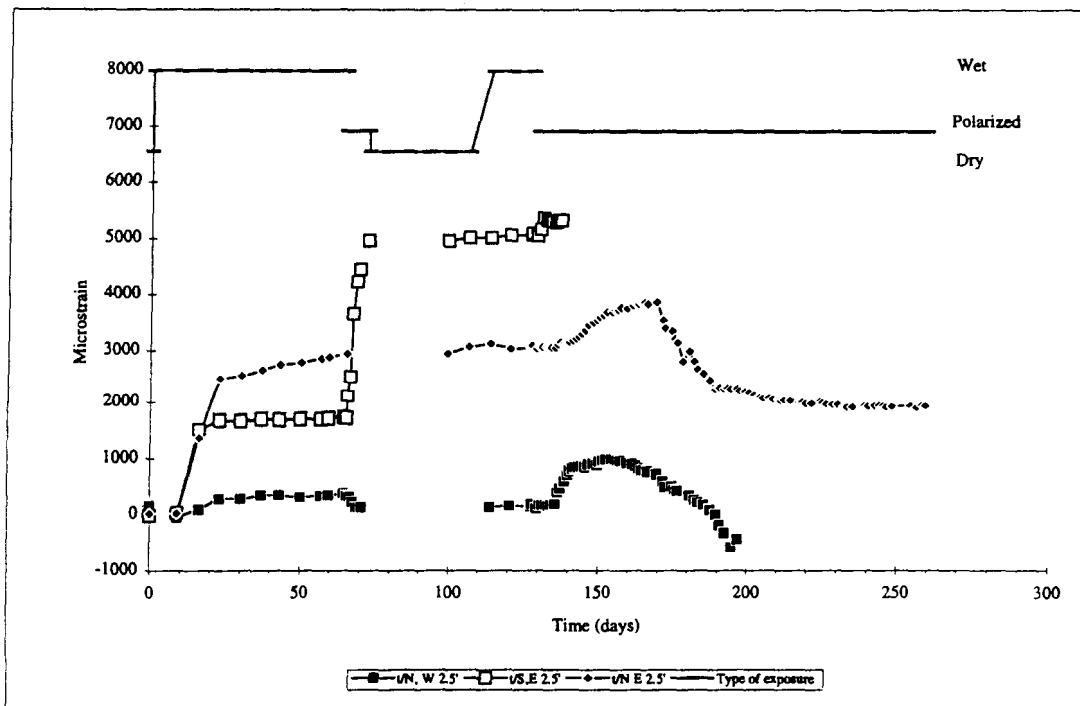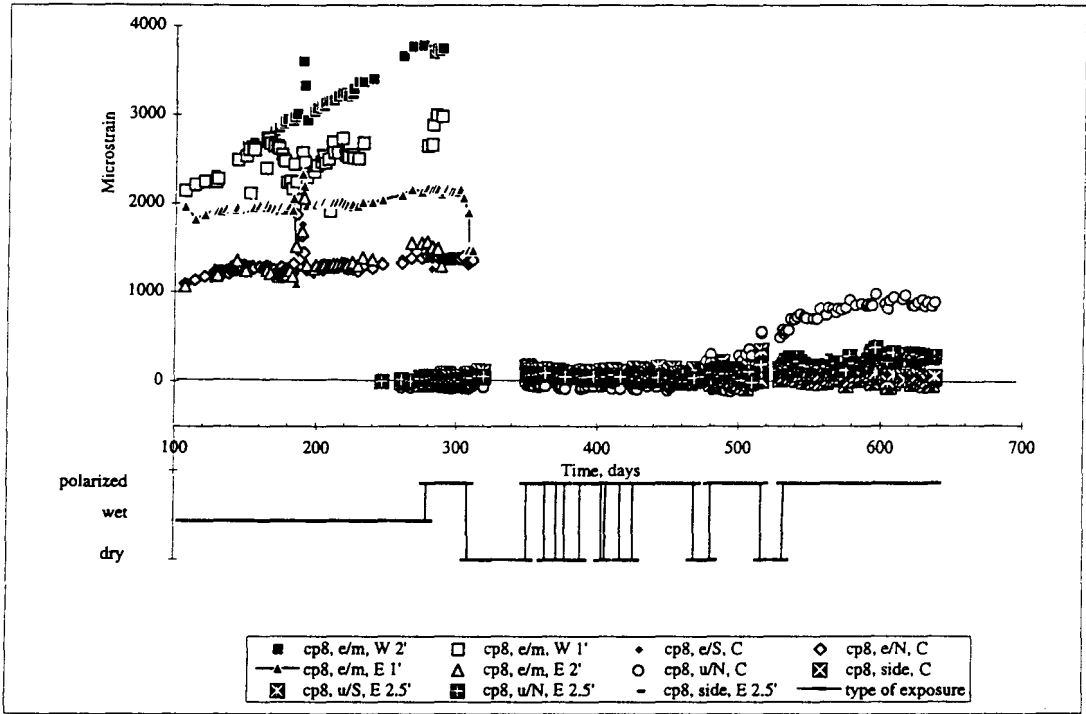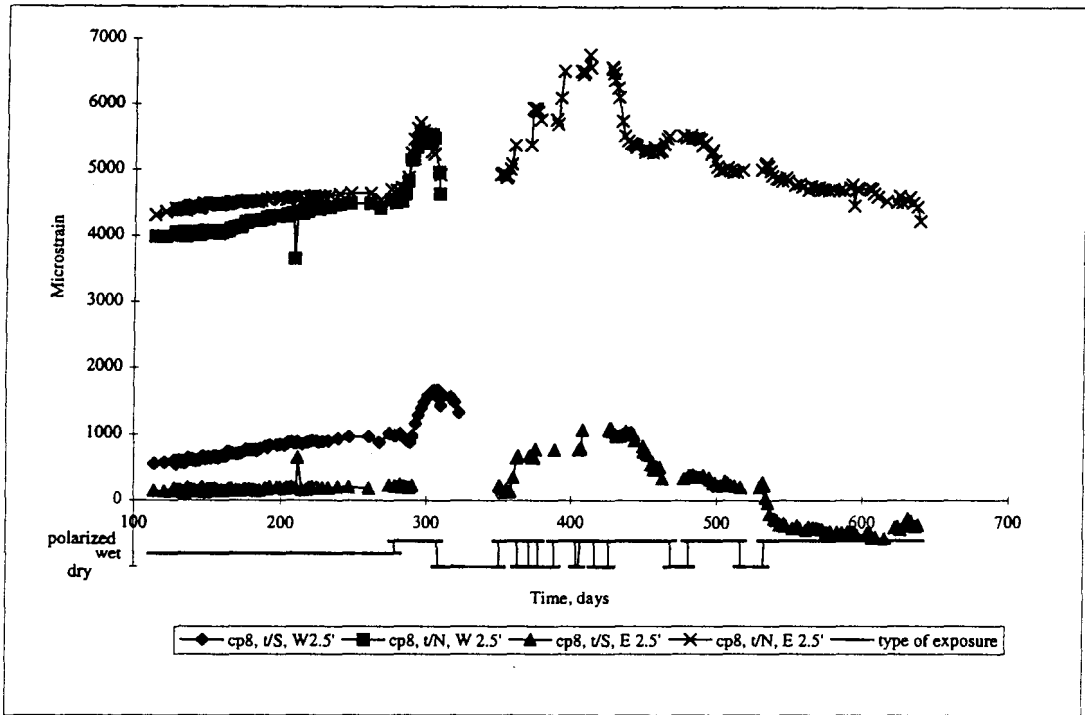
95

Figure 46: Output of (a) embedded strain gauges and (b) tendon strain gauges as a function of time for specimen B2cp8 with sea water ponding and cathodic current density of 2500 mA/m² of steel.
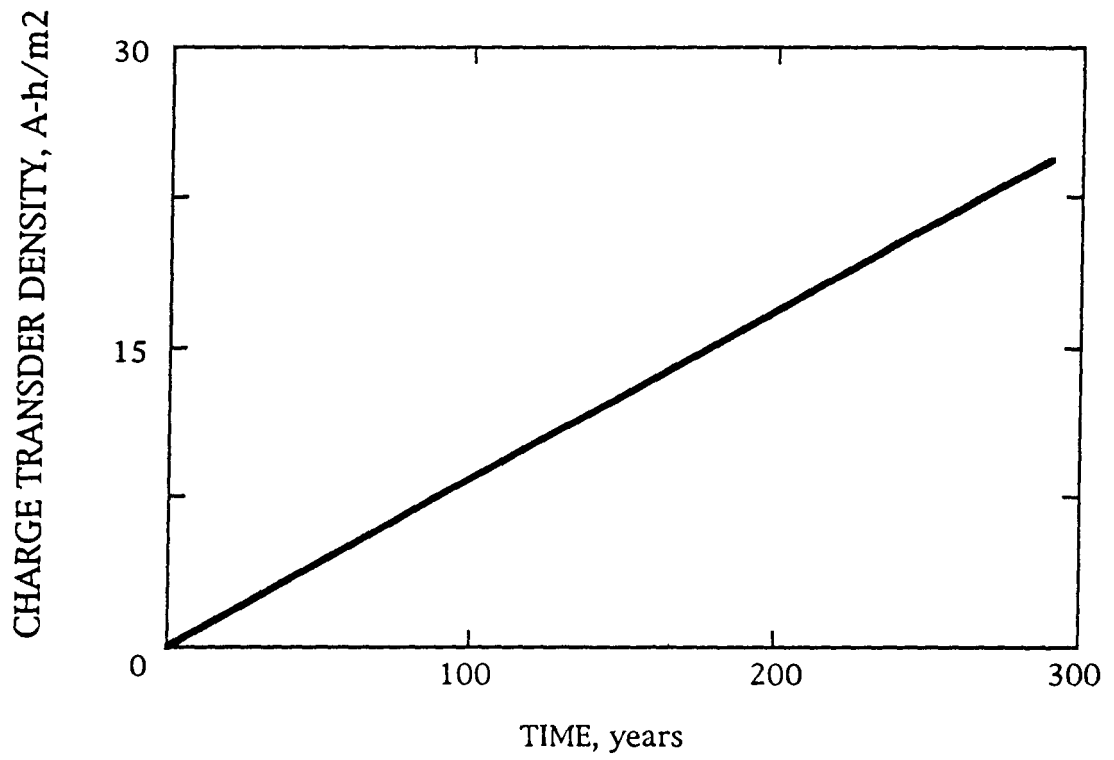
96

Figure 47: Charge transfer density accumulation at a cathodic current density of 10.8 mA/m2 of steel.

years at this same current density (10.8 mA/m^2). However, as noted earlier, not all historical data support a direct interdependence between charge transferred and bond reduction or loss.

The output from both tendon mounted and concrete embedded strain gauges upon the polarized specimens was generally similar to that for the sea water exposed, non-polarized specimens in that output increased initially but then moderated with time to a steady-state or near steady-state value after 100 to 200 days. In some cases (figure 43a, for example) the tendon gauge output progressively increased with time. A projected explanation for this is presented below. On the other hand, output for the concrete embedded and surface mounted gauges tended to eventually become constant. The latter observation is consistent with hydration expansion, as mentioned above for non-polarized specimens. Table 17 lists the average long-term strain readings for each polarized specimen (data for all non-polarized specimens (see figures 37 and 38) were averaged and are included for comparison) and shows that the lengthening of the tendon with time for these (polarized specimens) was almost three times greater than for the concrete embedded gauges. Data for specimen B2cp7 were excluded because polarization of this specimen was of relatively short duration as discussed below. Also, tendon data for specimen B2cp4 are excluded because of gauge problems at the time of the initial exposure which precluded normalization. Aside from these specimens, the average long-term strain output data are generally consistent with what was mentioned above for the non-polarized specimens. Interestingly, the time-to-failure of both tendon mounted and embedded gauges was less the higher the cathodic current density. Subsequent to the first set of gauge failures, alternative attachment procedures involving successive trial and error gauge reapplications were attempted. Visual examination revealed that premature failure of tendon mounted gauges was invariably accompanied by presence in the gauge area of a reddish liquid about and at the gauge-steel interface. While this had a rust-like appearance, the underlying steel was not corroded. As a part of one of the gauge replacements for specimen B2cp8 a new gauge on each of the two tendons was periodically inspected subsequent to cathodic polarization being reinstituted upon one of the tendons but not the other. Within several days the reddish liquid appeared upon the gauge on the polarized tendon, and the gauge output indicated relatively rapid expansion. At the same time the reddish liquid was bubbling, suggesting that a reaction involving a gaseous product was occurring. No liquid was present for the gauge upon the unpolarized tendon, where the gauge adhesive remained clear and readings were relatively constant. It was concluded that some aspect of the polarization process caused degradation of the polycyanoacrylate bonding agent with reaction rate increasing in proportion to current. The mechanism for this is unclear, however, since the gauges are in an air space within the PVC wells. Possibly some of the cathodic current matriculated along an adsorbed moisture layer upon the steel surface and reacted with the gauge adhesive. Irrespective of this, the abnormally large tendon extension relative to that of the concrete during the course of the present tests (table 16) is thought to have been a consequence of gauge swelling in association with this degradation process. More recent gauge applications using an epoxy bonding agent have resulted in greater gauge life and improved output stability.

Strain gauge data from the eight polarized specimens have been examined in detail to determine if there are any events that could be indicative of bond reduction or loss. Doing this necessarily involved addressing both data

98

Table 17:   Average long-term strain gauge output data for (a) tendon mounted gauges and (b) concrete embedded gauges. An average value for all non-polarized specimens is included for comparison.

Beam	Period over which average is computed (days)	Current density (mA/m^2) of steel	Charge transferred (Ah/m^2) of steel	mean deformation, μe
FC Beams	473-557	0	0	4353
B2cp1	563-594	50	610	5069
B2cp2	541-594	50	645	3695
B2cp3	541-594	50	645	3857
B2cp5	541-594	500	23111	10652
B2cp6	541-593	500	24166	6064
B2cp8	546-593	2500	14100	4736
Average deformation (cp specimens)				5679
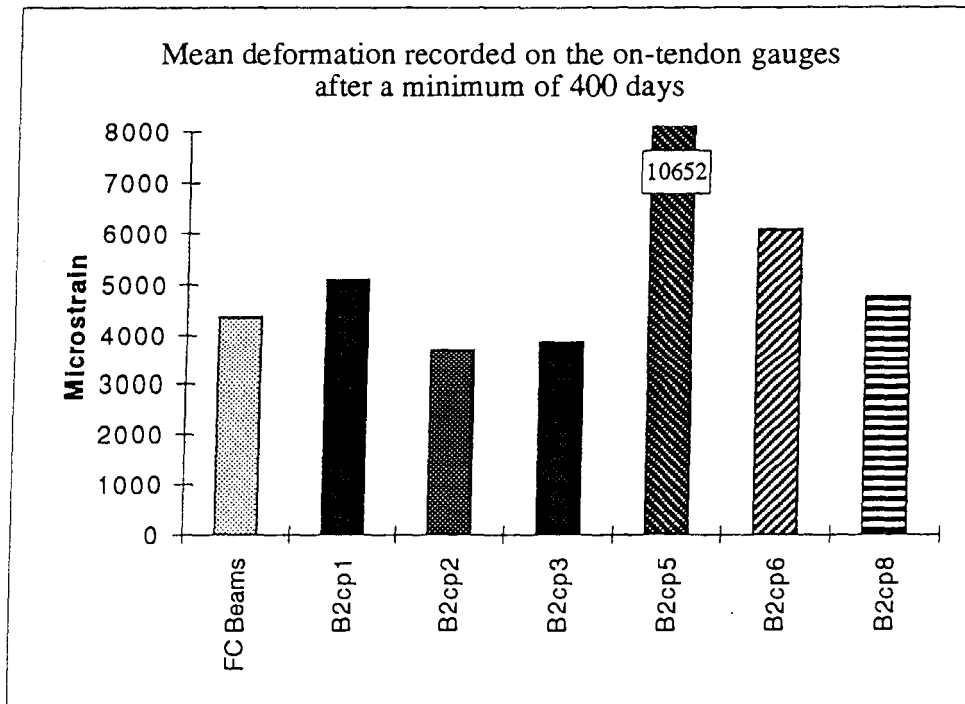
(a)

99

Table 17:   Average long-term strain gauge output data for (a) tendon mounted gauges and (b) concrete embedded gauges. An average value for all non-polarized specimens is included for comparison (continued).

Beam	Period over which average is computed (days)	Current density (mA/m^2) of steel	Charge transferred (Ah/m^2) of steel	mean deformation (μe)
FC beams	380-620	0	0	2320
B2cp1	398-500	50	514	2610
B2cp2	398-500	50	514	1868
B2cp3	398-500	50	514	1445
B2cp4	357-428	500	15300	2009
B2cp5	411-500	500	18000	2295
B2cp6	411-469	500	20000	1573
B2cp8	246-300	2500	2250	2030
Average deformation (cp specimens)				1976

(b)

100
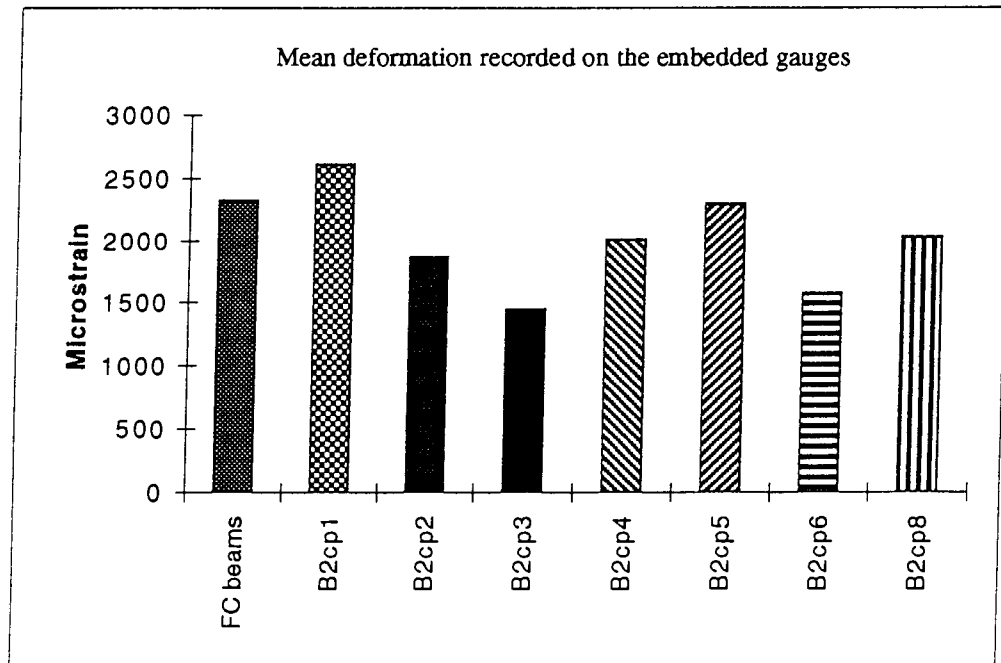
scatter and anomalies associated with gauge failures. In this regard, one of the two tendon strain gauges on specimen B2cp1 (figure 39b) exhibited an output decrease in the 425 to 490 days exposure time period. This was accompanied by an output increase for the embedded gauges (figure 39a); however, the latter occurred during the time when these gauges were failing; and so reliability of these data must be considered suspect. The single replacement surface mounted gauge exhibited a constant output between 475 and 515 days followed by a small increase. Relatedly, the two tendon mounted gauges on both specimens B2cp2 and B2cp3 (figures 40b and 41b) exhibited an output decrease at 490 days. However, the fact that these occurred concurrently suggests that an instrumentation problem may have been responsible. Also, the tendon contraction that is inferred to have occurred by these data was recovered (the tendon extended) subsequently with time. As was the case for specimen B2cp1, these output decreases occurred at the same time that embedded gauges were failing. No replacement surface gauge data are available for specimen B2cp2, but data from the single surface gauge on B2cp3 gave no indication of concrete expansion. The average tendon mounted gauge output decrease involved here was approximately 750 $\mu\varepsilon$ which, if this were due to a loss of bond event, would correspond to a 12 percent reduction in the prestress. From the representation in figure 47 the charge transfer density at the time of these events (approximately 484 A·h/m^2) corresponds to 5.5 years exposure at a current density of 10.8 mA/m^2 , assuming the charge transfer density is the parameter that governs bond reduction and loss. It is thought, however, that the strain gauge output transitions discussed above probably did not reflect any bond alteration; but if they did, the bond loss to which they corresponded were relatively modest. This does not preclude the possibility of bond reduction or loss upon continued charge transfer accumulation. Monitoring of these three specimens is continuing for the purpose of assessing this.

While no strain gauge output changes that can be related to bond reduction are apparent for specimens B2cp5 and B2cp6 (figures 43 and 44), output for the two tendon mounted gauges on Specimen B2cp4 decreased beginning at about 450 days (figure 42b). Strain continued to decrease to the extent of the exposure to date (approximately 600 days) for one of the gauges (t/S,E2.5') but reverted to an increase after about 500 days exposure for the other (t/N,E2.5'). During this same period output for several of the surface mounted gauges increased (figure 42a). Of particular interest is that the surface mounted gauge with the highest output was the one closest to tendon gauge t/S,E2.5'. If bond reduction was responsible, then the fact that output for one of the tendon gauges reverted from a decrease to increase could be a consequence of bond loss for one tendon being more extensive than for the other such that the concrete expansion resulting from the former tended to further extend the latter. The magnitude of strain decrease for gauge t/S,E2.5' corresponds to a prestress reduction of 12 percent. The charge transfer density at the onset of the tendon mounted gauge output decrease for specimen B2cp4 was about 14,400 Ah/m^2, which is equivalent to 164 years at a current density of 10.8 mA/m^2. The other two specimens tested at 500 mA/m^2, B2cp5 and B2cp6, have now accumulated approximately 24,840 A·h/m^2. The relatively high charge transfer densities for these three 500 mA/m^2 specimens with only one exhibiting an indication of a bond reduction event suggest that the strain output data for the 50 mA/m^2 specimens discussed above as possibly being bond reduction related were more likely experimental artifacts.

The two long-term tendon gauges that were mounted upon specimen B2cp8 (most of the polarization for this specimen was with a current density of 2,500 mA/m², see table 6) exhibited an output decrease at about 410 days exposure (figure 46b). Output for one of the surface mounted gauges began to increase noticeably after approximately 450 days with several others possibly showing this same trend but to a lesser extent. If these gauge output changes corresponded to a bond reduction event, then the magnitude of these to date (approximately 1,900 με for gauge t/N,E2.5') is equivalent to loss of about 21 percent of the prestress; and the charge transfer density at which this began (5,800 A h/m²) corresponds to 58 years of cathodic polarization at a current density of 10 mA/m².

Specimen B2cp7 was polarized at the highest current density 5,000 mA/m², (see table 6) and was the first test performed. As such, it constituted a learning experience with regard to gauge failures and data management during the course of this difficulty. As shown by figure 45a, the embedded gauges failed in less than 150 days; and these were not replaced by surface gauges. Irrespective of this, the two operative tendon mounted gauges both exhibited an output decrease, t/N,E2.5' after about 155 days exposure and t/S,E2.5' after 170 days. Correspondingly, the larger of the two strain decreases (1,800 με for gauge t/N,E2.5') is equivalent to a 20 percent prestress loss. Also, the charge transfer density at the onset of the gauge output decrease (4,160 A·h/m² for gauge t/N,W2.5') would be achieved at 48 years of exposure with a current density of 10.8 mA/m².

At about the same time at which the strain decrease occurred a liquid was observed oozing from each end on the tendons on specimen B2cp7. The cause of this is not clear, but apparently this material was able to migrate either along the tendon-concrete interface or through the tendon interstices to the specimen ends. No such liquid was detected for any of the other specimens.

Because a tendon contraction and concrete expansion could also result from tendon embrittlement and fracture, specimen B2cp7 was broken open subsequent to acquisition of the data in figure 45. This revealed that both tendons were in tact with no indication or either cracks or broken wires.

Table 18 summarizes the projected data for the pull-out specimens which have been tested to date. In the case of specimens for which bond reduction is thought to have occurred (B2cp4, B2cp7 and B2cp8), a trend of decreasing charge transfer density to initiate this bond reduction event with increasing current density is apparent. This, in conjunction with the fact that, first, the remaining two 500 mA/m² specimens (B2cp5 and B2cp6) do not yet appear to have experienced any bond reduction and, second, the equivalent time at a current density of 10.8 mA/m² would be even greater for these than for any of the above three specimens, suggests that the safe service life of cathodically protected prestressed concrete from a bond loss perspective should exceed what is likely to be the remaining anticipated useful life of most structures. Two considerations require that this conclusion be qualified, however. First, data have been acquired only from a limited number of specimens; and some difficulties were encountered in the experiments. Second, while the assumed current density of 10.8 mA/m² is a typical average value, local areas must be anticipated where current density is high. From the

SPECIMEN NUMBER	CURRENT DENSITY, mA/sqm of steel	CHARGE TRANSFER DENSITY AT INITIATION OF BOND REDUCTION, A-hr/sqm of steel	MAGNITUDE OF BOND REDUCTION, percent	EQUIVALENT TIME AT 10 mA/sqm OF STEEL, years
B2cp1	50	>640	0	>7
B2cp2	50	>640	0	>7
B2cp3	50	>640	0	>7
B2cp4	500	8,300	12	86
B2cp5	500	>26,000	0	>298
B2cp6	500	>26,000	0	>298
B2cp7	5,000	4,700	20	48
B2cp8	2,500	5,800	21	58

Table 18: Summary of charge transfer density data for polarized beam specimens and projected time for a bond reduction event at a current density of 10 mA/sqm.

most conservative perspective the lowest equivalent time to a bond loss event in table 18 (48 years for specimen B2cp7) becomes about 10 years if current density were locally concentrated by a factor of 5 and 5 years if it were concentrated by a factor of 10. Thus, particular attention should be provided to current distribution in the design and operation of cathodic protection systems for prestressed concrete structures. This applies not only from the perspective of bond loss but also with regard to hydrogen embrittlement.

Comparison of the charge transfer densities in table 18, for which bond reduction may have occurred, with those for the pull-out specimens (table 15) indicates that this parameter was less for the latter specimens tested to date than what corresponded to the apparent bond reduction events in the former. Thus, the two sets of data are mutually consistent since there was no indication of any bond strength reduction for the pull-out specimens (1,390 A·h/m^2 charge transfer density).

CONCLUSIONS AND RECOMMENDATIONS

Based upon the experiments and analyses performed the following conclusions and recommendations are made with regard to cathodic protection of prestressing steel in concrete:

1. The previously proposed -0.90 v (SCE) cathodic polarization limit for prestressing steel was confirmed as appropriate for non-microalloyed tendon material. However, microalloyed tendon specimens containing 0.24 weight percent chromium polarized to this same level (-0.90 v) often failed at stress levels which were only slightly above the pretensioning load. It is concluded that the appropriate lower potential limit for tendon microalloyed with this amount of chromium is more positive than -0.90 v. Additional experiments are required to 1) define an appropriate lower potential limit for chromium microalloyed prestressing steel and how this varies with chromium concentration and 2) define an appropriate lower potential limit for the other types of microalloyed prestressing steel (ones containing vanadium and chromium plus vanadium). In the meantime it is recommended that prestressed concrete members with microalloyed tendon material not be cathodically protected. Experiments to define quantitatively the influence of chromium upon prestressing steel embrittlement and the utility of cathodic protection for this material type are presently under way as a part of this project, and the results will be available in the final report.

2. Fracture properties of prestressing steel for which the cross section was locally reduced by either a notch or pit were governed by the relative influence of a) the magnitude of stress concentration, b) notch strengthening and c) hydrogen embrittlement. While notch strengthening appeared to be the dominant factor for notched specimens tested in air, at -1.30 v and for pitted specimens under both environmental conditions (air and polarization to -1.30 v), the combined influence of stress concentration and hydrogen embrittlement was most influential.

3. For prestressing steel wire containing a relatively modest notch or pit (remaining cross section approximately 75 percent or more of the original) the ultimate stress in air and with polarization in saturated $Ca(OH)_2$ to -1.30 v (SCE) was linearly related to the remaining cross section area independent of notch or pit shape. Based upon this disclosure a procedure for qualification of a particular prestressed concrete member for cathodic protection is proposed as follows:

   A. If no corrosion induced concrete cracking and spalling are evident, then the structure is automatically qualified.

   B. In cases where corrosion related cracking and spalling are evident, remove concrete from the damaged areas thereby exposing the tendon directly.

105

C. Identify locations on the exposed steel tendon where corrosion is uniform and where it is localized. Qualify the structural member for cathodic protection based upon the following criteria:

1. The remaining wire cross section at locations of uniform corrosion is no less than 85 percent of the original (uncorroded) area.

2. The remaining wire cross section at locations of any localized attack is at least 90 percent of the original. For locations where there is both uniform and localized corrosion this same 90 percent remaining cross section limit applies.

This new approach constitutes a straightforward procedure for qualifying a particular structure for cathodic protection and is simpler than the previously proposed Electrochemical Proof Testing methodology. At this time, however, it is limited to normal (non-microalloyed) prestressing only, for reasons discussed above.

4. Consideration that structures for which Grade 250 prestressing steel was specified might be more conducive for cathodic protection than ones with Grade 270 (the former may be less susceptible to hydrogen embrittlement than the latter because of its lower specified strength) is discounted since the specification for Grade 250 is met by Grade 270 material and the former is often substituted for the latter depending upon availability.

5. Pull-out tests upon tendon and wire in concrete block specimens (non-prestressed) that were previously polarized galvanostatically with current density 2,500 mA/m^2 of steel to achieve 1,390 A·h/m^2 charge transfer density (equivalent to 15.1 years at a current density of 10.8 mA/m^2) exhibited no decrease in bond strength but about a 70 percent decrease in bond stress at 0.25 mm free end slip. Significance of the latter change is under evaluation. Dimensional monitoring of prestressed concrete beams cathodically polarized with current density in the range 50 to 5,000 mA/m^2 of steel indicated that a 20 percent bond reduction event could begin after accumulation of a minimum of 4,700 A·h/m^2 of steel charge transfer density. On an equivalent charge transfer density basis this translates to 48 years if current density were 10.8 mA/m^2. Based upon the limited results that are available thus far, it appears that loss of prestressing steel-to-concrete bond in association with cathodic protection should not be a concern. This assumes, however, that current density is in the normal range for embedded steel cathodic protection (10.8 mA/m^2 or less) and is not locally concentrated.

REFERENCES

1. K. F. Dunker and B. G. Rabbat, "Highway Bridge Type and Performance Patterns," Journal of Performance of Constructed Facilities, Vol. IV, No. 3, 1990, p. 161.

2. J. E. Slater, *Corrosion of Metals in Association with Concrete*, ASTM STP 818, Am. Soc. for Test. and Matls., Phila., PA, 1983, pp. 16-22.

3. D. S. Spellman and R. F. Stratfull, "Concrete Variables and Corrosion Testing," Highway Research Record, No. 423, 1963, p. 27.

4. K. C. Clear, "Time-to-Corrosion of Reinforcing Steel in Concrete Slabs", FHWA-RD-76-70, Federal Highway Administration, Washington, DC, 1976.

5. D. A. Hausmann, Materials Protection, Vol. 8, No. 10, 1969, p. 23.

6. E. G. Nawy, *Prestressed Concrete: A Fundamental Approach*, Prentice Hall, Englewood Cliffs, N. J., 1989.

7. J. E. Bennett, "Cathodic Protection Field trials on Prestressed Concrete Components," Draft Interim Report on FHWA Contract No. DTFH61-91-C-00030, March, 1995.

8. Standard Specification for Steel Strand, Uncoated Seven Wire for Prestressed Concrete, A 416-90a, Annual Book of ASTM Standards, American Society for Testing and Materials, Phila., PA, 1994.

9. R. A. Barnhart, Federal Highway Administration Memorandum entitled, "FHWA Position on Cathodic Protection Systems." FHWA, April, 1982.

10. "A Manual for the Corrosion Control of Bridge Decks", Ed. R. F. Stratful, Report No. FHWA/CrEng/1 Federal Highway Administration, Washington, DC, February, 1984.

11. R. B. Mears and R. H. Brown, Trans. Electrochem. Soc., Vol. 74, 1938, pp.519.

12. M. Pourbaix, Corrosion, Vol. 26, 1970, p. 431.

13. J. E. Bennett, T. R. turk and R. Savinell, "Mathematical Modeling of the Effects of Current Flow through Concrete," paper no. 94285 presented at CORROSION/94, February 27-March 4, 1994, Baltimore.

14. G. K. Glass, J-Z. Zhang and N. R. Buenfeld, Department of Civil Engineering, Imperial College, London, SW7 2BU, unpublished research.

15. J. E. Bennett and T. A. Mitchell, "Depolarization Testing of Cathodically Protected Reinforcing Steel in Concrete," paper no. 373 present at CORROSION/89, April 17-21, 1989, New Orleans.

16. M. Funahashi and J. B. Bushman, Corrosion, Vol. 47, 1991, p. 376.

17. O. Chaix, W. H. Hartt, R. Kessler and R. Powers, Corrosion, Vol. 51, 1995, p. 386.

18. NACE Standard Recommended Practice RP0290-90, "Cathodic Protection of Reinforcing Steel in Atmospherically Exposed Concrete Structures," NACE International, Houston, 1990.

19. R. J. Kessler and R. G. Powers, "Conductive Rubber as an Impressed Current Anode for Cathodic Protection of Steel Reinforced Concrete," paper no. 374 presented at CORROSION/89, April 17-21, 1989, New Orleans.

20. B. Bazzoni and L. Lazzari, Materials Performance, Vol. 31(12), 1992, pp. 13-18.

21. J. Wagner and M. Funahashi, "Laboratory Study on New Cathodic Protection Criterion Proposed for Prestressing Steel," paper no. 300 presented at CORROSION/95, Feb. 28-March 4, 1994, Baltimore.

22. J. E. Bennett, J. Bartholomew and T. Turk, "Cathodic Protection Criteria Related Studies under SHRP Contract," paper no. 323 presented at CORROSION/93, March 8-12, 1993, New Orleans.

23. R. Pangrazzi, W. H. Hartt and R. Kessler, Corrosion, Vol. 50, 1994, pp. 186-196.

24. J. P. Hirth, Met. Trans., Vol. 11A, 1980, p. 861.

25. R. A. Oriani, Corrosion, Vol. 43, 1987, p. 390.

26. J. D. Gilchrist and R. Narayanan, Cor. Sci., Vol. 11, 1971, p. 281.

27. W. H. Hartt, C. C. Kumria and R. J. Kessler, Corrosion, Vol. 49, 1993, p. 377.

28. W. T. Scannell and W. H. Hartt, Materials Performance, Vol. 26(12), 1987, p. 32.

29. R. N. Parkins, M. Elices, V. S. Galvez and L. Caballero, Corrosion Sci., Vol. 22, 1982, p. 379.

30. W. S. Galvez, L. Caballero and M. Elices, ASTM STP 866, American Society for Testing and Materials, Phila., PA, 1985, p. 428.

31. J. Wagner, W. Young, S. Scheirer and P. Fairer, "Cathodic Protection Developments for Prestressed Concrete Components", Report No. FHWA-RD-92-056, Federal Highway Administration, Washington, DC, March, 1993.

32. W. H. Hartt, "A Critical Evaluation of Cathodic Protection for Prestressing Steel in Concrete," in Corrosion of Reinforcement in Concrete, Eds.: C. L. Page, K. W. J. Treadaway and P. B. Bamforth, Soc. Chem. Ind., London, 1990.

33. S. T. Ewing, "Effect of Cathodic Current on Bond Strength between Concrete and Reinforcing Steel," Report No. WC-IR-60, Jersey Research Co., January, 1960.

34. J. B. Vrable, "Cathodic Protection of Reinforced Concrete Bridge Decks", NCHRP Report No. 180, National Research Council, Washington, DC, 1977.

35. B. M. Casad, "Effect of Cathodic Protection on Bond between Concrete and Reinforcing Steel", MS thesis, Oklahoma State University, Stillwater, OK, 1981.

36. C. E. Locke, C. Dehghanian and L. Gibbson, "Effect of Impressed Current on Bond Strength between Steel Rebar and Concrete", paper no. 178 presented at CORROSION/83, April 18-22, 1983, Anaheim, CA.

37. J. E. Bennett, T. J. Schue, K. C. Clear, D. L. Lankard, W. H. Hartt and W. J. Swiat, "Electrochemical Chloride Removal and Protection of Concrete Bridge Components: Laboratory Studies," Strategic Highway Research program Report No. SHRP-S-657, June, 1993.

38. Rasheeduzzafar, M. G. Ali and G. J. Al-Sulaimani, ACI Materials Journal, Vol. 90, 1993, pp. 8-15.

39. N. R. Buenfeld and J. P. Broomfield, "Effect of Chloride Removal on Rebar Bond Strength and Concrete Properties," Proceedings of International Conference held at the University of Sheffield, Vol. II, Ed. R. N. Swamy, Sheffield Academic Press, p. 1438.

40. E. B. Rosa, B. McCollum and O. S. Peters, "Electrolysis in Concrete," Technologic Papers of the Bureau of Standards, No. 18, March 19, 1913.

41. K. C. Clear, Kenneth C. Clear, Inc., Boston, VA. Personnel communication.

42. R. Pangrazzi, L. Ducroq and W. H. Hartt, "An Analysis of Strain Changes in Cathodically Polarized Pretensioned Concrete Specimens," paper no. 554 presented at CORROSION/91, March 11-15, 1991, Cincinnati.

43. W. T. Nutter, A. K. Agrawal and R. W. Staehle, ASTM STP 665, American Society for Testing and Materials, Phila., PA, 1979, p. 375.

44. R. Baboian, L. McBride, R. Langlais, G. Haynes, Materials Performance, Vol. 18 (12), 1979, p. 40.

45. R. W. Hertzberg, *Deformation and Fracture Mechanics of Engineering Materials*, third edition, J. Wiley and Sons, New York, 1989, pp. 20-26.

46. J. H. Hollomon, Trans. AIME, Vol. 162, 1945, p. 268.

47. R. D. Cook and W. C. Young, *Advanced Mechanics of Materials*, Macmillan Publishing Company, New York, 1985, pp. 28-29.

48. R. W. Hertzberg, *Deformation and Fracture Mechanics of Engineering Materials*, third edition, J. Wiley and Sons, New York, 1989, pp. 246-248.

49. R. Hill, *The Mathematical Theory of Plasticity*, Oxford University Press, Oxford, 1956, pp. 245-252.

50. H, Nisitani and N. Noda, *Stress Intensity Factors Handbook*, Society of Materials Science, Japan, Vol. 1, 1990, p. 643.

51. M. Regourd, "Physico-Chemical Studies of Cement Pastes, Mortars and Concretes Exposed to Sea Water," in *Performance of Concrete in the Marine Environment*, SP 65, Am. Concrete Inst., Detroit, 1980.

52. A. M. Paillere, M. Raverdy and J. Millet, "Effect of Cement on the Degradation of Concrete in the Marine Environment," Bulletin de Liaison des Laboratoires des Ponts et Chaussees, Paris, Vol. 35, Jan.-Feb., 1985, pp. 5-10 (in French).

53. A. M. Paillere and M. Raverdy, "Possibilities of Using Sulfur in Combination with Hydraulic Binders," Bulletin de Liaison des Laboratoires des Ponts et Chaussees, Paris, Vol. 129, Jan.-Feb., 1984, pp. 71-80 (in French).

54. J. Mijnsbergen and H. W. Reinhardt, "Long-Time Creep and Expansion Behavior of Concrete in a Marine Environment," SP 109, Am. Concrete Inst., Detroit, 1988.